

**Ministry of Higher Education and Scientific Research
University of Baghdad
Institute of Laser for Postgraduate Studies**



Computational Study of Al Emission Spectra in The XUV Region Using Nd:YAG Laser

**A Thesis Submitted to the Institute of Laser for
Postgraduate Studies, University of Baghdad in Partial
Fulfillment of the Requirements for the Degree of
Master of Science in Laser / Physics**

By

Shaymaa Neamah Ayyash

B.Sc. Physics Sciences – 2014

Supervisor

Dr. Mahmoad shakir Mahmoad

2018 AD

1439 AH

Certification

I certify that this thesis was prepared under my supervision at the Institute of Laser for Postgraduate Studies, University of Baghdad, as a partial fulfillment of requirements for the degree of "Master of Science in Laser/ Physics Sciences".

Signature:

Name: **Dr. Mahmoad Shakir Mahmoad**

Title: **Lecturer**

Address: Institute of Laser for Postgraduate studies,
University of Baghdad.

Date: / / 2018

(Supervisor)

In view of the available recommendation, I forward this thesis for debate by Examining Committee.

Signature:

Name: **Asst. Prof. Dr. Shelan Khasro Tawfeeq**

Title: Head of the Scientific Committee.

Address: Institute of Laser for Postgraduate studies,
University of Baghdad.

Date: / / 2018

Examination Committee Certification

We certify that we have read this thesis " Computational Study of Al Emission Spectra in The XUV Region Using Nd:YAG Laser " and as Examination Committee, we examined the student in its content and in our opinion, it is adequate with standards as a thesis for a degree of Master in science in Laser /Physics

Signature:

Name: Dr. Sabah Noori Mazhir.
Title: Assistant Professor.
Address: College of Science for Women/ University of Baghdad
Date: / / 2018
(Chairman)

Signature:

Name: Dr. Majida Hamdan Khadar.
Title: Assistant Professor.
Address: College of Science/
University of Mustansiriya
Date: / / 2018
(Member)

Signature:

Name: Dr. Fadhil Abbas Umran.
Title: Lecturer
Address: Institute of Laser for
Postgraduate Studies/ University
of Baghdad
Date: / / 2018
(Member)

Signature:

Name: Dr. Mahmoad Shakir Mahmoad
Title: Lecturer
Address: Institute of Laser for Postgraduate Studies,
University of Baghdad.
Date: / / 2018
(Supervisor)

Approval by the Deanship of Institute of Laser for Postgradgate Studies, University of Baghdad.

Signature:

Name: Prof. Dr. Abdual Hadi M. Al-Janabi.
Title: Dean.
Address: Institute of Laser for Postgraduate Studies, University of Baghdad.
Date: / / 2018

بِسْمِ اللَّهِ الرَّحْمَنِ الرَّحِيمِ

وَلَسَوْفَ يَعْطِينَا اللَّهُ فَتْرَتِي

صَدِّكَ يَا اللَّهُ الْعَظِيمِ

(سورة الضحى آية "5")

Dedication

*To my dear father, dear mother,
my sisters, my brothers, my
friends, and my husband
I dedicate my work.*

Shaymaa

Acknowledgements

I would like to thank first Allah for help me to complete this work. I would like to express my deepest thanks and appreciation to my supervisor **Dr. Mahmoud shakier Mahmoud** for his guidance.

I would like to express my sincere thanks to **Dr. Zainab, Dr. Hanan, Dr. Shelan, Dr. Ziad, Dr. Tahreer, Dr. Mohammed, Dr. Hussien, Dr. Fadil, and Dr. Jwad** Dean of the Institute of Laser for Postgraduate Studies, University of Baghdad for them great support during the period of my work.

Abstract

In this work, the hydrodynamic properties of laser produced plasma (LPP) have been investigated. For the purpose a light source working in the EUV region was created which is very important for lithography semiconductor manufacturing.

Cowan code was used to calculate the electrons transitions between atomic configurations using the mathematical method called (The Hartree-Fock).

The improved MEDUSA (Med103) code calculated 1- dimensional hydrodynamic properties (velocity, electron density, pressure, electron temperature, ion density, ion temperature and average ionization Z^*) of aluminum target ($Z=13$).

This work was done using laser source at wavelength of 1064 nm with three values of laser power densities (10^{11} , 10^{12} and 10^{13} W/cm²), and with pulse width of 10 ns and 10 ps.

The laser power densities with 10 ns pulse width gave a high ionization stage range for the aluminum from 2.4 -11 and with electron temperature ranging from 16.5 -3000 eV. For the 10 ps laser pulse width, the average ionization range was 3.35-13 while the electron temperature ranging was from 16.5 to ~ 2000 eV.

The aluminum target has been given a good emission spectrum in the XUV region at 10 nm with oscillator strength of 1.82.

List of symbols

A^Z	ion in charge state Z
c	Speed of light
e	electron charge
$e_1(\varepsilon_1')$	free electron with increased energy after the capture of the other free electron by the ion.
$e_1(\varepsilon_1)$	free electrons before the interaction
E_n	total energy of the system in state n
F	fractional absorption
H	Hamiltonian operator
K	propagation direction
\mathcal{K}	thermal conductivity
\mathcal{K}	rate of energy exchange between ions and electrons
k_B	Boltzmann constant
K_o	effective absorption coefficient
LPP	Laser produced plasma
m_e	mass of the electron
m_H	proton mass
n_c	critical density
N_D	number of electrons in Debye sphere
n_e	Plasma electron density
λ_D	Debye length
M_k	mass number
S	energy rate per unit mass
T_e	electron temperature
T_o	isothermal temperature of the plasma
V	specific volume
Λ	ratio of the maximum and minimum impact parameters
Z	ion charge state

Z	nuclear charge
H	flow of heat due to thermal conduction
α	absorption coefficient
γ	Photon
ε_1	energy of the free electron before the process
ε_2	energy of the free electron after the process
ν_{ei}	electron-ion collision frequency
ν	frequency of the incident radiation
ψ_n	total wave function
ω_o	the frequency of the electromagnetic wave
ω_p	plasma oscillation frequency
ϕ	resonance parameter
Z_k	charge number
Z^*	Average ionization
Z	Atomic number

List of contents

Chapter one: Introduction and Basic Concepts	
1.1 Introduction	1
1.2 Laser produced plasma	3
1.3 Interaction processes in laser produced plasma	5
1.3.1 Linear processes	5
1.3.1.1 Collisional absorption (inverse bremsstrahlung)	6
1.3.1.2 Resonance Absorption	7
1.3.2 Nonlinear Processes	7
1.4 Plasma expansion	7
1.5 Atomic processes in a plasma	9
1.5.1 bound – bound transition	9
1.5.2 bound - free transition	10
1.5.3 free-free transition	11
1.6 Equilibrium in a laser produced plasma	12
1.7 Wavelength Regimes and Nomenclature	13
1.8 The simulation codes	15
1.8.1 The cowan code	15
1.8.2 The Medusa code (Med103 code)	15

1.9 Literature review	16
1.10 Aim of the work	19
Chapter two: Computational Methods and Codes	
2.1 Introduction	20
2.2 Atomic Structure Theory	20
2.3 Single Configuration Hartree-Fock Approximation	21
2.4 Calculation of Atomic Structure	22
2.4.1 Configuration Interaction Hartree-Fock	22
2.4.2 Multiconfiguration Hartree-Fock	23
2.5 The Cowan Code	23
2.5.1 The Cowan Code Structure	23
2.5.2 Cowan output files	24
2.6 The Medusa Code	26
2.6.1 The Physical model	27
2.6.2 Medusa output	28
Chapter three: Results, Discussion Conclusions and Future Work	
3.1 Introduction	30
3.2 Atomic Structure Results	30
3.3 MEDUSA Code Results	39
3.3.1 Spatial and temporal electron density variation	39
3.3.2 Spatial and temporal velocity variation	46

3.3.3 Spatial and temporal electron temperature variation	54
3.3.4 Spatial and temporal pressure variation	61
3.3.5 Spatial and temporal average ionization variation (Z^*)	68
3.4 Conclusions	75
3.5 Future work	76

Chapter One

Introduction and Basic

Concepts

1.1 Introduction:

Plasma can be defined as the 4th state of the matter in the universe of partial or completed ionization, the matter state of purely solid, liquid, and gas [1]. As a solid is heated, it becomes liquid, as it is heated further it evaporates to become a gas. If the matter is still heated, the atoms will begin to dissociate into negative electrons and positive ions, this process is called ionization. The degree of ionization in the plasma increases when the plasma is heated, [1, 2].

Plasma represents 99% of the matter in the universe .It can be considered a very good radiation source which emits in the different regions from electromagnetic radiation [2].

The fundamental parameters that can be used to characterize plasma are the electron number density (n_e), temperature (T_e) and steady state magnetic field (B). The electron density is the measure of the probability of an electron which is being present at a specific location.[3, 4].

$$n_e = n_i z \quad (1.1)$$

Where n_e is electron density, n_i is the ion density, and z is the average charge state.

The fundamental characteristic of the plasma is the ability to shield out electric potentials that are applied to it. This distance which is measured called "Debye length" can be defined as a distance travels by a particle at the thermal velocity in $1/2 \pi$ of the plasma cycle. This distance can be defined by the relation [5, 6]:

$$\lambda_D = \left(\frac{k_B T_e}{4\pi n_e e^2} \right)^{1/2} \quad (1.2)$$

where k_B is Boltzmann constant, T_e is the electron temperature and e is the electron charge, λ_D is Debye length.

The electron (or ion) has individual behavior on a scale shorter than the Debye length. The number of electrons (ions), N_D , is given by

$$N_D = \frac{4\pi n_e \lambda_D^3}{3} \quad (1.3)$$

The plasma oscillation frequency (ω_{pe}) is given by

$$\omega_{pe} = \left(\frac{n_e e^2}{m_e \epsilon_0} \right)^{1/2} \quad (1.4)$$

Where (m_e) is the mass of the electron, $\epsilon_0 =$ the permittivity of the vacuum (8.854×10^{-12} F/m) [7].

The propagation of the electromagnetic radiation wave (with frequency ω) through the plasma, will be related to a dispersion relation which is dependent on the electron density. For an electromagnetic wave travelling through plasma, the dispersion relation is given by [8]:

$$\omega^2 = \omega_{pe}^2 + c^2 k^2 \quad (1.5)$$

where ω_{pe} is the plasma frequency, $k = 2\pi/\lambda$, which represents the propagation direction of the wave, and c is the speed of light.

For $\omega > \omega_p$, k is real and the wave propagates through the plasma, and for $\omega < \omega_p$, k is imaginary and the wave doesn't propagate through the plasma. Also If $\omega = \omega_p$, the reflection occurs so it is called the critical density where the plasma density is maximum and can be represented by:

$$n_c = \epsilon_0 m_e \omega^2 / e^2 \quad (1.6)$$

where m_e is the electron mass and e is the electron charge [9].

The most important methods of the ionization in nature and in the laboratory can be classified into:

- 1- Ionization by heat.
- 2- Ionization by radiation.
- 3- Ionization by electric discharge.

1.2 Laser produced plasma

There are four specific features that characterize the laser produced plasma, which are [10]:

- 1- High temperature (up to 100 eV)
- 2- High density (electron density $\approx 10^{18} - 10^{21} \text{ cm}^{-3}$)
- 3- Relatively high degree of ionization
- 4- High expansion velocities

The plasma formed by laser has a very short lifetime of a few microseconds. The plasma lifetime is divided into three main stages, which are:

- 1- Early life (from initiation to about 100 ns)
- 2- Mid-life (100-1000 ns)
- 3- Late life (1-10 μs)

Neodymium doped yttrium aluminum garnet ($\text{Nd Y}_3\text{Al}_5\text{O}_{12}$) laser can be defined as a crystal that is used as an active medium for solid state lasers. The Nd YAG solid state laser has an important aim due to its high efficiency, and the pulse duration can be changed from millisecond down to ultra-short pulse [11, 12].

The principle of laser produced plasma is very simple, depends on high power density laser beam strike target material. When a high intensity laser beam hits of the target material, the laser energy can be absorbed by the target, and hot plasma can be created that emits extreme ultra violet (EUV) radiation and all electromagnetic spectrum [13].

A laser beam, focused with a sufficient power density on a target material, can produce very high temperature, high density plasma, which can be localized in a small spatial volume.

The density of free electrons and the electron temperature of such plasma can reach values as high as $n_e \approx 10^{20} - 10^{23} \text{ cm}^{-3}$ and $T_e \approx 10^2 - 10^3 \text{ eV}$ ($1 \text{ eV} \approx 11600 \text{ K}$) [14].

The Plasma formation begins when the laser beam hits target surface through multiphoton absorption, and produces free electrons. The target material is heated, and these free electrons causing collisions with the target. As the target surface is rapidly heated, it vaporizes and forms a layer of vapor at the surface [14, 15].

These collisions between the target vapor and free electrons lead to ionization of the vapor and thus plasma formation. Also, the particles, ions or atoms, near the free electrons are either ionized to the next ionization state or excited to a higher excitation level in the same ionization stage [15].

If the laser power density reaches the value ($>10^8 \text{ W/cm}^2$), the plasma can be reached a sufficient high temperature for a significant number of atoms to be ionized by collisions. As a result of this ionization, opaque plasma will be produced; therefore the intensity of the laser beam can be calculated from the following relation [16]:

$$I = \frac{1}{2} \epsilon_o c E^2 . \quad (1.7)$$

Where I is the power density in (W/m^2), c = the speed of light ($3 \times 10^8 \text{ m/s}$), E = the electric field strength (V/m).

The plasma rapidly expands; it continues to absorb laser energy. The propagation of electromagnetic wave in plasma is effected by the free electrons and follows this dispersion relation [16, 17].

For a Nd:YAG laser at wavelength of 1064 nm, the critical density is about 10^{21} cm^{-3} [15]. Only up the critical density, the laser beam hits on the plasma can be reflected.

The interference of the incident and reflected waves produces a large amplitude field near the critical density [17].

Due to high density at the point of reflection and the large amplitude of the electromagnetic field, most of the laser energy can be absorbed near the critical density. When the plasma electron density is higher than the critical density, the laser cannot penetrate the region; more target material is ablated through absorbed laser energy by the target surface [15, 16].

1.3 Interaction processes in a laser produced plasma

There are many processes in laser produced plasma can explain the incident electromagnetic waves interact with the plasma. These interactions are classified into two types, linear and nonlinear processes.

1.3.1 Linear processes

This process can be achieved when a high intensity laser beam hits any target material, and these processes can be mainly divided into types [17]:

- 1- Collisional absorption (inverse bremsstrahlung)
- 2- Resonance absorption

1.3.1.1- Collisional absorption (inverse bremsstrahlung)

This process can be described as a free – free transition process and it happen in plasmas with density less than the critical density (n_{cr}).

The incident wave energy at a collisional absorption ν is:

$$\nu = \nu_{ei} \omega_{pe}^2 / \omega_o^2 \quad (1.8)$$

Where ν_{ei} is the collision frequency of electron-ion, and ω_o is the frequency of the electromagnetic wave.

In the case of a Maxwellian velocity distribution for the electrons, the damping average of the incident wave is ν_{ei}

$$\nu_{ei} = 3 \times 10^{-6} \ln \Lambda n_e Z / (\theta_e)^{3/2} \quad (1.9)$$

where Λ is the ratio of the Debye length and DeBroglie wavelength, and θ_e is the electron temperature of the plasma and Z is the ion charge state where [9,15]

$$\theta_e = k_B T_e \quad (1.10)$$

θ_e is a function of T_e and K_B , If the temperature of the plasma increases, the collision becomes less.

The absorption coefficient of this process is given by [9]:

$$\alpha = 5.61 \times 10^{-11} Z n_e^2 \ln \Lambda / (\omega_o^2 T_e^{3/2}) (1 - (\omega_{pe}^2 / \omega_o^2))^{1/2} \quad (1.11)$$

where ω_o is the frequency of the incident wave, when $\omega_{pe} = \omega_o$, the absorption coefficient is maximum.

1.3.1.2- Resonance Absorption

This process is a linear process which explains the absorption of the incident wave energy near the critical surface and it plays a very important role in interaction processes during laser produced plasma process [16, 17].

$$F = \phi^2 (\tau_o) / 2 \quad (1.12)$$

where F is refers to the fractional , ϕ is the resonance parameter which can be described as the strength of oscillation, and τ_o is a function of the incidence angle and the length L, as given by the formula

$$\theta (\tau_o) = 2.31 \exp (2 \tau_o^3/3) \quad (1.13)$$

where

$$\tau_o = (K_o L)^{1/3} \sin\theta \quad (1.14)$$

1.3.2 Nonlinear Processes

At threshold intensities, the nonlinear processes can be occurred. There are different processes can explain nonlinear processes;

- 1- Raman instability
- 2- Brillouin instability.
- 3-Two Plasmon decay instability

1.4 Plasma expansion

The interaction of laser light with plasma can be happed in different ways. The laser light can be refracted, reflected, and absorbed by the plasma [18].

To get plasma, high external power densities (high intensity laser) should be used. When a high power density laser hits a material, the plasma is created and the dynamic equilibrium happens between the plasma absorption coefficient and the energy transfer of thermal energy to kinetic energy [19, 20].

There are several steps of plasma formation as shown in Fig.(1.1):

1-absorption and thermal diffusion.

2- melting of target material.

3- vaporization of target material.

4-absorption of laser radiation that means plasma is created.

5-plasma expansion.

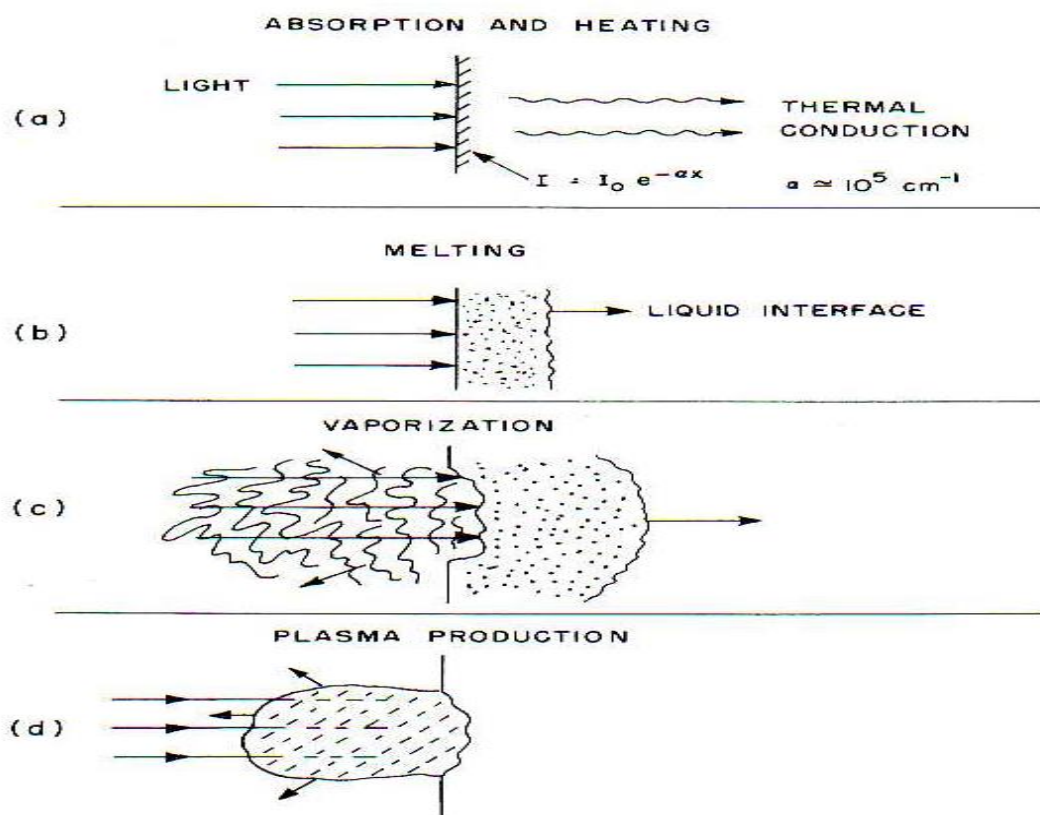


Fig.(1.1) Schematic diagram of physical process occurring when a high power laser beam strikes an absorbing surface [20].

1.5 Atomic processes in a plasma

If the laser beam strikes the absorber surface target, the laser photons can be absorbed by an atoms, and the following atomic processes can be occurred [21]:

- 1- bound-bound transition
- 2- free-bound transition
- 3- free-free transition

1.5.1- bound – bound transition

This transition depends on the transition of an electron in atoms or ions from one energy level to another following collision with another electron, or depend on the absorption or emission of a photon.



(a) electron impact excitation(i) and de-excitation (ii).

(b) spontaneous decay and resonant photoabsorption

Fig.(1.2) Schematic diagram of bound-bound transitions in laser-produced plasmas. (a) Collisional processes and (b) radiative processes [21].

In the collisional process the moving electron near an ion can induce a transition of a bound electron to a higher excited level (electron-impact excitation) or inversely can be induced toward down transition of an excited bound electron to a lower bound state (electron-impact de-excitation) [21, 22].

1.5.2- bound - free transition

When a free electron collides with an atom or ion, the bound-free transition process can be achieved. Enough energy can be transferred from the free electron to a bound electron, then, the amount of energy obtained by the bound electron is equal to the energy wasted by the free electron. This process is known as electron impact ionization and can be explained by [23]:



where A^Z represents ion in charge states Z , and A^{Z+1} represents ion in charge state $Z+1$. Also e_1 and e_{11} are indicates to free electron before and after the collision, and e_2 is the ionized electron [24].

In high density plasmas, the inverse of this process can be achieved. In this case, one free electron of an ion is catch into an outer state while the second electron can get the lost energy by capturing an electron. The following equation can explain the previous case:



where A^{Z+1} is refer to an ion in charged state $Z+1$, and A^Z is the ion in charge state Z , while $e_1(\varepsilon_1)$ and $e_2(\varepsilon_2)$ are the free electrons before the interaction and $e_1(\varepsilon_1')$ is a free electron with the increased energy after the capture of the other free electron by the ion [23, 24]:

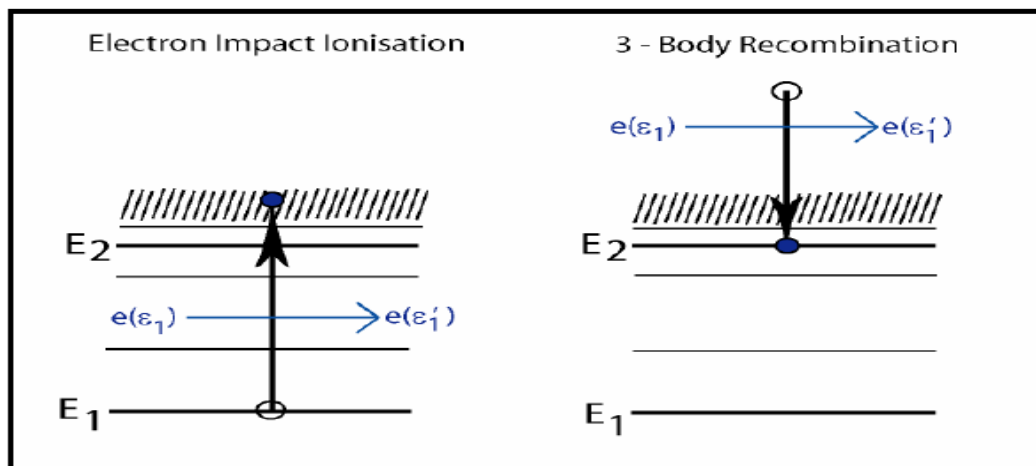


Fig.(1.3) Schematic diagram explained the electron impact ionization (left) and 3- body recombination (right) [23].

1.5.3-free-free transition

When the photon is absorbed by a free electron, the kinetic energy of this electron can be increased by the absorbed quantum of energy. This process is known as Inverse Bremsstrahlung (IB) and can be played a major role in absorption of the laser radiation by the plasma and can be described by [25]:

$$e(\varepsilon_1) + A + \gamma \quad A + e(\varepsilon_2) \quad (1.17)$$

where e is refer to the free electron, while ε_1 and ε_2 are the energies of the free electron before and after this process, and A represents the ion and γ

represents the photon. The corresponding free-free emission process is called Bremsstrahlung.

Braking of the radiation can be occurred when an electron is passing through the electric field of each ion. The electron may be overdue in the electric field and emit a photon.

Bremsstrahlung can be classified by [26]:

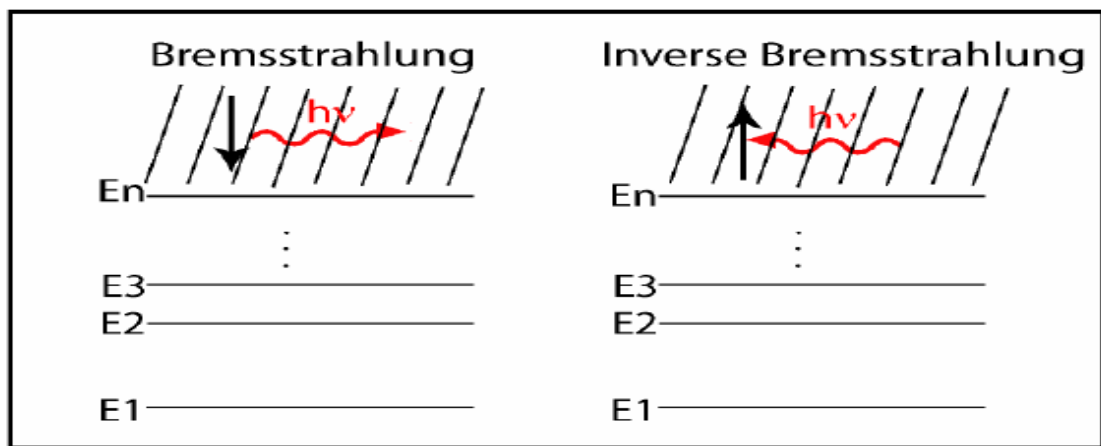
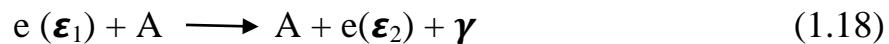


Fig.(1.4)Schematic diagram of the Bremsstrahlung (left) and Inverse Bremsstrahlung (right) [25].

1.6 Equilibrium in a laser produced plasma

When the electrons, ions and photons are all in the equilibrium, thermodynamic equilibrium (TE) of plasma can be achieved [27].

The most common equilibrium models can be used to describe plasmas as shown in Fig.(1.5) [28]:

- 1-Collisional Radiative Equilibrium
- 2-Local Thermodynamic Equilibrium
- 3-Coronal Equilibrium

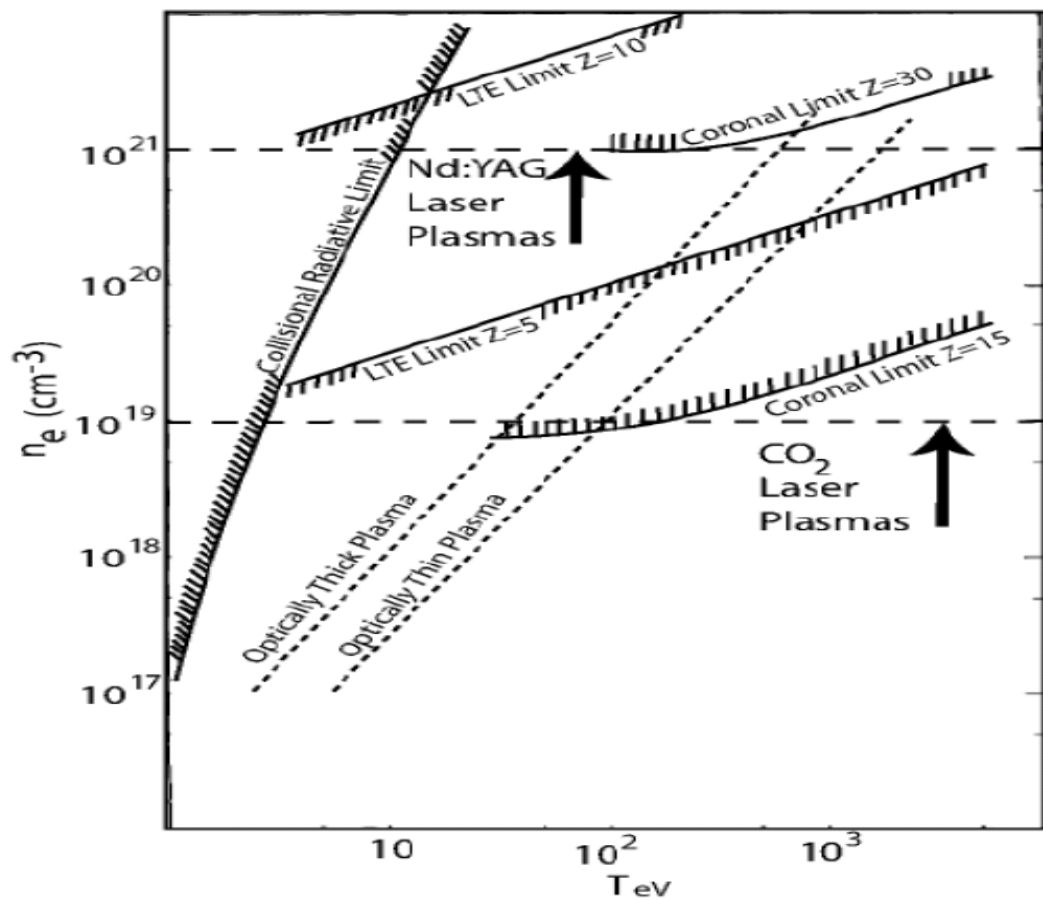


Fig.(1.5) The idea about the validity of each model for a temperatures and plasma densities [27].

1.7 Wavelength Regimes and Nomenclature

The wavelengths regions of the electromagnetic radiation below 200 nm can be given by various names and depend on the nature of the optical instruments [30, 31].

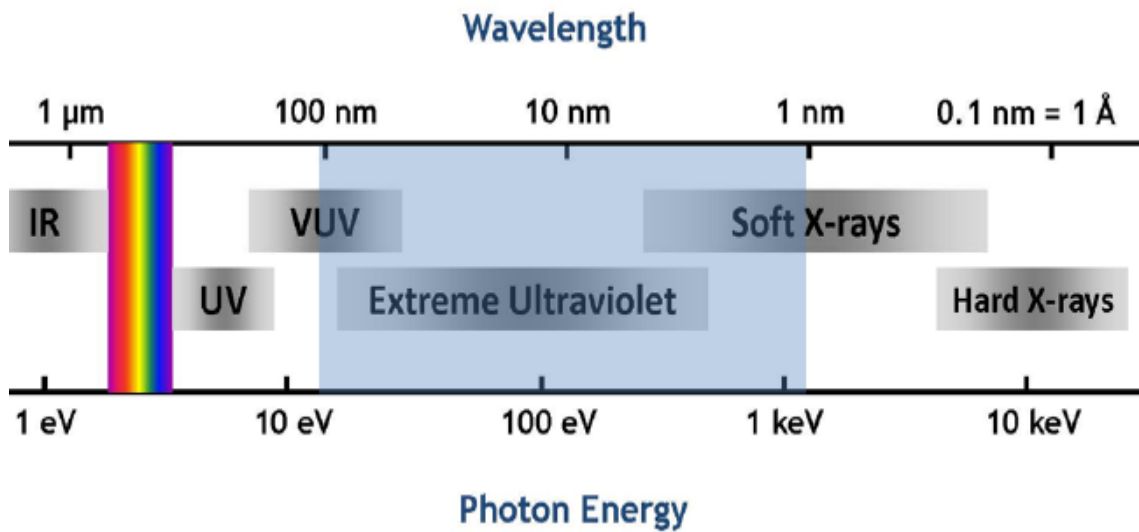


Fig.(1.6)Wavelength regions and nomenclature used below 200 nm [34].

The emission spectrum can be defined as the spectrum of the frequencies of electromagnetic radiation due an atom or molecular by transition from high energy to the lower energy levels [29].

Extreme ultraviolet radiation has a high energy ultraviolet radiation. Moreover, its range is 2-100nm in the electromagnetic spectrum. Planck Einstein equation has photons with energies from 10 eV to 124 eV. Extreme ultraviolet can be generated naturally by the solar corona and artificially by the plasma [34],[35].

Energy of the emitted photon is equal to the energy difference between the two energy levels.

These different transitions can give different wavelength emission spectrum. [36].

1.8 The simulation codes

Simulation is the process that can explain the designing of a model of a real system and experiments in order to understand the behavior of this system [37].

The basic reason for using simulation is to find easy solution of standard mathematical techniques of many processes that cannot be solved easily. In this case the interactions between variables have been considered as nonlinear in the system [38], [39].

1.8.1 The cowan code

The energy emitted from the radiation sources can be measured by atomic structure calculations using different codes. For example, the Cowan code uses Hartree-Fock mathematical method to solve the Schrödinger equation for atoms [40].

The Cowan code can calculate the atomic structures and the emission spectra by the superposition of configuration and also it can calculate the wave length (λ), and weighted oscillator strength(gf) for a transition between two energy levels. This code was developed by Robert Cowan.

This code consists of four sub codes which are RCN, RCN2, RCG and RCE[41].

1.8.2 The Medusa code (Med103)

This code is important to calculate the spatial and temporal velocity, electron temperature, pressure, ion and electron temperature and ion distribution in laser produced plasmas (LPP) [42].

The spatial and temporal hydrodynamics parameters can be calculated by using the laser material interaction.

Medusa (Med103) code is known as an improved MEDUSA code which was created by Christiansen for the UKAEA group at Culham laboratory in 1974 [43].

The Medusa code can calculate the one dimensional hydrodynamic parameters and thermodynamic behavior of plasma irradiated by an intense laser beam (high power density laser) [44].

The output results from medusa code are: plasma expansion velocity, Pressure, electron and ion temperature, electron density, average ionization (Z^*), and mass density [45].

The detailed description of laser-matter interactions (laser plasma interaction) can be calculated by numerical simulation. The differential equations describe the motion of the plasma produced by an intense laser. Also, it can describe the calculated plasma properties which can be compared with the experimental work [46].

1.9 Literature review

In 1949, C. E. Moore listed the atomic energy levels in three parts which is played a major role in the revolution in physics [47].

R. Bates *et al* in 1962 studied the recombination between atomic ions and electrons in optically thin plasma [48].

In 1967, J. Bearden and A. Burr studied all the x-ray emission wavelengths from electromagnetic spectrum [49].

U. Fano and J. Cooper in 1968 studied the information of neutral atoms in the ground states on the spectrum of oscillator strength in the far uv-soft x-ray range [50].

M. Mansfield and J. Connerade in 1975, studied the absorption spectrum between 40 and 95 Å of Sr I [51].

In 1979 the laser induced gas breakdown model was done by J. Gauthier and J. Geindre [52].

In 1989, I. Martinson described Spectroscopic investigations of the structure of highly ionized atoms [53].

In 1991, extreme-ultraviolet (EUV) region absorption spectroscopy has been worked on by J. Costello [54].

P. Sladeczek et al studied photoionization experiments with an atomic of Tungsten in the region of the sub-levels $5p$ and $4f$ excitation in 1995 [55].

In 1999, G. O'Sullivan et al made a study on the super complex spectra and continuum emission spectra from rare - earth ions [56].

The absorption spectrum of vacuum-ultraviolet of the Rb^{2+} ion in a laser generated plasma was done by Neogi et al (2002) [57].

A Cummings, G O'Sullivan et al in 2004 studied one dimensional hydrodynamic model using Medusa code from laser produced Tin plasma [58].

In 2007, N. Shaikh et al studied nonlinear process fundamental, second and third harmonic generation of Nd:YAG laser to produced aluminum plasma [59].

P. Hough et al studied the ion and electron stagnation at the collision front between two laser produced plasmas in 2009 [60].

C. Suzuki et al made an interpretation of spectral emission of the tungsten ions in the 20 nm region from electromagnetic spectrum in 2011[61].

The studies of spectroscopic of the laser produced lead plasma generated by the wavelengths (1064 nm) and (532 nm) of a Q-switched pulsed Nd:YAG laser, the emission lines of neutral atoms and ions lead were shown predominantly lead lines observed were used to extract the excitation temperature using Boltzmann plots in 2011 [62].

In 2012, C. Pagano, Goncharov, and J. G. Lunney described the first results of an experiment to investigate the compression and focusing of a low temperature copper laser produced plasma using an electrostatic plasma lens [63].

M. Hanif et al made a study of characteristics of the titanium plasma produced by an intense laser beam (1064 nm) and second harmonics (532 nm) of a Q-switched Nd : YAG laser beam .They observed line profiles of neutral titanium can be used to extract the electron temperature by using the Boltzmann plot method in 2013 [64].

In 2014, H. Hegazy et al studied the the characteristics of the plasma generated by an intense laser beam on Zn targets in air at atmospheric pressure by using Nd-YAG pulsed laser using pulse duration being 6 ns, and laser energies of 350, 200, and 100 mJ [65].

The dynamics of the laser plasmas is characterized by time resolved and time integrated optical emission spectroscopy with (20, 10) ms time resolution using Nd:YAG laser by M. Favre1 and et al were be done in 2016 [66].

C. IORGA et al used high intensity laser beam to produce aluminum plasma by focusing a Nd-YAG laser ,the energy of the 50mJ,

15ns full width half maximum duration and wavelength is equal to 1064 nm in 2016 [67].

1.10 Aim of the work

The aim of this work is to study the emission spectra of the aluminum target in order to get the emission spectrum in the XUV region. Moreover, it aims also to study the hydrodynamic parameters of the plasma in order to find the optimum conditions for obtaining a new emission wavelength that can be used in lithography. Using Cowan and improved MEDUSA (med103) codes for those purposes.

Chapter Two

Theoretical Work

2.1 Introduction

The Lorentz force equation and the Maxwell equations of motion for charged particles can describe the plasma physics. These equations are difficult to solve for the realistic problems. Therefore, the plasma equations can be solved numerically by using plasma simulation codes.

Plasma simulation codes divided into two categories [46]:

- 1- Kinetic model which is following the plasma in phase space can be used for many plasma phenomena such as wave-particle interactions.
- 2- Fluid model used to find the integrated velocity to maintain only basic information about distribution functions, like temperature and fluid velocity.

The fluid model used for the most simulations of the complete experiments, such as laser produced plasmas. The kinetic simulation models can represent only one element of a complete system such as the absorption of laser irradiation in a laser-plasma experiment [8, 46].

2.2 Atomic structure theory

The atomic structure theory was written by Slater and Condon. The standard approach can use the variation principle to obtain the energies of the states within the atom by Hartree Fock approximation [68]. The Schrödinger equation is a fundamental equation of the quantum mechanics that explains the steady state of multi-electron system by:

$$H\psi = E_n \psi_n \quad (2.1)$$

where E_n is the energy of the system of level n .

ψ_n represents the total wave function that can describe the state of the system, and H is the Hamiltonian operator of the system which is depends on the properties of the system [69].

The atomic structure theory concerns with the solving of Schrodinger equation for an atomic system with electrons and nucleus and obtaining the eigenvalues (E_n) and eigenfunctions (ψ_n) of the system.

These eigenvalues and eigenfunctions can be used to calculate the values of energy levels and energy values of electronic transitions determined from spectroscopic measurements [70]. For atomic system with number of electrons, the non-relativistic Hamiltonian can be achieved which contains of the total kinetic energy of the number of electrons and the total potential energy according to their interaction with each other and with the nucleus.

The equation of the Hamiltonian is

$$H = \sum_{i=1}^N \left(-\frac{1}{2} \nabla_i^2 - \frac{ZZ}{r_i} \right) + \sum_{i>j} \frac{1}{r_{ij}} \quad (2.2)$$

where ZZ represents the nuclear charge, r_i is the distance of the i th electron from the nucleus, and r_{ij} is the distance between the i th and the j th electron.

The solutions of the Schrödinger equation are possible only dealing with one electron system (for H-like atoms). For two-electron system, the Schrödinger equation depends of the inter-electronic distance r_{ij} . This distance prevents the Shrodinger equation from being amenable to the separation of the variables [71].

2.3 Single configuration Hartree-Fock approximation

The method for obtaining approximate total wave functions of many electrons is called Hartree-Fock method.

For hydrogen-like atom of the one-electron, the Hamiltonian in equation (2.1) consists of one term from the 1st summation of equation (2.2). When the Schrödinger equation and the Hamiltonian are expressed by the spherical polar coordinates r , θ , and ϕ , the equation can be solved by the method of the separation of variables [72].

2.4 Calculation of Atomic Structure

The Hartree-Fock and the conventional Hartree are approaches to the atomic bound state problems involving many electrons which have been developed in the past years.

The self-consistent field is the appropriate method for solving the particle problems physically with details numerical computations [73].

2.4.1 Configuration Interaction Hartree-Fock

The method of the configuration interaction of the extending Hartree-Fock approximation is not preferred to do with the interaction of electrons and it prefer to do with the configuration mixing [74].

The Cowan code uses numerical approach to calculate the radial wave functions by assuming an initial approximation to the radial wave function [41].

The single-configuration of the atomic radial wave functions can be taken initially to describe the Slater-type orbitals and also can be describe by self-consistency. One of these options in cowan code is the ability to include only one continuum wavefunction electronic configuration [75].

2.4.2 Multiconfiguration Hartree-Fock

In this (MCHF) method, the wavefunction can be found as an eigenvector of the energy matrix. The basis wavefunction set is fixed as Hartree-Fock wavefunctions at the configuration interaction method. Moreover, if the multi-configuration Hartree-Fock method, the electron orbital functions must be optimized at any time after the mixing coefficients (describing the eigenvector). The energy matrix can be calculated and diagonalised. The multi-configuration Hartree-Fock calculation method can be done just for one specific eigenvector [76, 77].

2.5 The Cowan Code

The Cowan code is a numerical computer code to calculate atomic structure. FORTRAN code can be comprised by the Robert D. Cowan in 1968 [40]. In 1961, this code was originally written, and developed over a long period by Robert D. Cowan and co-workers since 1964.

Hartree-Fock equations employ several approximations such as Hartree-Fock with exchange in different methods for self-interaction and method to approximate the remainder of the Hartree-Fock exchange term [78].

2.5.1 The Cowan code Structure

The cowan code consists of the following sub-codes [40, 41, 79, 80];

- 1- RCN can calculate only one-electron radial wavefunction which is bound or free for any number of electron configurations, and this code uses the Hartree-Fock method.

-
-
- 2- RCN2 is using the output wavefunctions from RCN for calculating the configuration-interaction between each pair of the interacting.
 - 3- RCG uses energy matrices for possible value of the total angular momentum (J), diagonalises of each matrix to give energy levels (eigenvalues) and multi-configuration, intermediate coupling (eigenvectors).
 - 4- RCE this code can be used to very various radial energy parameters F^k , G^k , E_{av} , ζ and R^k , when the higher accuracy results to make a least square fit of experimental energy ststes. The resulting least-square fit parameters using to repeat the RCG calculation with energy levels and wavefunctions.

2.5.2 Cowan input files

There are two input files for the cowan code [40], [41]:

- 1- Input filename includes a multiline configuration file as it is shown in Fig.(2.1)
- 2- Input filename.in2 is a single line which consists of also a single line (as shown in Fig.(2.2)).

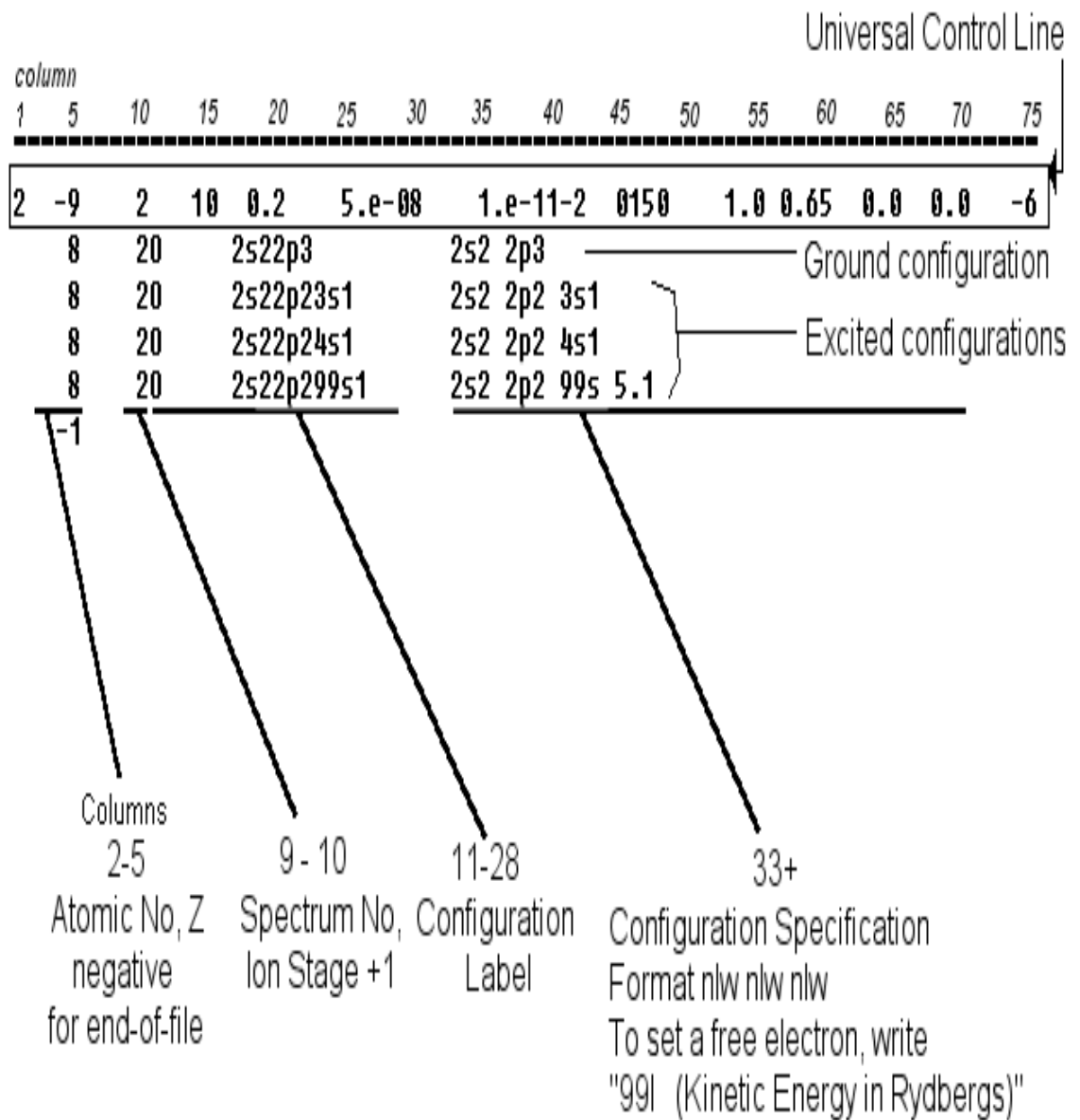


Fig.(2.1) A multiline input file [80]

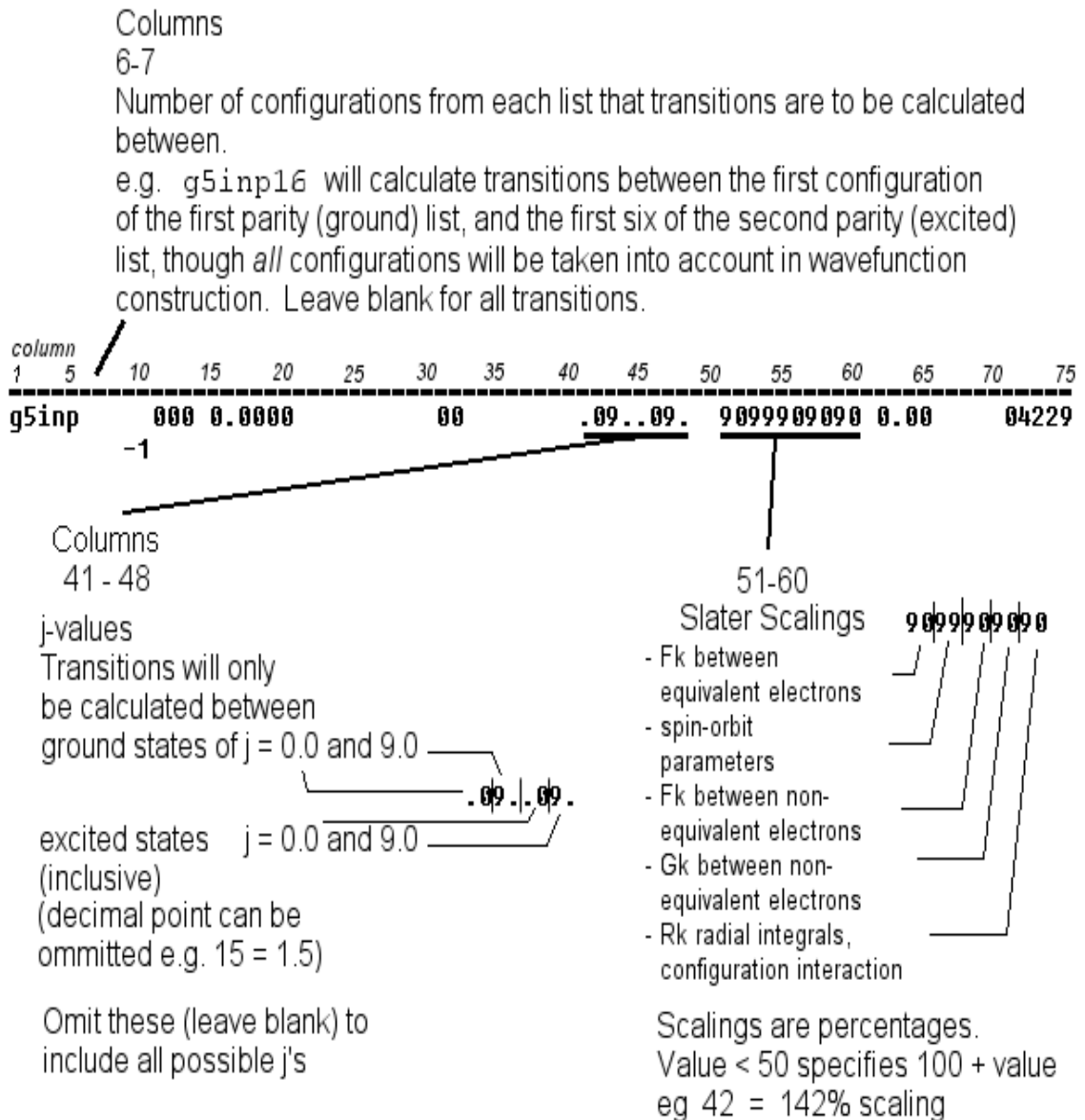


Fig. (2.2) Standard input file [80]

2.6 The Medusa Code

Medusa code can calculate the 1-dimensional thermodynamic and hydrodynamic behavior of the plasma which is irradiated by high intensity laser beam. In 1974, this code was created by J. P. Christiansen and *et al.* in UK [43].

Medusa code can describe the plasma by many variables. These variables are ion temperature (T_i), electron temperature (T_e), density (ρ), and velocity (v), which are functions of the time (t) and space [43].

2.6.1 The physical model

The plasma is assuming to be consisting of charged-neutral mixture for electrons and various species of the ions, atoms, and molecules.

The chemical composition can be described by a set of the fractions f_k [81,82].

$$n_k = f_k n_i \quad (2.3)$$

The number density of the ion of species k , where

$$\sum_k f_k = 1 \quad (2.4)$$

The charge numbers and average mass can be given by these formula:

$$Z = \sum_k f_k Z_k \quad (2.5)$$

$$M = \sum_k f_k M_k \quad (2.6)$$

where M_k is the mass density and Z_k is the charge number. The ion and electron densities are given by:

$$n_e = Z n_i \quad (\text{m}^{-3}) \quad (2.7)$$

the physical density is

$$\rho = n_i M m_H = \frac{M}{V} \quad (\text{kg} / \text{m}^{-3}) \quad (2.8)$$

where m_H represents the proton mass, V is the volume and M is the total mass.

The energy equation is

$$C_v \frac{dT}{dt} + B_T \frac{d\rho}{dt} + p \frac{dV}{dt} = S \quad (\text{W/kg}) \quad (2.9)$$

Where C_v is the specific heat, S represents the energy rate per unit mass

$$C_v = \left(\frac{\partial U}{\partial T} \right)_\rho \quad (2.10)$$

$$B_T = \left(\frac{\partial U}{\partial \rho} \right)_T \quad (2.11)$$

The thermal conduction term is given by [83]

$$H = \frac{1}{\rho} \nabla \cdot \underline{k} \nabla T \quad (2.12)$$

where \underline{k} is the thermal conductivity.

The absorption occurs via inverse bremsstrahlung when the densities are below critical density. The absorption coefficient of this given by:

$$\alpha_c = 13.51 \lambda^{-2} \beta^2 (1 - \beta)^{1/2} T_e^{-3/2} \times (5.05 + \log \lambda T_e) Z^2 \quad (2.13)$$

Where $\beta = \frac{\rho}{\rho_c} < 1$ and λ is the laser wavelength.

2.6.2 Medusa output

The output files of the medusa code contains of many files as shown in Fig. (2.3). these output files are [83]:

- 1- Output1: this file gives the cell edge, cell number, velocity, electron density, pressure, mass density, ion temperature, electron temperature, and average charge state.
- 2- Output2: which gives the average ionization and occupation numbers $\{P_n\}$ for K to P shell (from $n = 1$ to $n = 6$).
- 3- Output3: gives the total time of the all-time steps.
- 4- Output4: gives information about ion distribution.

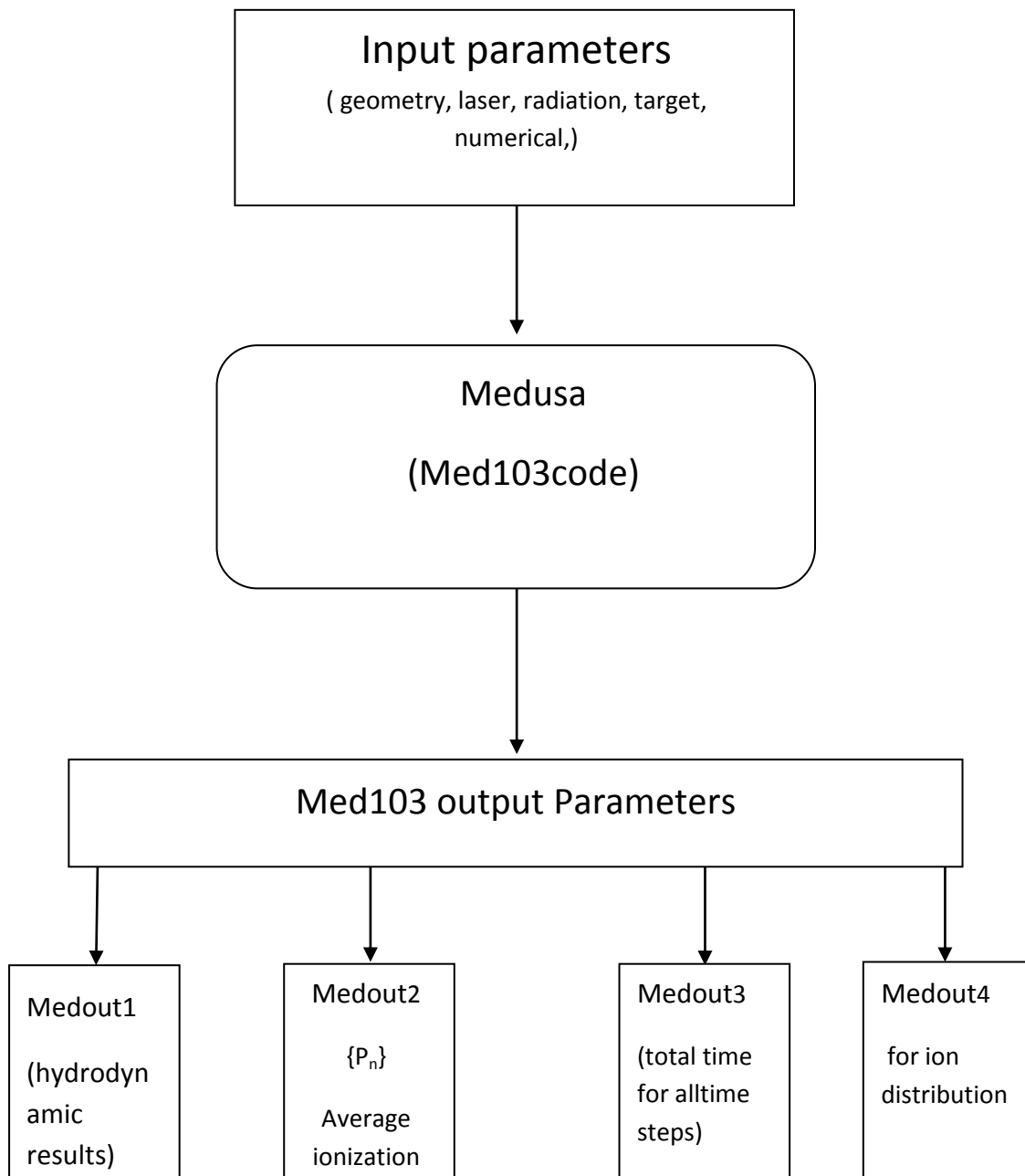


Fig. (2.3) Schematic diagram of the Medusa code [83].

Chapter Three

Results and Discussion

3.1 Introduction

This chapter explains the results of laser plasma interaction mechanisms for aluminum target in different conditions which can be classified into two parts:

- 1- Atomic structure properties of Al using Cowan code to get the emission spectra for different transitions of the Aluminum.
- 2- Spatial and temporal hydrodynamic properties of the plasma using the Medusa (med103 code).

3.2 Atomic Structure Results

Emission from Al Target

Figure (3.1) represents the emission spectrum for Al II (Mg like) ion. The first ionization stage (Al II) ion computed by using Cowan code. There was one emission range lying in 95.00 nm. The results and discussion was in the nanometer scale as it is nowadays the standard for wavelength. The maximum oscillator strength in this range was 0.058 at $\lambda = 95.00$ nm. The emission oscillator strengths of the second ionization stage (Al III) were represented in Fig.(3.2). The AL III (Na like) ion was emitting a spectrum with oscillator strength of 0.135 at $\lambda = 16.05$ nm.

Figure (3.3) represents the wide range of the emission spectrum for Al IV (Ne like) ion. The strongest transition was at $\lambda = 127.50$ nm with oscillator strength of 4.25, and the minimum emission spectrum with small oscillator strength was 0.10 at $\lambda = 140.20$ nm. This result shows the emission spectrum range can cover a wide range which means that the decrease of the ionization number leads to increase the emission spectrum wavelength, according to coulomb forces.

The emission wavelength spectrum decreases as the number of electrons releases from the Aluminum atom increases. The Al V (F like) emission spectrum as shown in Fig.(3.4) where the maximum emission spectrum was at $\lambda = 10$ nm with strongest oscillator strength (1.82) . The emission spectrum for the fifth ionization stage of Al VI (O like) can be shown in Fig.(3.5). The highest oscillator strength was 3.25 at $\lambda = 107.50$ nm.

The emission wavelength covered a wide range from different transitions. The minimum emission spectrum was at $\lambda = 200$ nm with oscillator strength of 0.05.

Figure (3.6) describes the emission spectra for Al VI (N like) ion with a maximum emission wavelength of 115.50 nm and with oscillator strength of 2.18. The minimum wavelength was 185.85 nm with oscillator strength of 0.05. In this form, there were thousands of lines in a very narrow region like oscillator strength of 1.85 with wavelength of 117.85 nm. Moreover, the emission spectrum at $\lambda = 112.25$ nm was with oscillator strength of 1.20, and the emission spectrum with oscillator strength of 0.45 was at $\lambda = 140.00$ nm.

Figure (3.7) shows the Al VIII (C like) ion oscillator strength behavior with a maximum emission spectrum at $\lambda = 127.50$ nm and with oscillator strength of 1.25.

In this form, there were many lines from emission spectrum transitions like both the oscillator strength of 0.88 with wavelength 132.25 nm, at $\lambda = 153.50$ nm and with oscillator strength 0.58, and oscillator strength of 0.15 at $\lambda = 182.00$ nm.

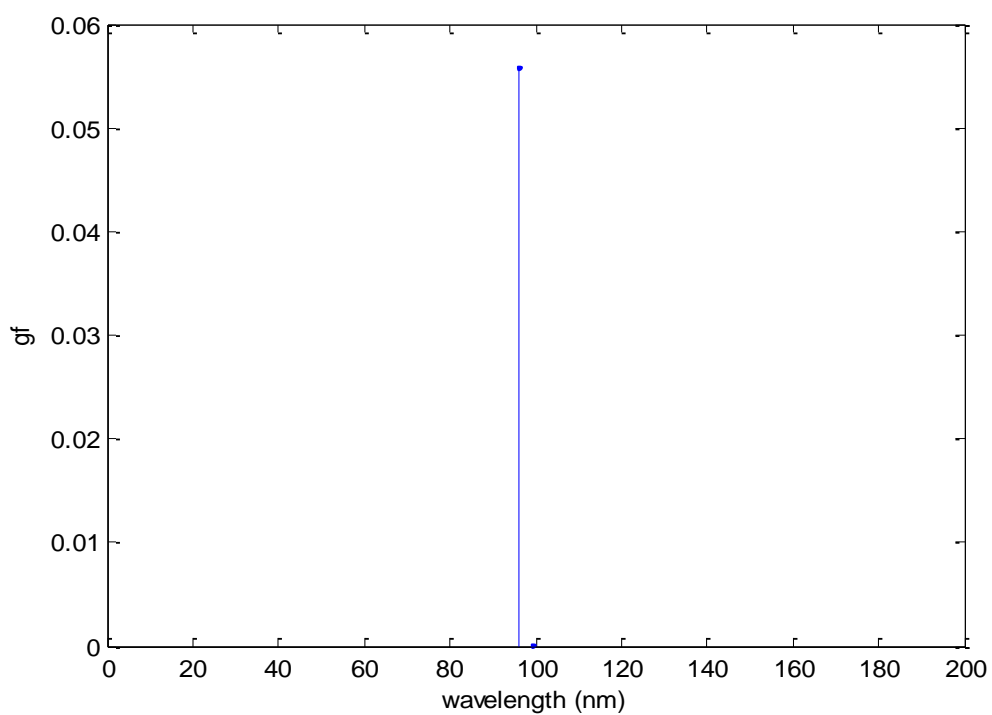


Fig.(3.1)Emission spectrum of the first ionization of(AlII).

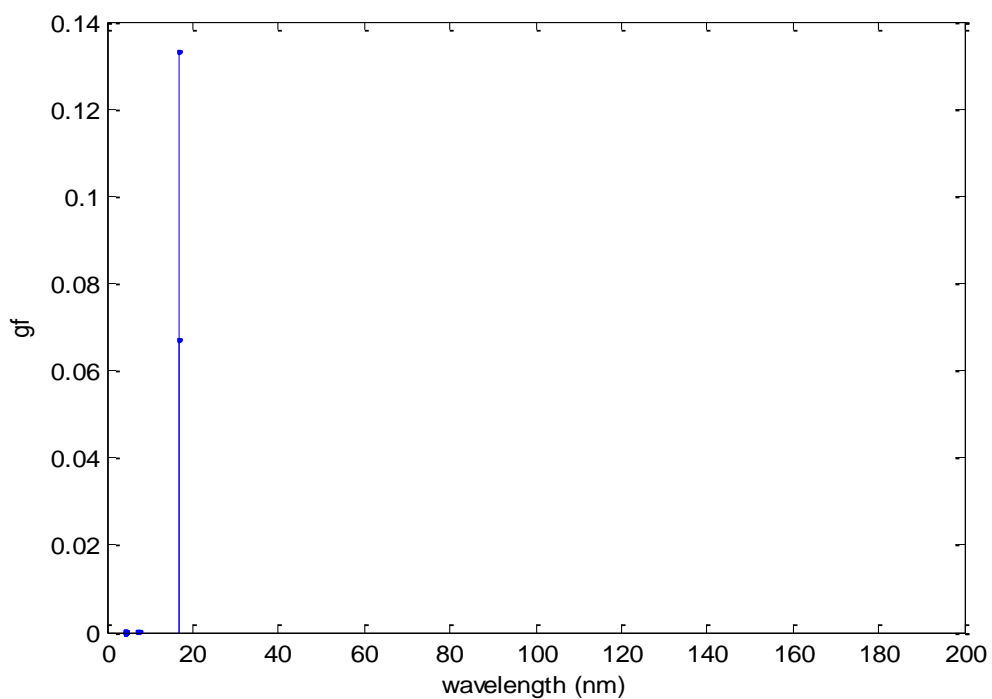


Fig.(3.2)Emission spectrum of the second ionization of(AlIII).

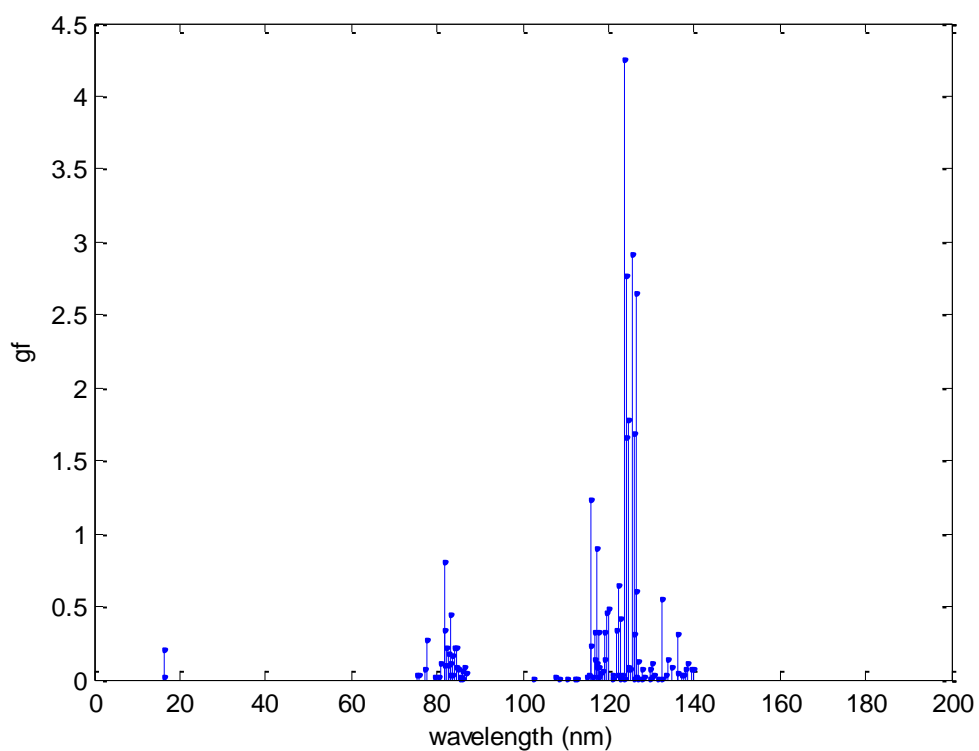


Fig.(3.3)Emission spectrum of the third ionization of (AlIV).

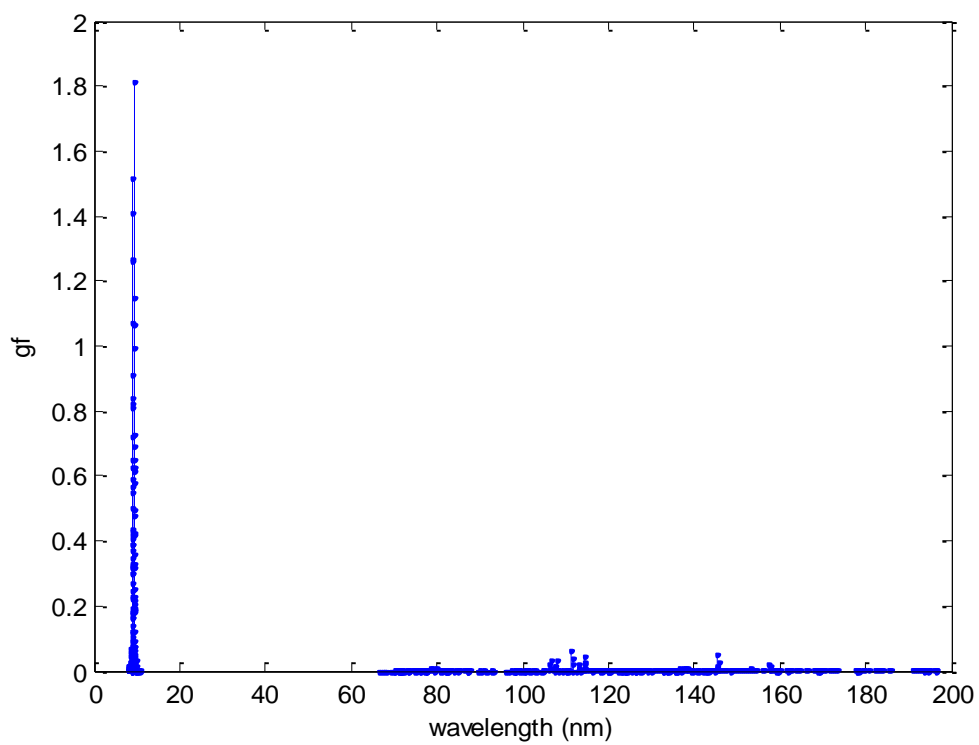


Fig.(3.4)Emission spectrum of the fourth ionization of (AlIV).

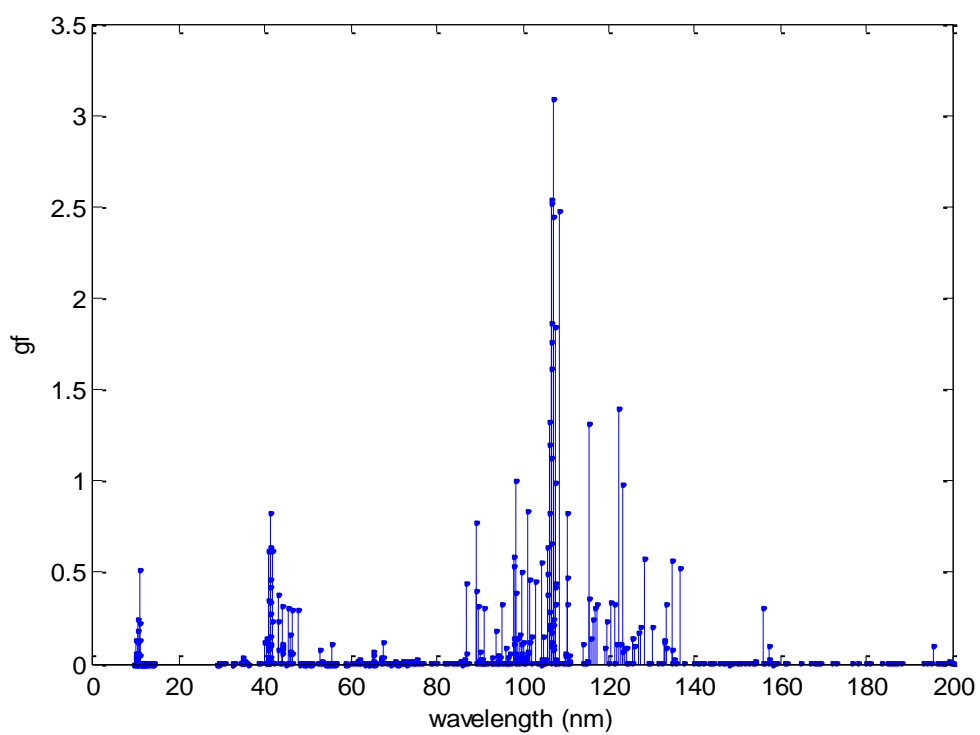


Fig.(3.5)Emission spectrum of the fifth ionization of (AlVI).

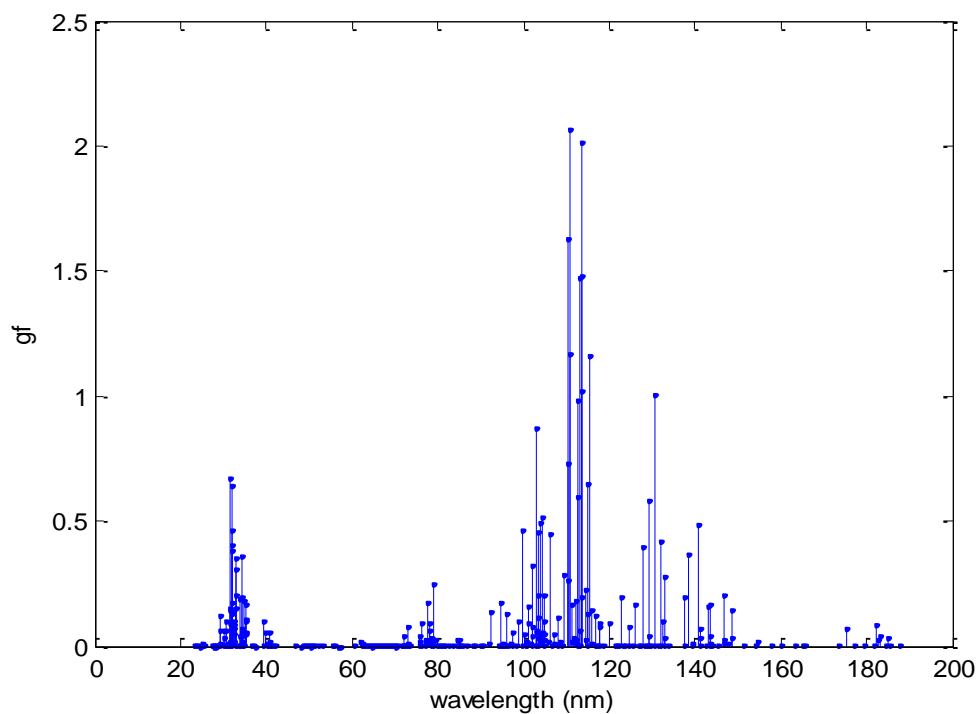


Fig.(3.6)Emission spectrum of the sixth ionization of (AlVII).

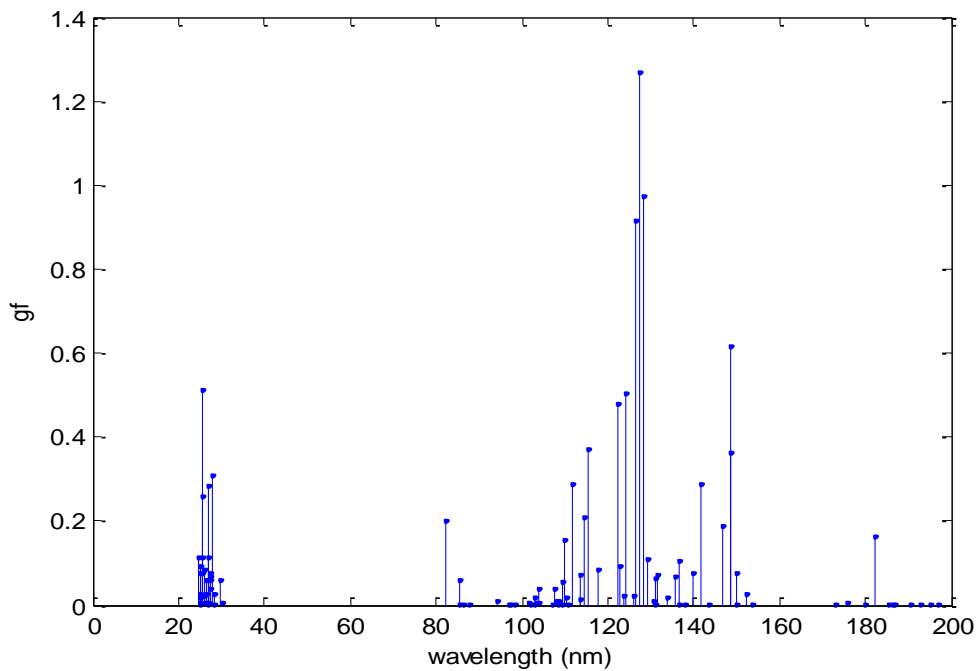


Fig.(3.7)Emission spectrum of the seventh ionization of (AlVIII).

Figure (3.8) describes the emission spectra for Al IX (Be like) ion at a maximum emission wavelength of 320 nm and with oscillator strength of 3.18. In the extreme ultraviolet region the maximum wavelength was 125.85 nm and with oscillator strength of 2.20.

The Al X (B like) ion gave a maximum oscillator strength of 0.85 at $\lambda = 1720.25$ nm (Fig. 3.9).The minimum emission wavelength was at $\lambda = 2000.30$ nm and with oscillator strength of 0.03. In this form, there was another emission spectrum line near the strongest transition which had a wavelength about 1450.00 nm and with oscillator strength of 0.83. The maximum oscillator strength in the extreme ultraviolet radiation was 0.49 at $\lambda = 198$ nm.

The emission spectrum for the tenth ionization stage of Al XI (Li like) can be shown in Fig.(3.10). The highest oscillator strength was 3.7 at $\lambda = 112$ nm.

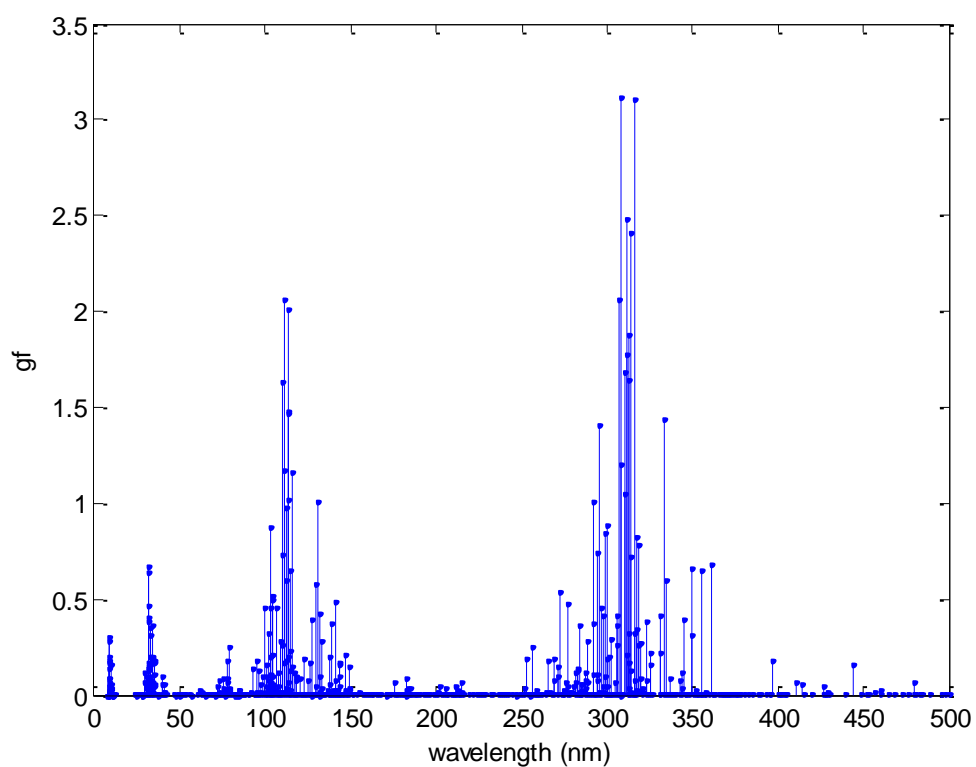


Fig.(3.8)Emission spectrum of the eighth ionization of (AlIX).

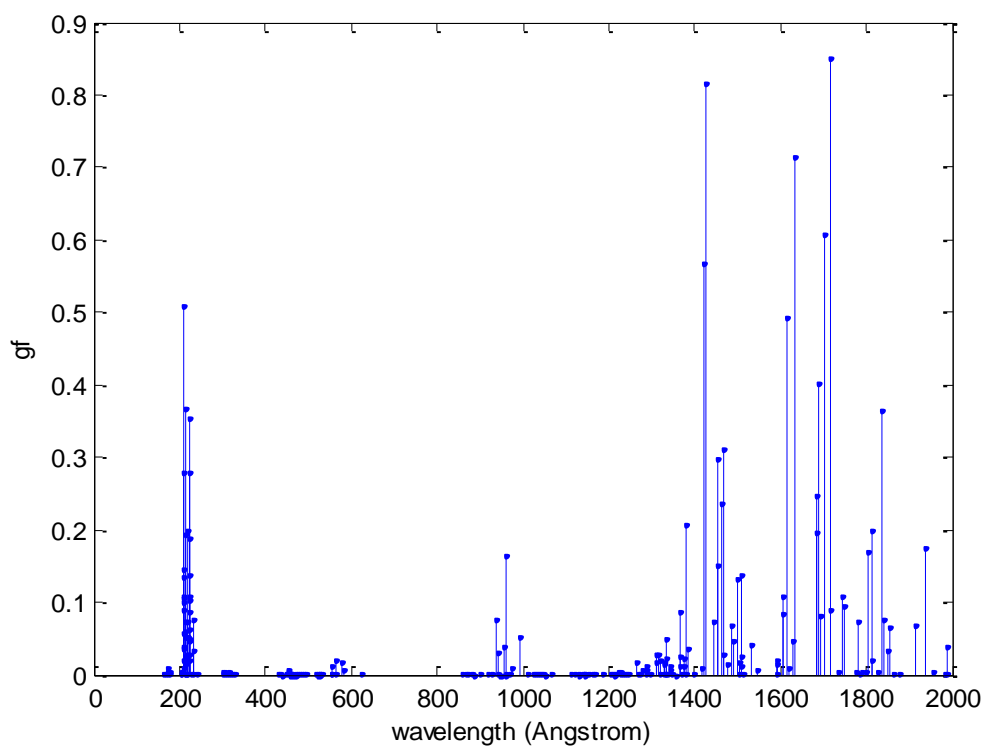


Fig.(3.9)Emission spectrum of the ninth ionization of (AlIX).

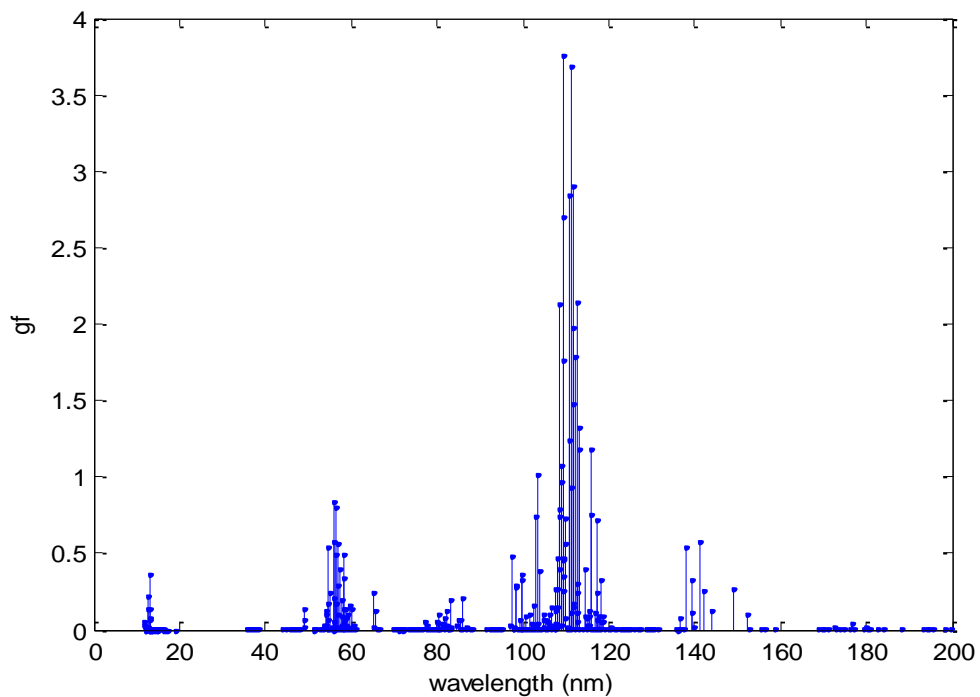


Fig.(3.10)Emission spectrum of the tenth ionization of (AlXI).

The emission spectrum of the eleventh ionization of the Aluminum target Al XII (He like) can be shown in Fig.(3.11). The strongest oscillator strength was 5.9 at $\lambda = 1010$ angstrom. The minimum emission spectrum wavelength was at $\lambda = 4500$ angstrom with an oscillator strength of 0.5. There were many lines emission spectrum between maximum and minimum emission spectrum like the line with oscillator strength of 0.98 at $\lambda = 1520$ angstrom.

The Al XIII (H like) ion gave a maximum oscillator strength of 5.40 at $\lambda = 1090.25$ angstrom (Fig. 3.12). In the range of the extreme ultraviolet radiation the minimum emission wavelength was at $\lambda = 1085$ angstrom and with oscillator strength of 1.2.

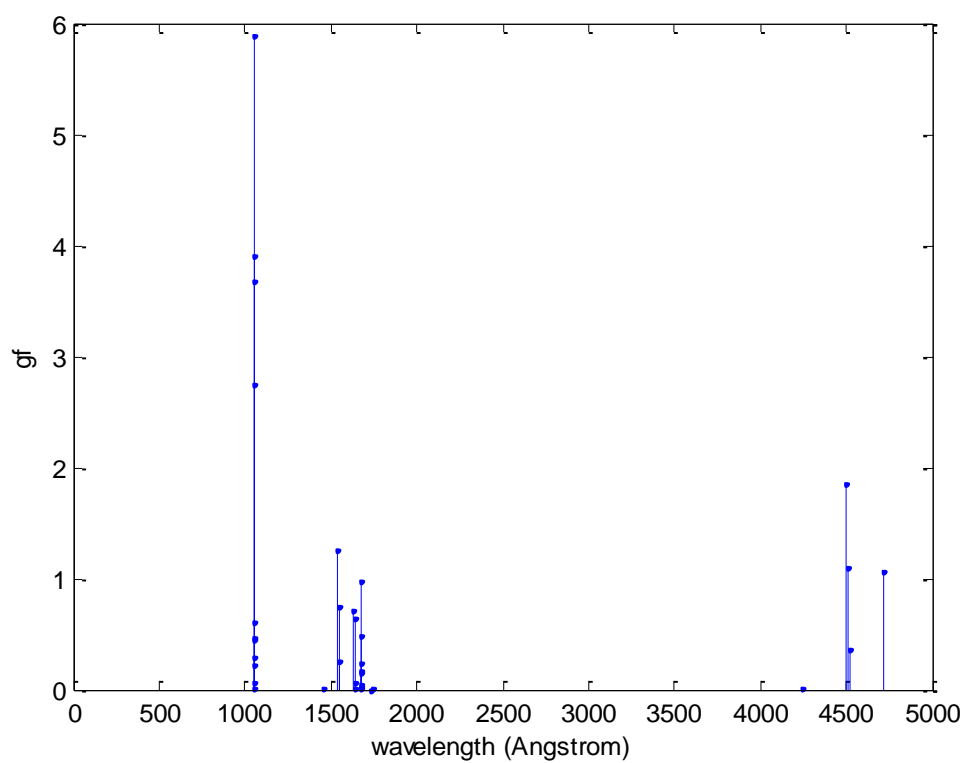


Fig.(3.11)Emission spectrum of the eleventh ionization of (AlXII).

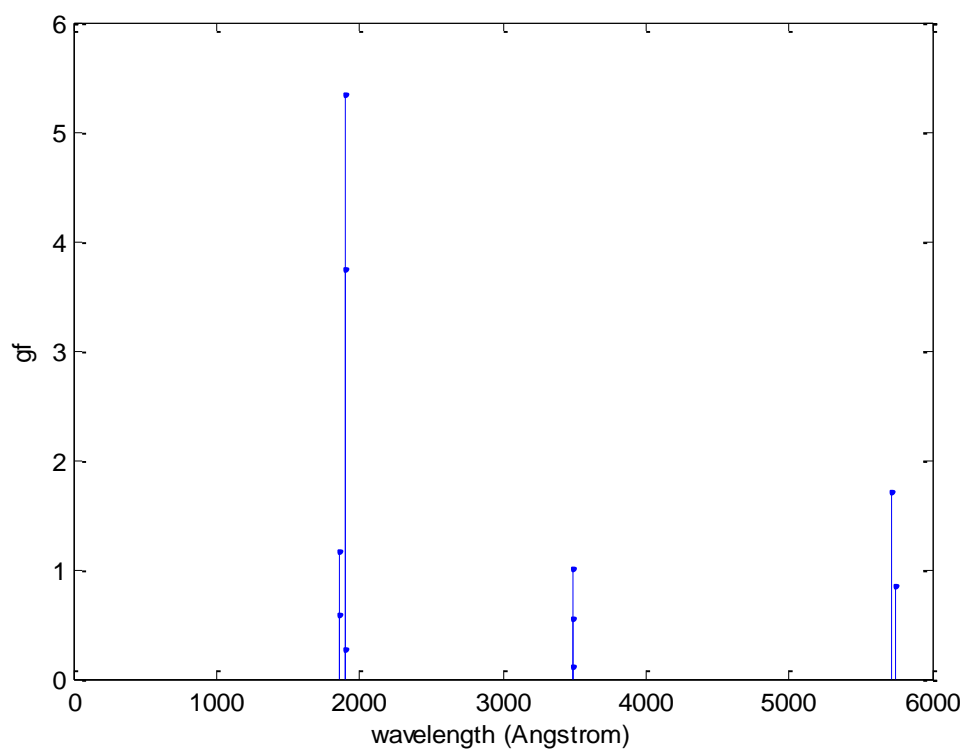


Fig.(3.12)Emission spectrum of the twelfth ionization of (AlXIII).

3.3 MEDUSA(Med103)Code Results

In this section, MEDUSA (med103) code calculated the plasma hydrodynamics properties, such as the velocity, mass density, pressure, electron temperature, electron density, and the average ionization. The planar shape of solid target was tested, namely, Al (Z=13).

In this work, a high power density of laser beam at $\lambda = 1064$ nm with two pulse widths of 10 ns and 10 ps were utilized. For nanosecond pulse width, two different laser power densities were used. These power densities were 10^{11} , and 10^{12} W/cm². For picosecond pulse width, there were three values of laser power densities have been used. These power densities were (10^{11} , 10^{12} and 10^{13} W/cm²). Gaussian pulse shape was employed in all laser types.

Medusa was developed to study the plasma parameters. The Aluminum planar shape target was proposed and an Nd: YAG laser beam with power densities 10^{11} , 10^{12} , and 10^{13} W/cm² were used.

3.3.1 Spatial and temporal electron density variation

Figure (3.13) and Fig.(3.14) describe the behavior of electron density as a function of space and time when the laser power density is 10^{11} W/cm² and with pulse width of 10 ns. The plasma expanded rapidly by an intense laser beam, Thermal energy converts into kinetic energy and the density and temperature decrease which agree with references [84, 85].

The density of the plasma begins from far the critical density (10^{23}cm^{-3}) then a strong drop happens to the electron density.

When the laser power density increased to 10^{12}W/cm^2 as shown in Fig.(3.15), the electron density began from far critical density of the plasma and strongly dropped to higher than the value of 10^{21}cm^{-3} at $85\ \mu\text{m}$. The electron density with the temporal variation of the plasma (Fig. 3.16) shows that the maximum electron density was 10^{23}cm^{-3} at the beginning and decreased rapidly with the time. The decreasing in temporal electron density of the plasma was relatively linear until 10 ns. The effect of the 10 ps laser on the electron density profile (Fig.3.17) was at 10^{11}W/cm^2 laser power density. The electron density began from higher than 10^{23}cm^{-3} and dropped to less than 10^{22}cm^{-3} . Figure (3.18) describes the electron density began from far 10^{23}cm^{-3} and decreased to 10^{20}cm^{-3} at 10 ns. The obtained electron density from the 10 nanosecond laser pulse width was greater than that from the 10 picosecond laser pulse width.

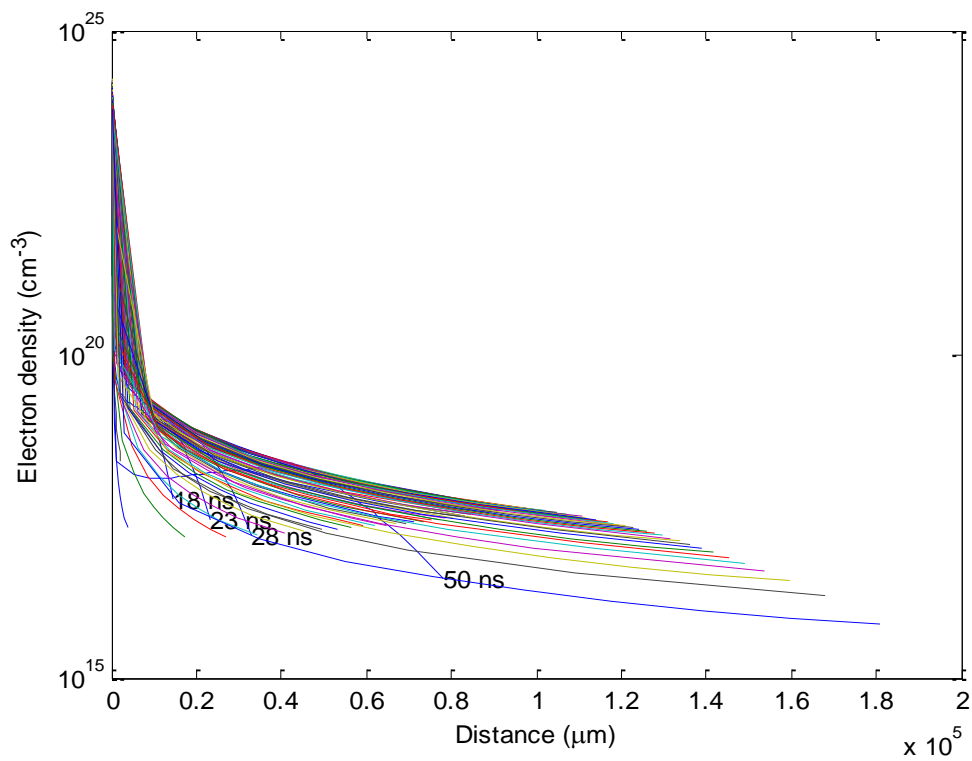


Fig.(3.13) Spatial variation of electron density at intensity 10^{11} W/cm² with pulse width 10 ns.

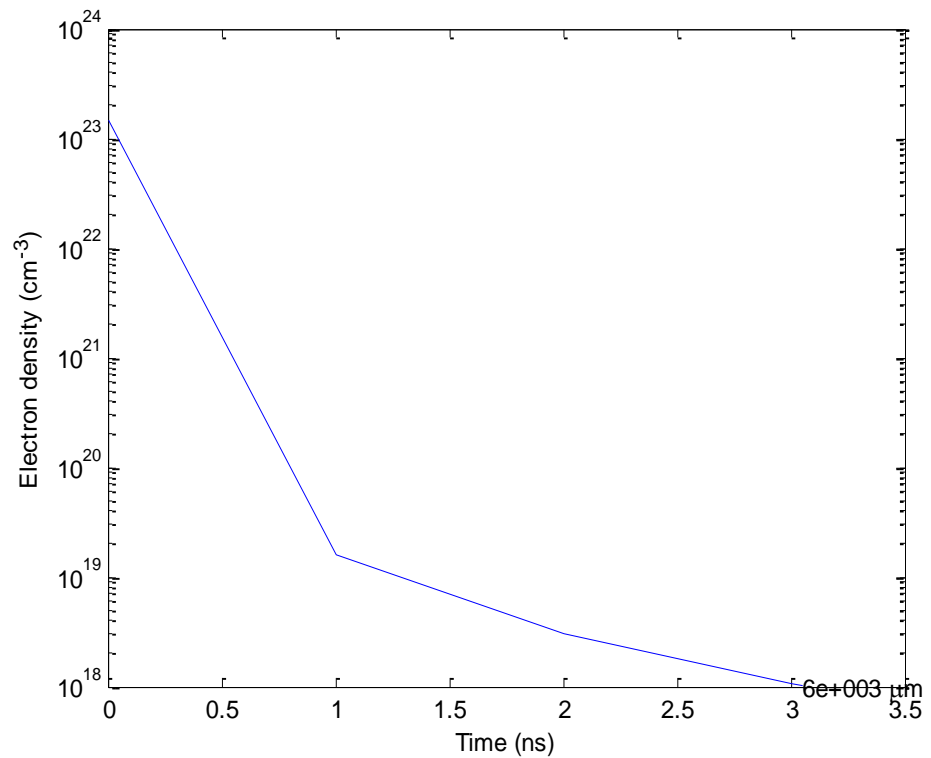


Fig.(3.14) Temporal variation of electron density at intensity 10^{11} W/cm² with pulse width 10 ns.

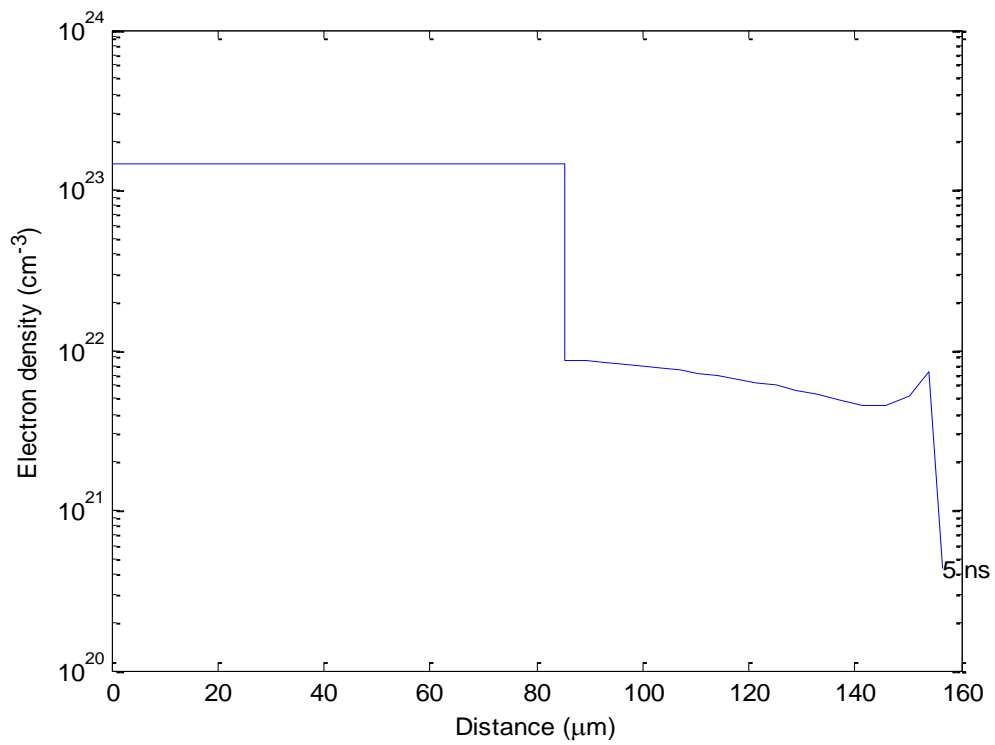


Fig.(3.15) Spatial variation of electron density at intensity 10^{12} W/cm² with pulse width 10 ns.

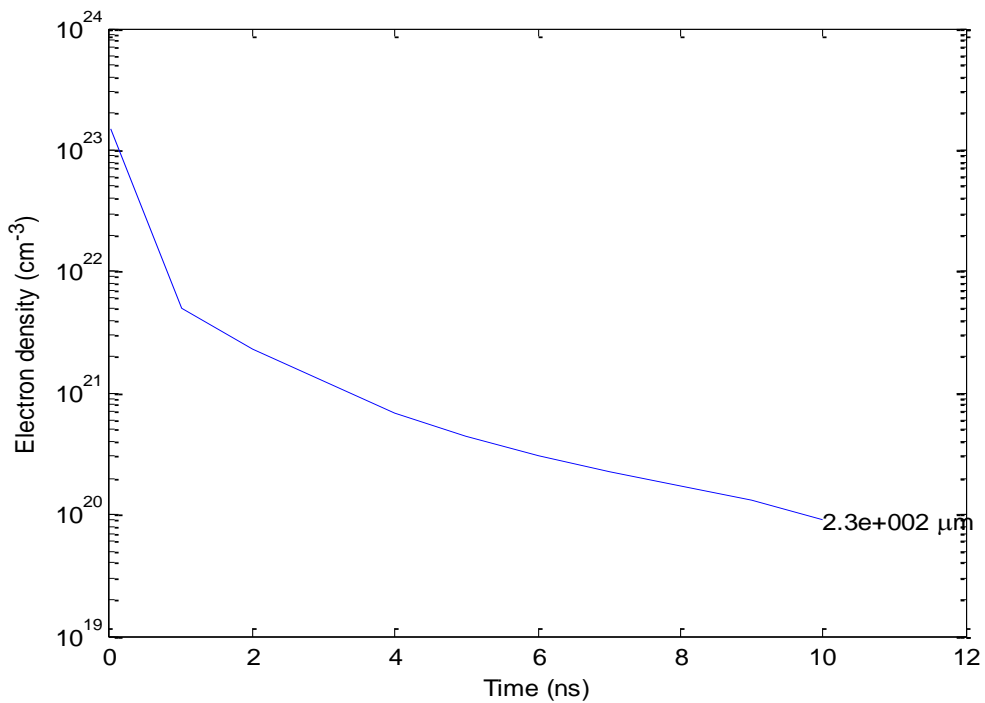


Fig.(3.16) Temporal variation of electron density at intensity 10^{12} W/cm² with pulse width 10 ns.

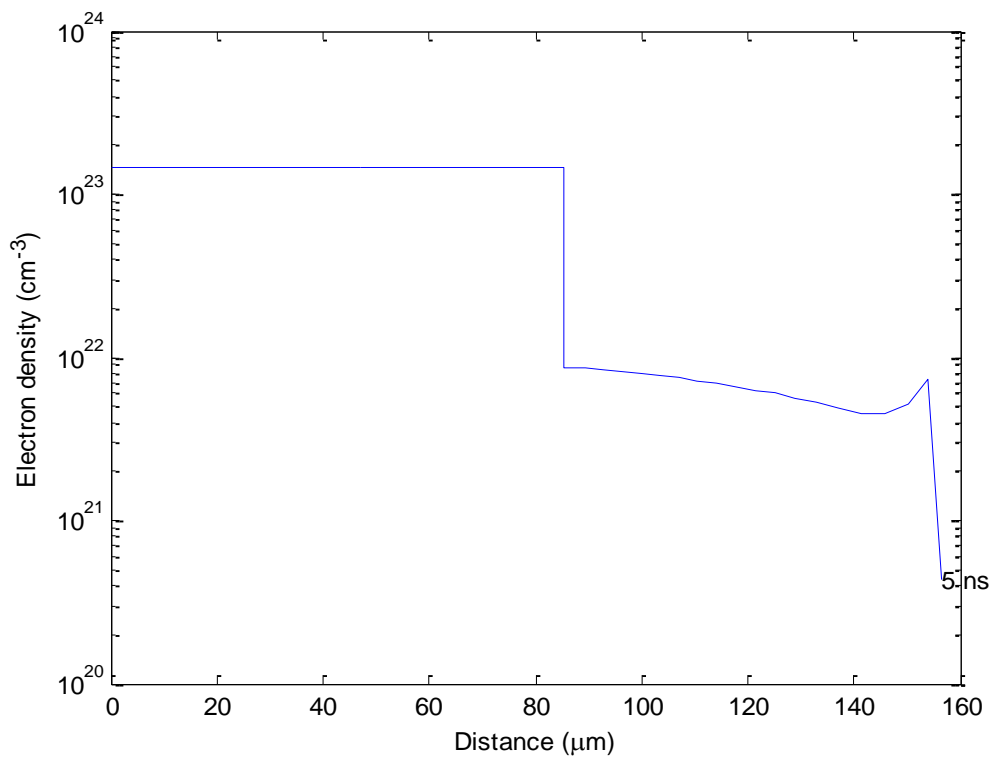


Fig.(3.17) Spatial variation of electron density at intensity 10^{11} W/cm² with pulse width 10 ps.

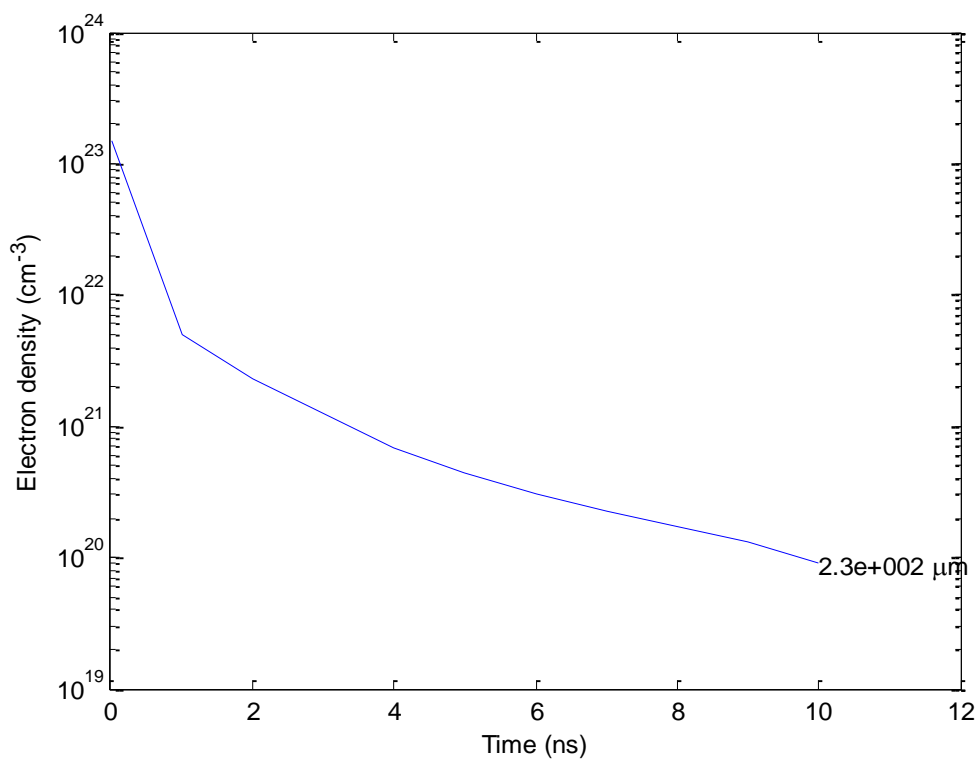


Fig.(3.18) Temporal variation of electron density at intensity 10^{11} W/cm² with pulse width 10 ps.

When the laser power density increased to 10^{12} W/cm² as it is shown in Fig.(3.19) and Fig.(3.20), the maximum electron density was higher than 10^{23} cm⁻³ at 98 μ m and then decreased gradually to reach 10^{19} cm⁻³. Figure (3.20) describes the relationship between the electron density and the time. The electron density began from far critical density 10^{23} cm⁻³ and then decreased to greater than 10^{18} cm⁻³ at 10 ns.

Figure (3.21) and Fig.(3.22) can explain the relationships between the electron density with space and time. It has been noticed that the results of both the laser power density at 10^{13} W/cm² and 10^{12} W/cm² were the same .

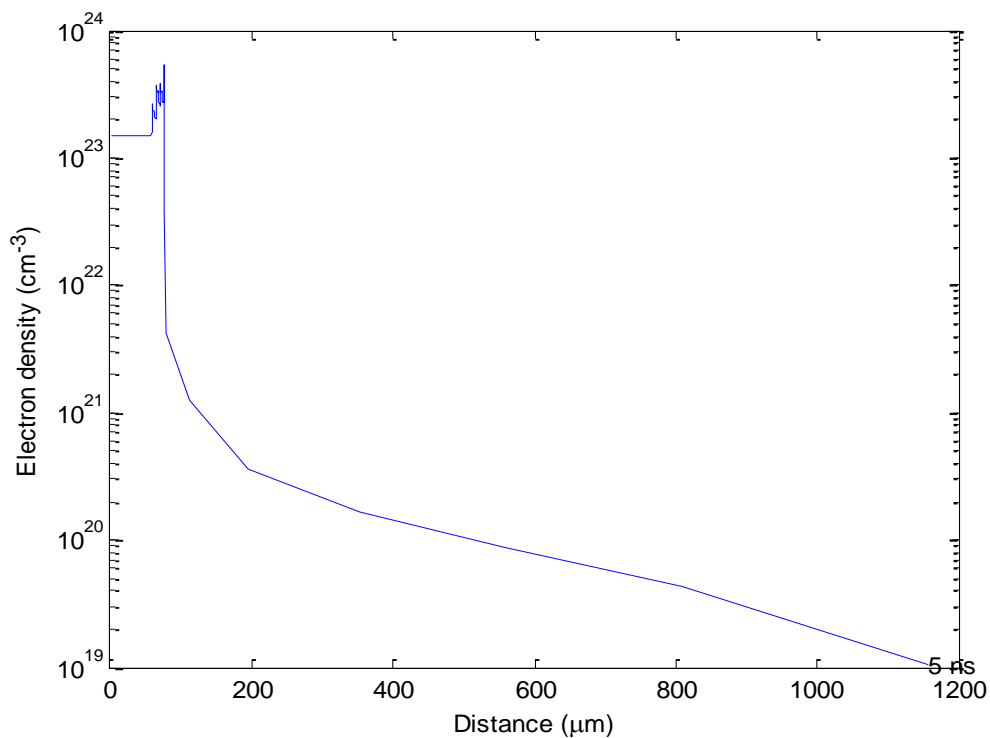


Fig.(3.19)Spatial variation of electron density at intensity 10^{12} W/cm² with pulse width 10 ps.

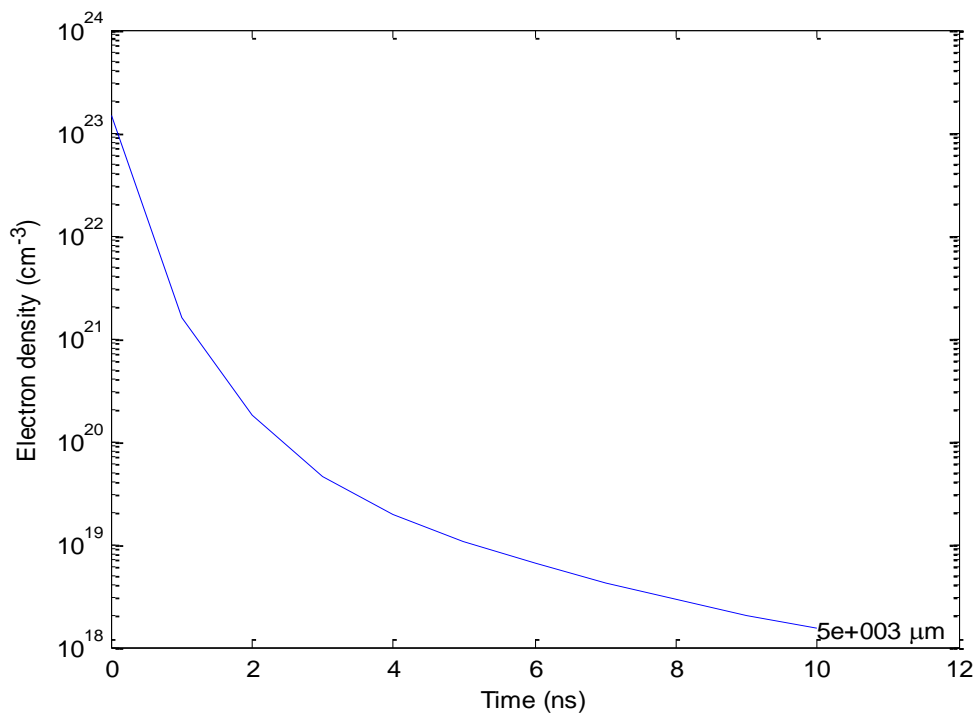


Fig.(3.20) Temporal variation of electron density at intensity 10^{12} W/cm² with pulse width 10 ps.

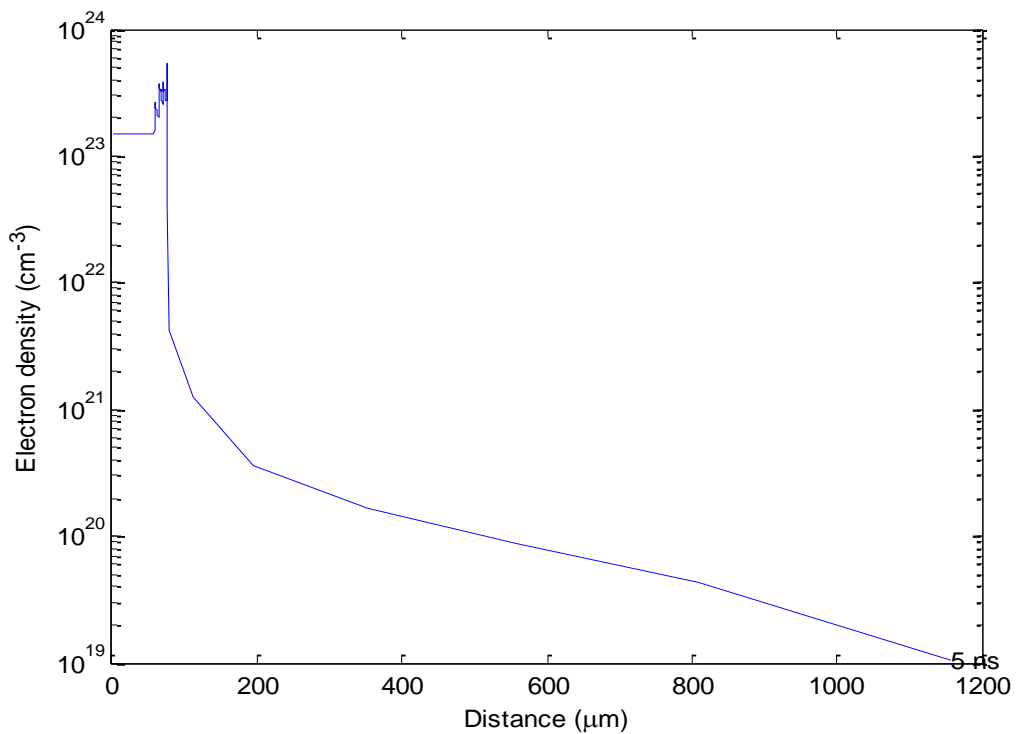


Fig.(3.21) Spatial variation of electron density at intensity 10^{13} W/cm² with pulse width 10 ps.

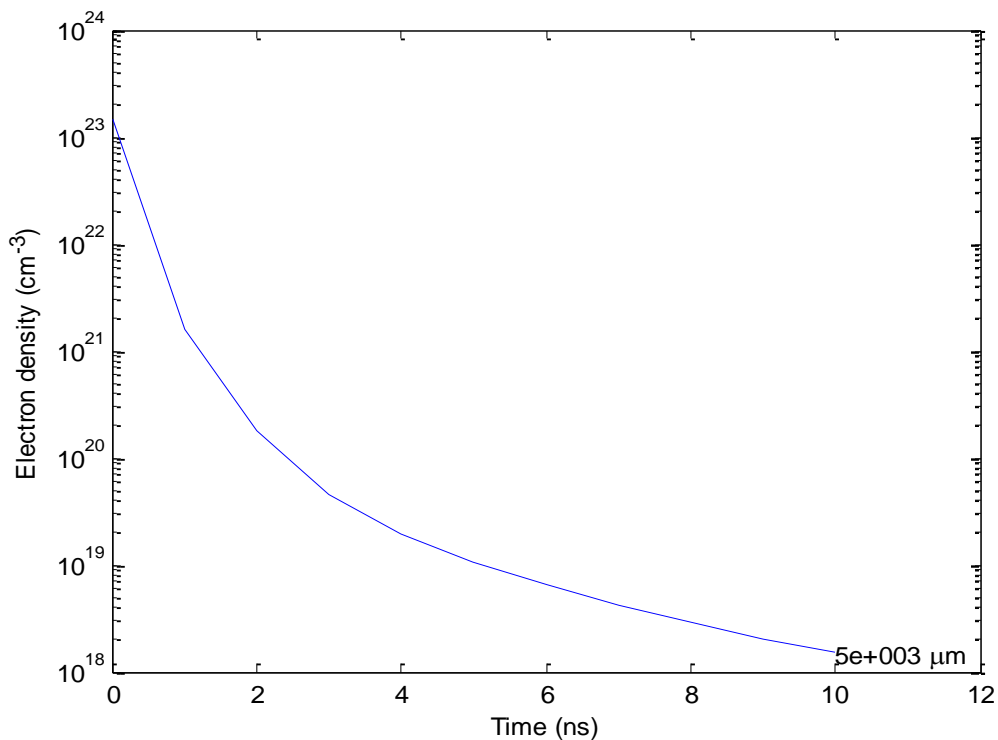


Fig.(3.22) Spatial and temporal variation of electron density at intensity 10^{13} W/cm² with pulse width 10 ps.

3.3.2 Spatial and temporal velocity variation

Figure (3.23) represents the spatial velocity variation of the plasma expansion when the laser power density was 10^{11} W/cm² with pulse width of 10 ns. The plasma velocity began from zero and increased to reach about 0.9×10^8 cm/sec after about 120 μ m distance, and it increased to reach value of 2.45×10^8 cm/sec with about 3100 μ m distance.

The temporal variation of the plasma expansion velocity when the laser power density of 10^{11} W/cm² and pulse width of 10 ns can be shown in Fig.(3.24). The velocity of the plasma began from zero and increased to reach about 1.4×10^6 cm/sec after 1 ns and decreased to 1.2×10^6 cm/sec after 4ns, then increased the plasma reaching to reach the value 4.45×10^6 cm/sec after 9.5 ns.

After increasing the power density to 10^{12} W/cm² (Fig3.25), the spatial velocity variation will stay at zero until reaching ~ 85 μm and then increased to reach the value 14×10^5 cm/sec at ~ 150 μm and decreased to the value 12×10^5 cm/sec at about 158 μm .

Figure (3.26) represents the temporal variation of the plasma expansion velocity. The velocity begins from zero and increases to reach about 1.35×10^6 cm/sec at 1 ns, then decreases to reach about 1.2×10^6 cm/sec after 7 ns, and increases after 8 ns reaching to 2.3×10^6 cm/sec.

The spatial variation of the plasma expansion velocity was shown in Fig.(3.27). When the laser power density is 10^{11} W/cm² and pulse width is 10 ps, the spatial velocity variation will stay at zero until about 85 μm and then increases to reach 14×10^5 cm/sec at about 150 μm and decreases to the 12×10^5 cm/sec at about 158 μm .

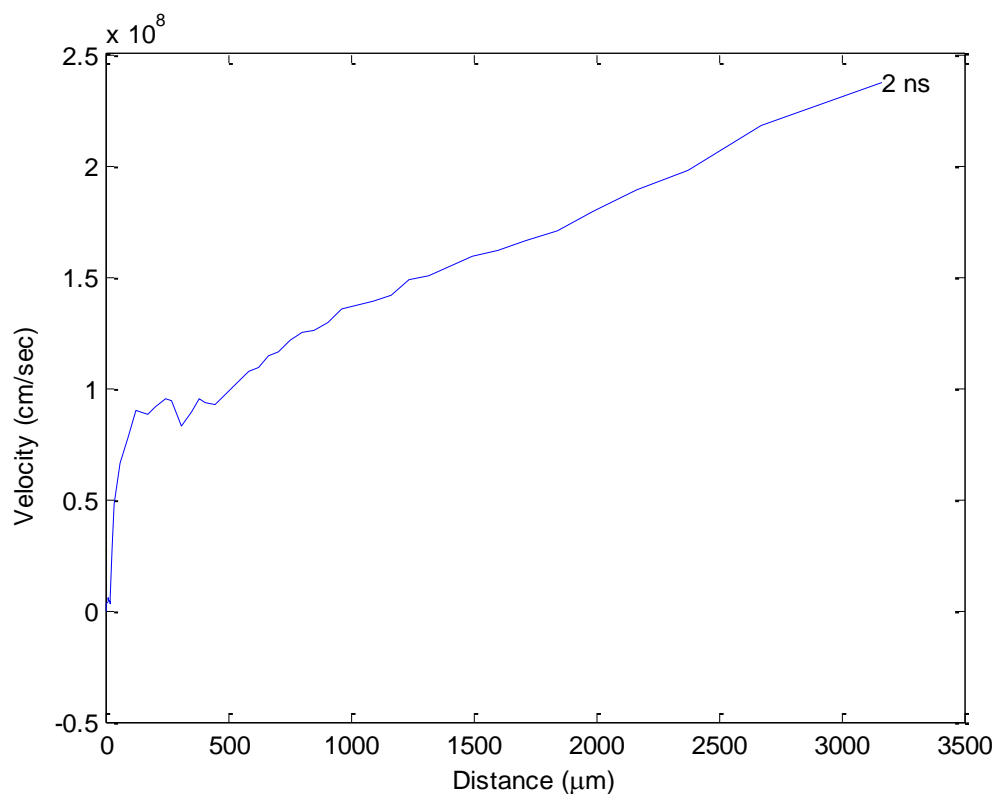


Fig.(3.23) Spatial variation of plasma expansion velocity at intensity 10^{11} W/cm² with pulse width 10 ns.

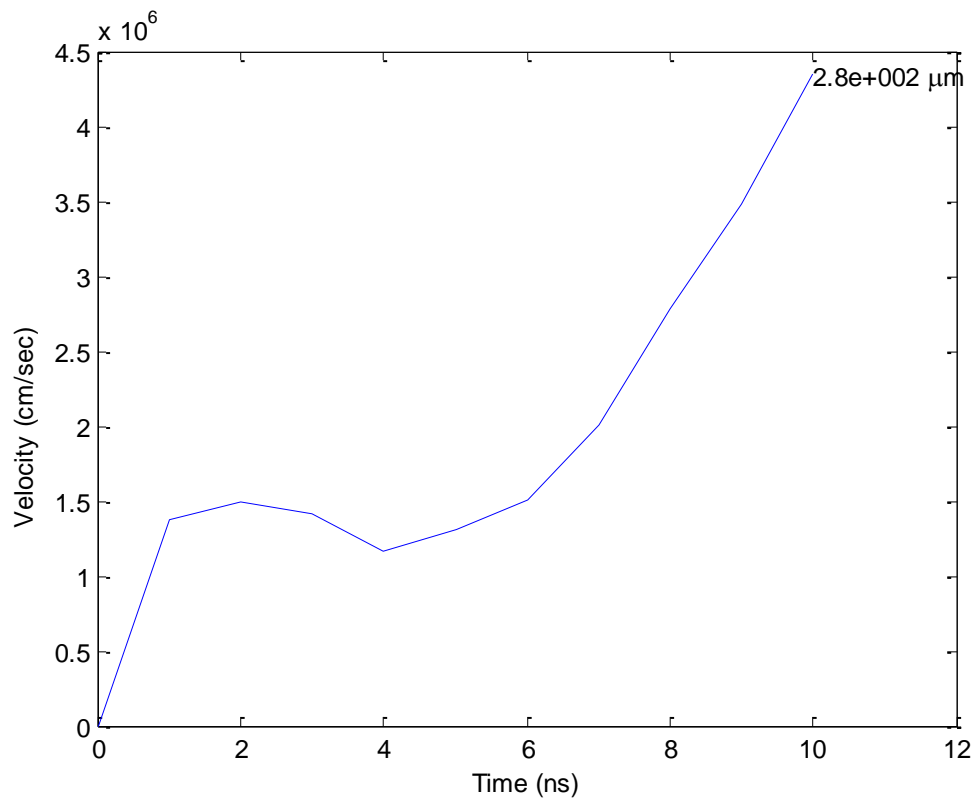


Fig.(3.24) Temporal variation of plasma expansion velocity at intensity 10^{11} W/cm^2 with pulse width 10 ns.

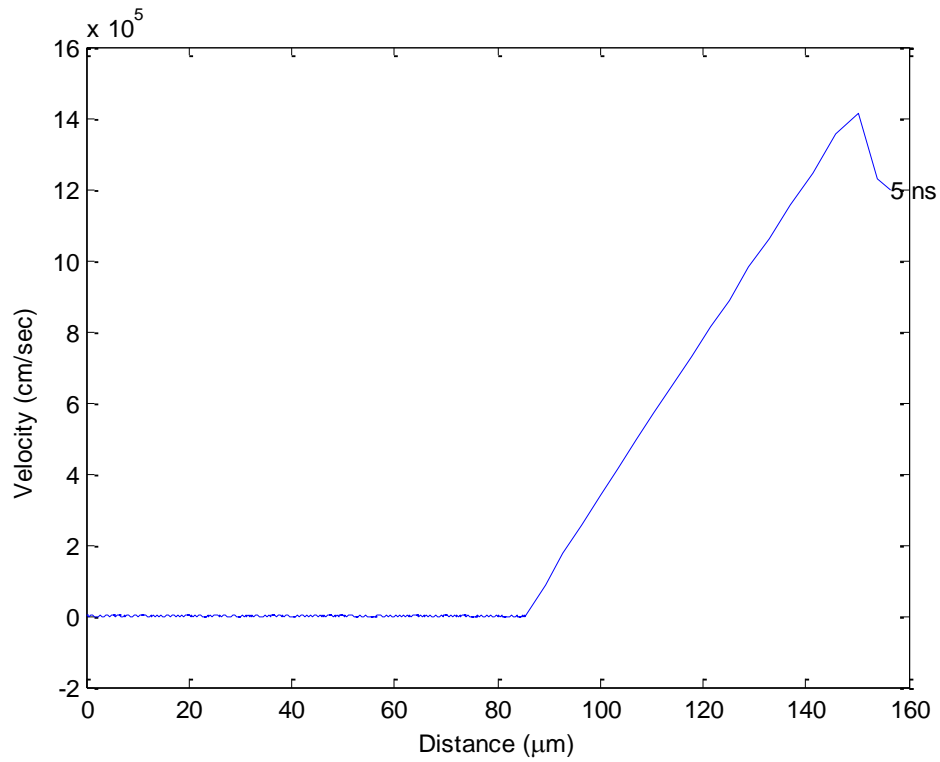


Fig.(3.25) Spatial variation of plasma expansion velocity at intensity 10^{12} W/cm^2 with pulse width 10 ns.

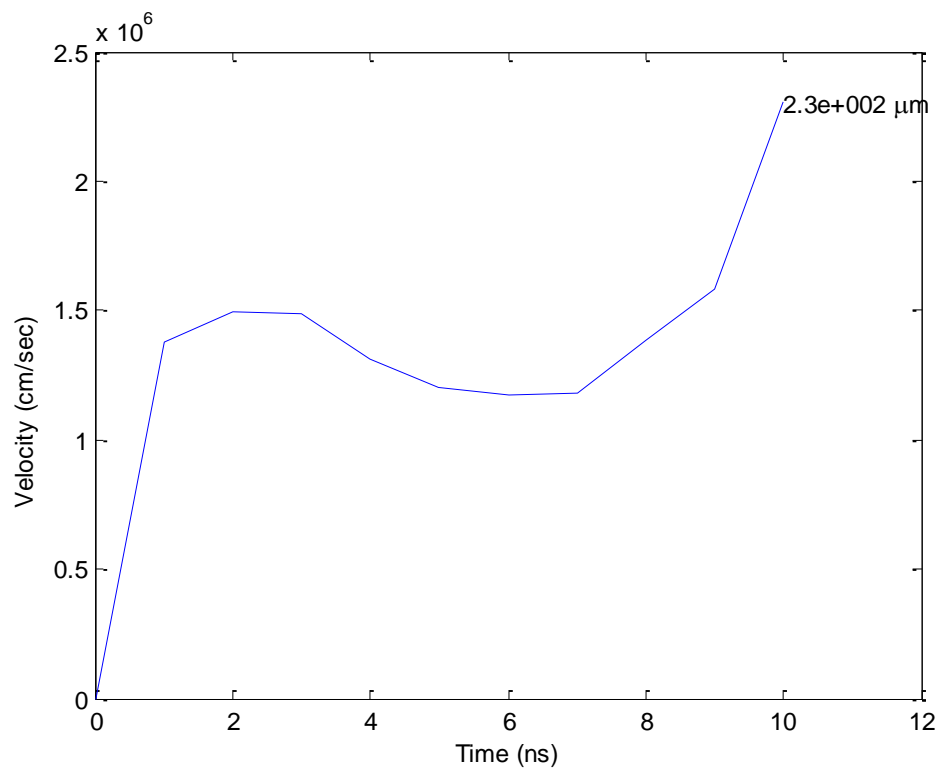


Fig.(3.26) Temporal variation of plasma expansion velocity at intensity 10^{12} W/cm^2 with pulse width 10 ns.

Figure (3.28) represents the temporal variation of the plasma expansion velocity. The velocity began from zero and increased to reach $\sim 1.35 \times 10^6$ cm/sec at 1 ns, then decreased to reach $\sim 1.2 \times 10^6$ cm/sec after 7 ns, and increased after 8 ns reaching the value 2.3×10^6 cm/sec.

The spatial variation of the plasma expansion velocity can be shown in Fig.(3.29). The laser power density was 10^{12} W/cm² with pulse width of 10 ps. The plasma expansion velocity will stay zero until ~ 90 μ m and increased to reach $\sim 5.2 \times 10^7$ cm/s at ~ 1150 μ m. Figure (3.30) shows that the plasma velocity began from zero and reached the value of 1.8×10^8 cm/s after 1 ns.

Figure (3.31) describes the spatial variation of the plasma expansion velocity with laser power density of 10^{13} W/cm² and pulse width 10 ps. It has been noticed that the plasma expansion velocity will stay zero value until ~ 100 μ m and increased to reach the value 5×10^7 cm/sec at 1170 μ m. The temporal variation of the plasma expansion velocity can be shown in Fig.(3.32). The plasma expansion velocity began from zero value and increases to reach the value 1.38×10^6 cm/sec and decreased to 1.38×10^6 cm/sec and then increased to reach the value 2.3×10^6 cm/sec at 10 ns.

In laser produced plasma, the plasma can be formed by the laser pulse leading target edge, and the plasma will heat by the rest of the pulse [86]. The electrons were initially heated to very high temperatures compared to the cold target. Therefore, the lattice became hot and these results agree with reference [87].

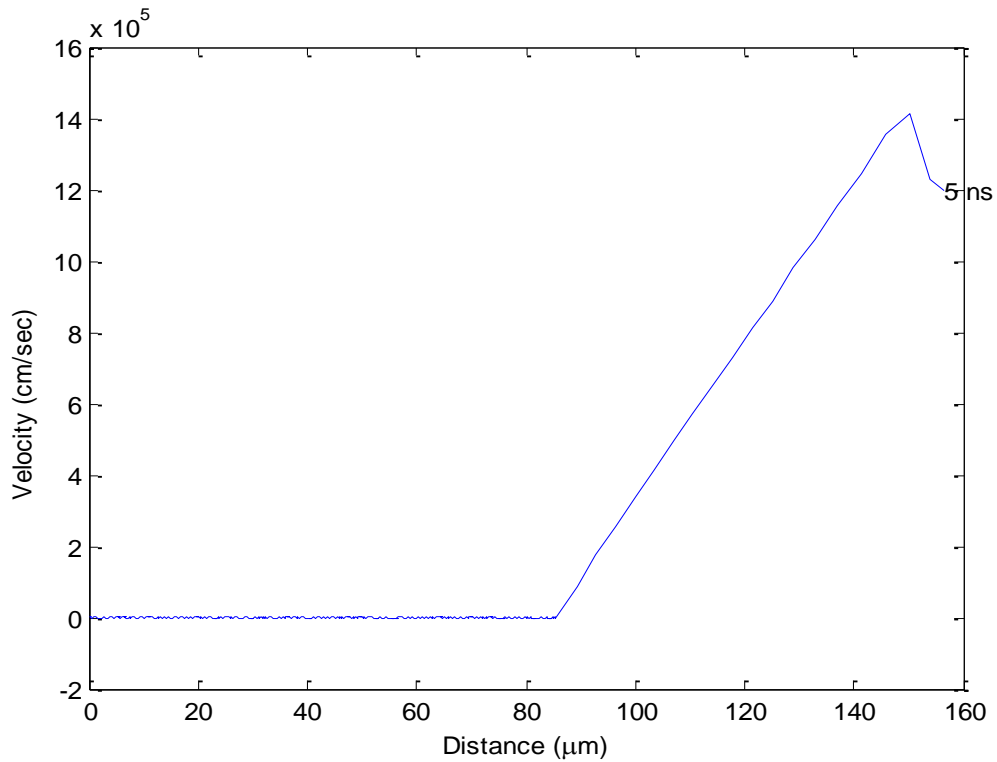


Fig.(3.27) Spatial variation of plasma expansion velocity at intensity 10^{11} W/cm^2 with pulse width 10 ps.

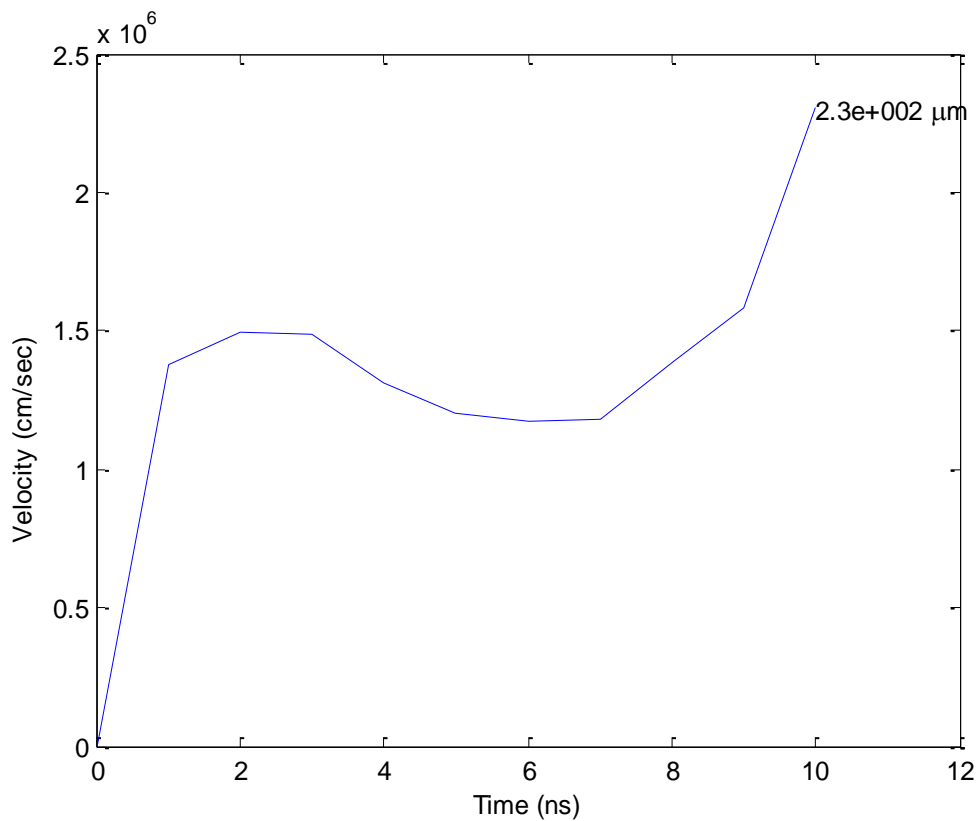


Fig.(3.28) Temporal variation of plasma expansion velocity at intensity 10^{11} W/cm^2 with pulse width 10 ps.

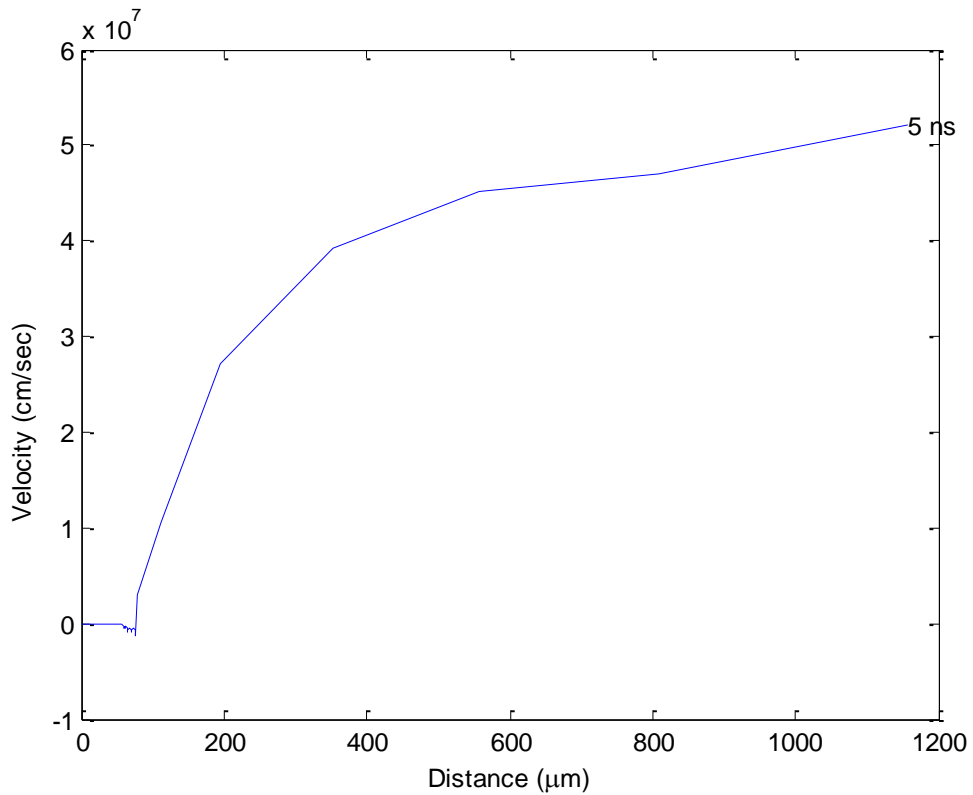


Fig.(3.29) Spatial variation of plasma expansion velocity at intensity 10^{12} W/cm^2 with pulse width 10 ps.

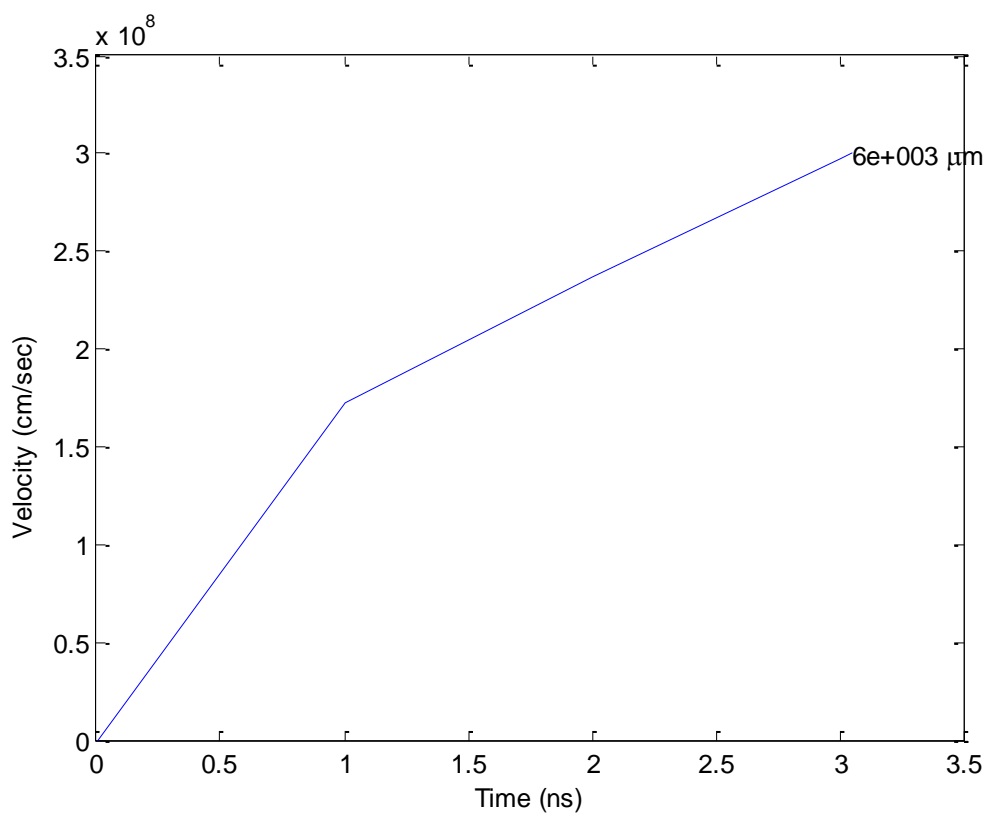


Fig.(3.30) Temporal variation of plasma expansion velocity at intensity 10^{12} W/cm^2 with pulse width 10 ps.

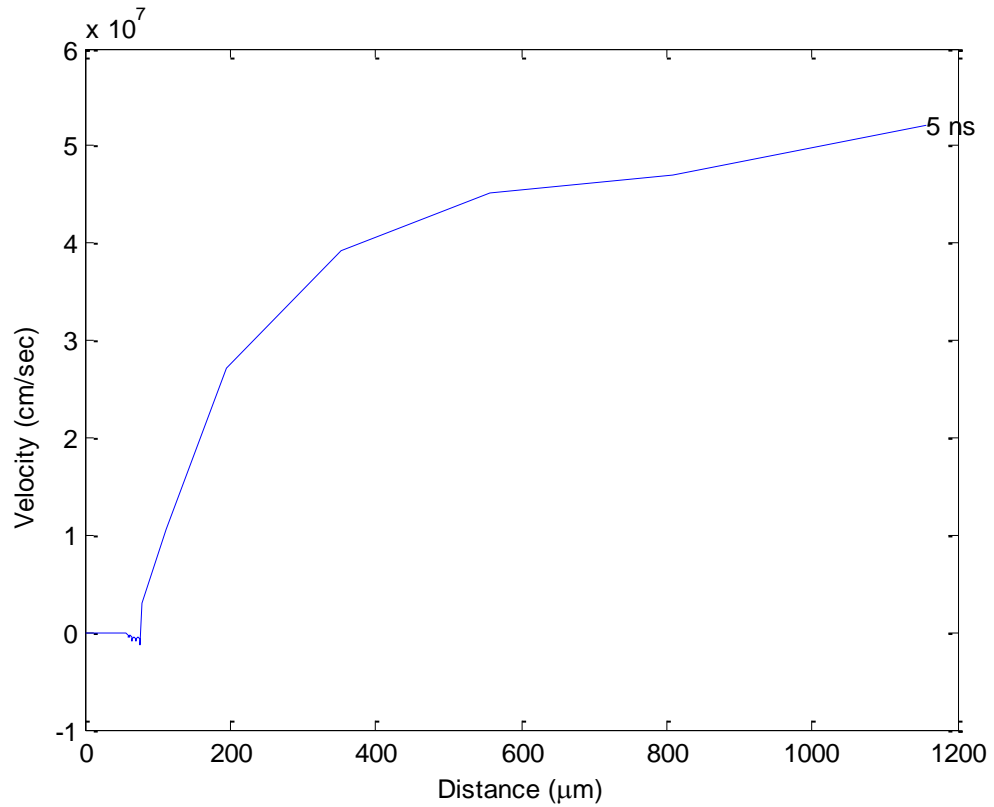


Fig.(3.31) Spatial variation of plasma expansion velocity at intensity 10^{13} W/cm^2 with pulse width 10 ps.

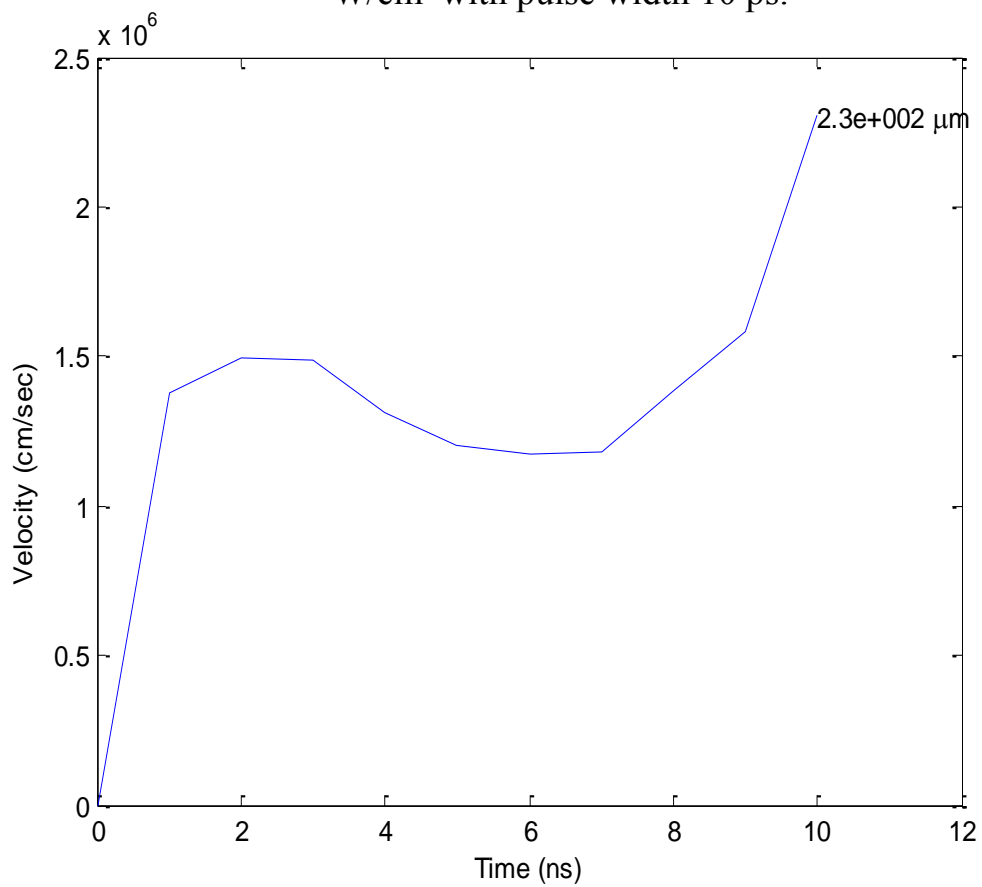


Fig.(3.32) Temporal variation of plasma expansion velocity at intensity 10^{13} W/cm^2 with pulse width 10 ps.

3.3.3 Spatial and temporal electron temperature variation

The electron temperature was a function of the laser power density, and it has been considered as one of the important parameter of the plasma. Figure (3.33) represents the spatial variation of the plasma electron temperature when the laser power density was 10^{11}W/cm^2 and the pulse width was 10 ns. The peak of the electron temperature is 3000 eV after $0.02 \times 10^5 \mu\text{m}$ distance.

The temporal variation of the plasma electron temperature can be shown in Fig.(3.34), the plasma electron temperature began from zero and increased reaching to 12.5 eV at about 4 ns, and increased rapidly to reach 56 eV at 9.5 ns.

Figure (3.35) explains the spatial variation of the plasma electron temperature when the laser power density increases to 10^{12}W/cm^2 . The electron temperature after 150 μm distance increases reaching to 17 eV. The temporal variation of the plasma electron temperature was shown in Fig.(3.36), the plasma electron temperature begins from zero and increases to 13 eV at 4 ns, and then increases to reach 85 eV after 9 ns.

The spatial variation of the plasma electron temperature when the laser power density is 10^{11}W/cm^2 and pulse width is 10 ps was shown in Fig.(3.37), the plasma electron temperature after 150 μm increases reaching to 16.5 eV. The temporal variation of the plasma electron temperature was shown in Fig.(3.38), the electron temperature begins from zero and increases reaching to 13 eV at 4 ns, and then increases to reach 84 eV at 9.5 ns. Figure (3.39) describes the spatial variation of the plasma electron temperature when the laser power density is 10^{12}W/cm^2 and pulse width is 10 ps. The plasma electron

temperature increases to reach 900 eV after 80 μm , and then decreases rapidly to reach 750 eV at 1800 μm .

Figure (3.40) represents the temporal variation of the plasma electron temperature when the laser power density is $10^{12}\text{W}/\text{cm}^2$. The plasma electron temperature begins from zero and increases to reach 350 eV at 2 ns, and then increases reaching to 1900 eV after 9.5 ns.

The spatial variation of the plasma electron temperature when the laser power density is $10^{13}\text{W}/\text{cm}^2$ and pulse width 10 ps was shown in Fig.(3.41), the maximum plasma electron temperature is 950 eV at 240 μm and then decreases to 750 eV at 1180 μm . Figure (3.42) represents the temporal variation of the plasma when the laser power density is $10^{13}\text{W}/\text{cm}^2$. The electron temperature begins from zero to 280 eV at 2 ns, and increases reaching to 1950 eV at 9.5 ns. From these results, when the laser power density increases, the plasma electron temperature also increases.

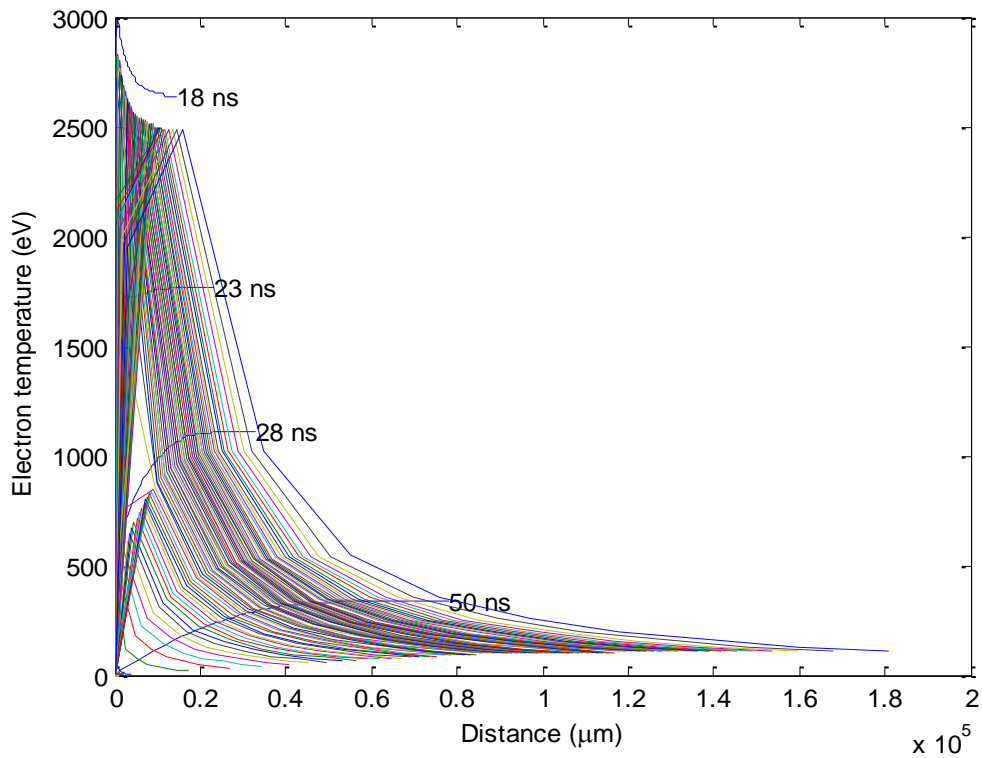


Fig.(3.33) Spatial variation of plasma electron temperature at intensity 10^{11} W/cm² with pulse width 10 ns.

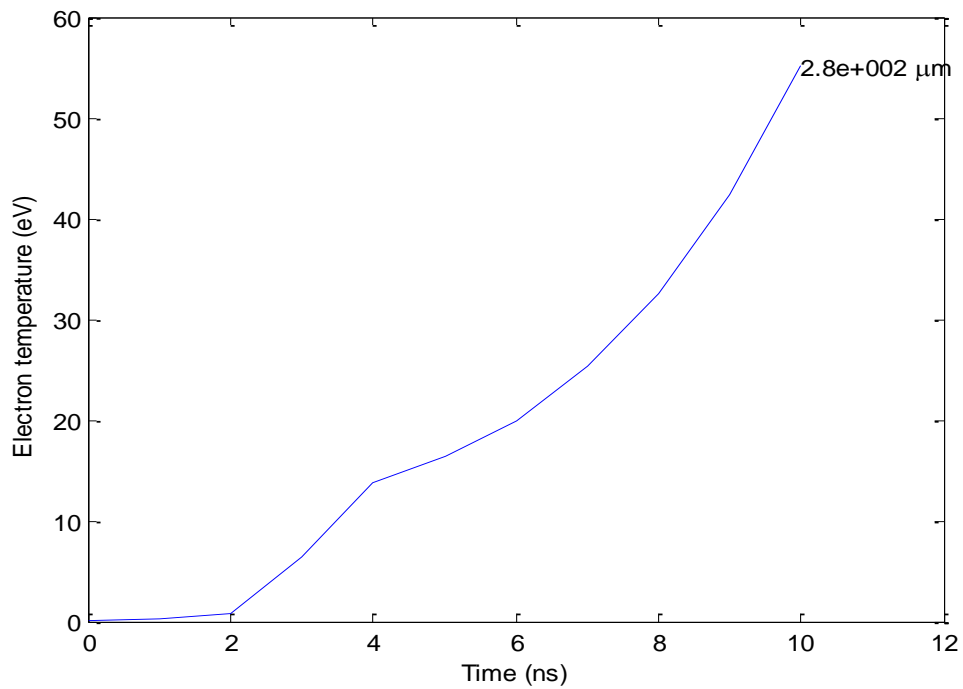


Fig.(3.34) Temporal variation of plasma electron temperature at intensity 10^{11} W/cm² with pulse width 10 ns.

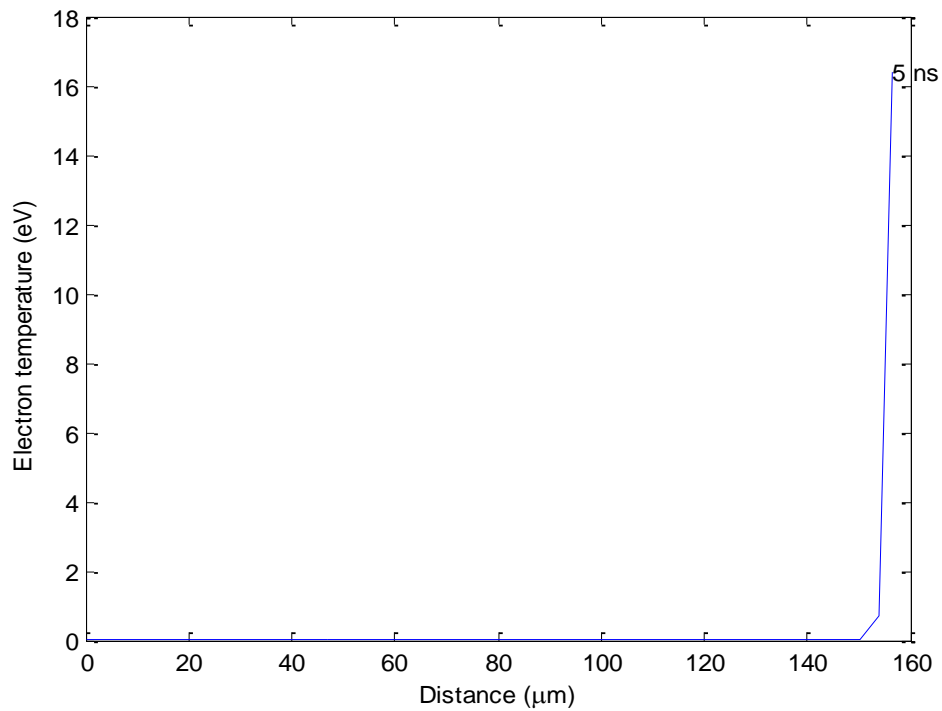


Fig.(3.35) Spatial variation of plasma electron temperature at intensity 10^{12} W/cm^2 with pulse width 10 ns.

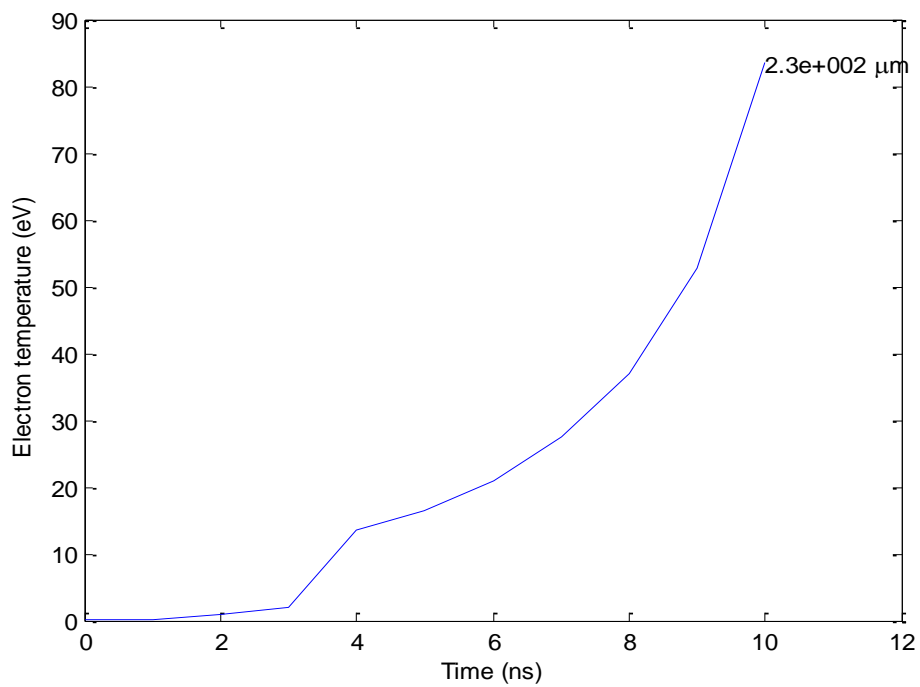


Fig.(3.36) Spatial variation of plasma electron temperature at intensity 10^{12} W/cm^2 with pulse width 10 ns.

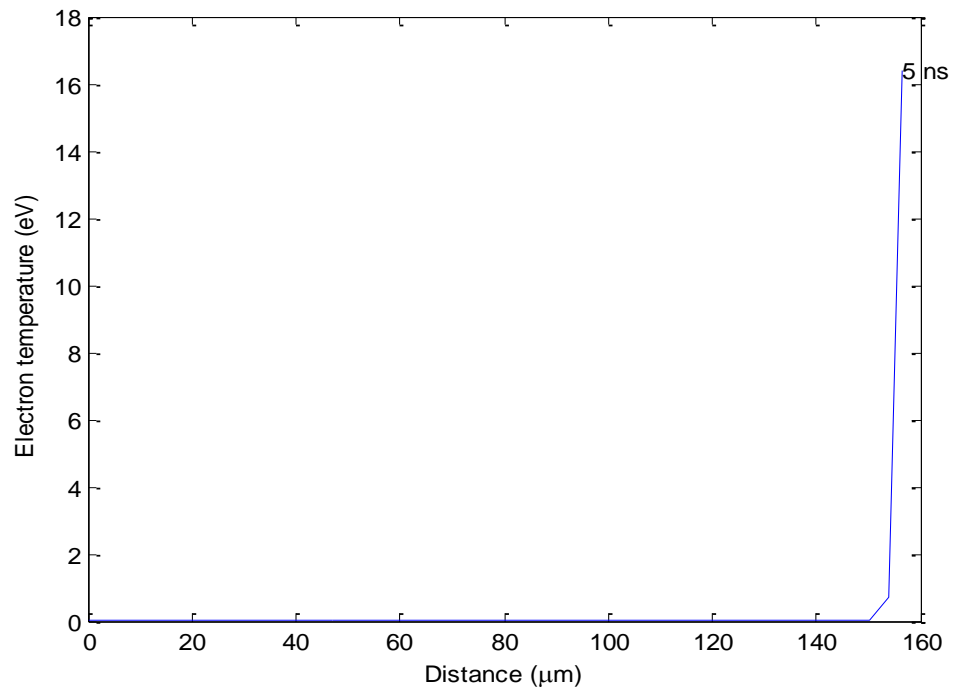


Fig.(3.37) Spatial variation of plasma electron temperature at intensity 10^{11} W/cm^2 with pulse width 10 ps.

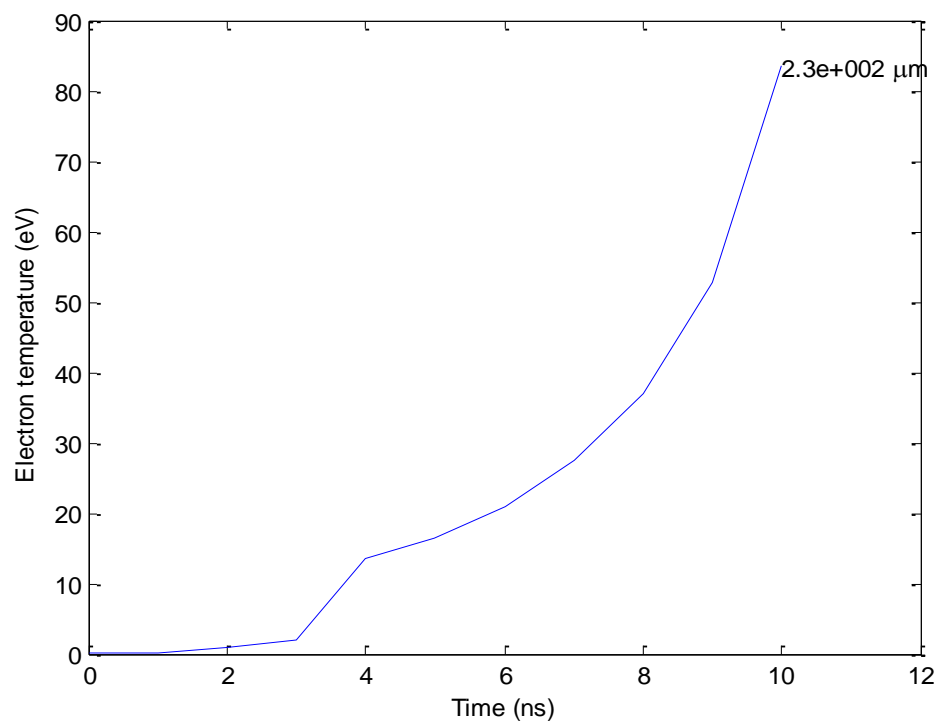


Fig.(3.38) Temporal variation of plasma electron temperature at intensity 10^{11} W/cm^2 with pulse width 10 ps.

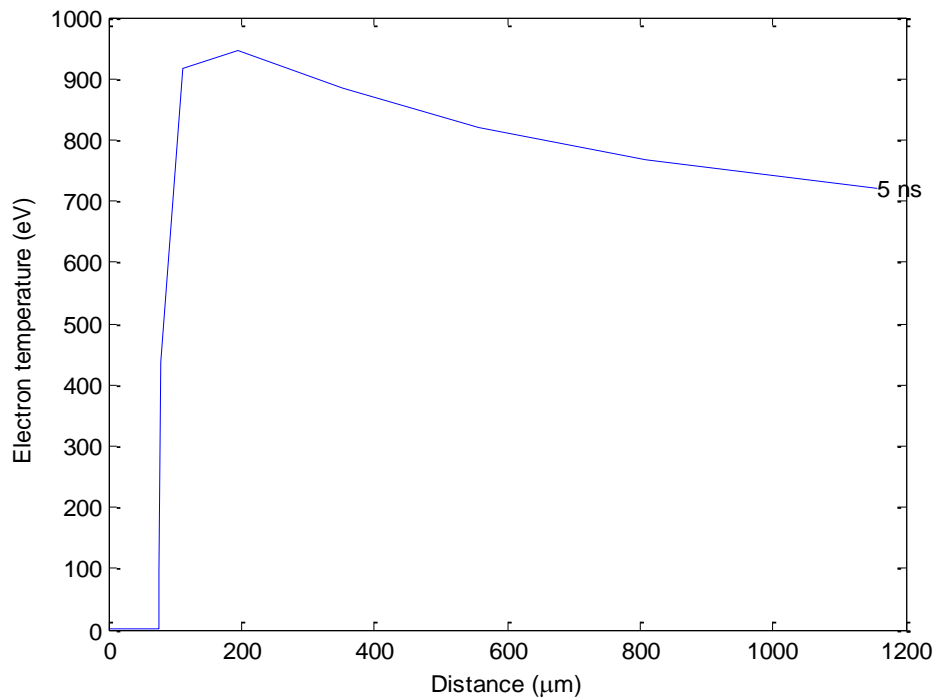


Fig.(3.39) Spatial variation of plasma electron temperature at intensity 10^{12} W/cm^2 with pulse width 10 ps.

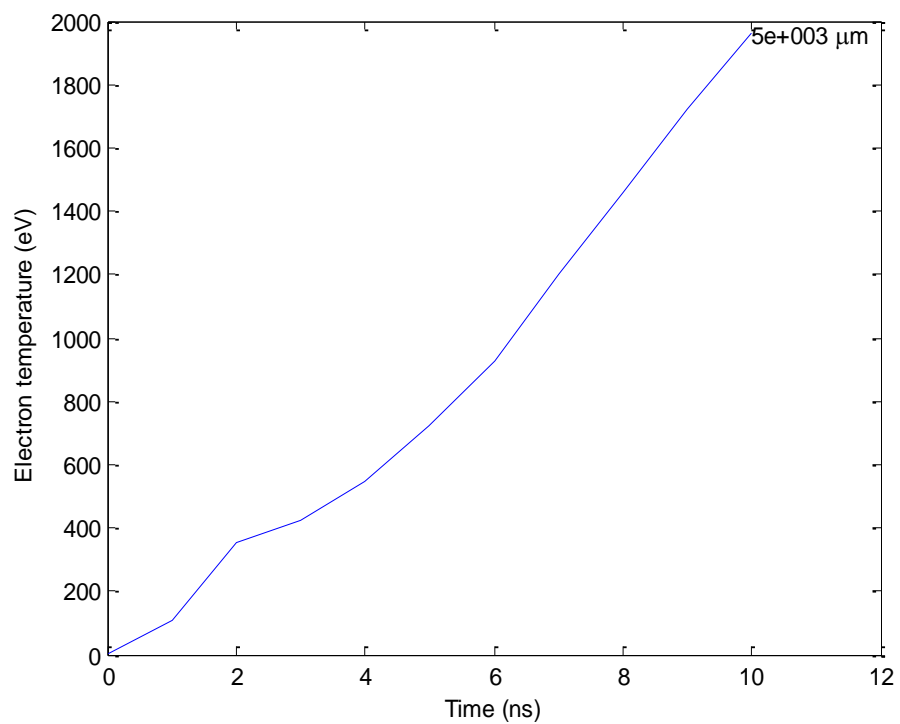


Fig.(3.40) Temporal variation of plasma electron temperature at intensity 10^{12} W/cm^2 with pulse width 10 ps.

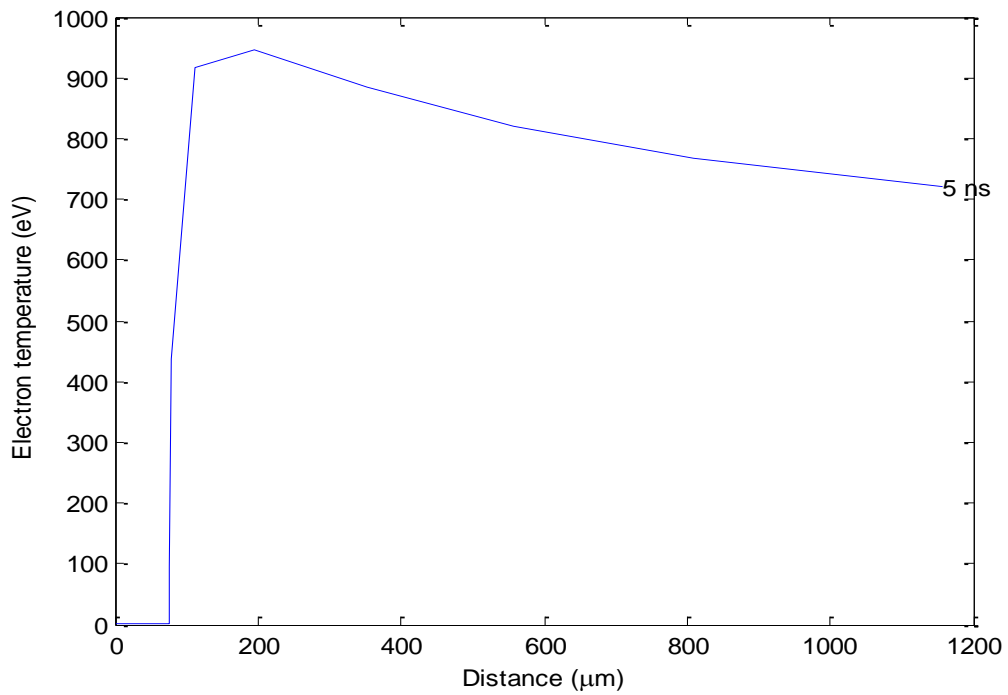


Fig.(3.41) Spatial variation of plasma electron temperature at intensity 10^{13} W/cm^2 with pulse width 10 ps.

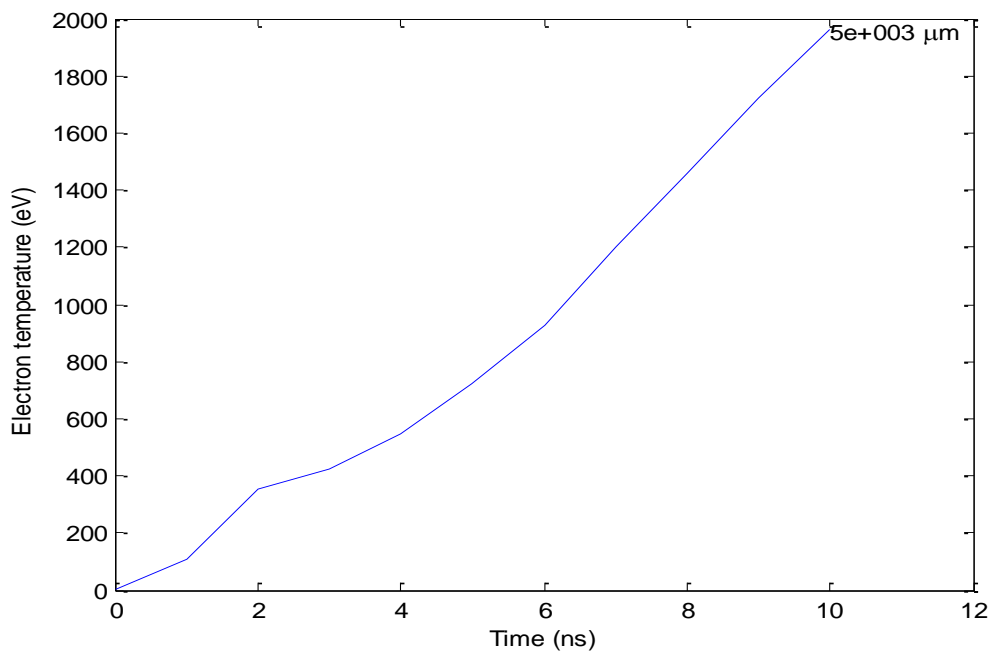


Fig.(3.42) Temporal variation of plasma electron temperature at intensity 10^{13} W/cm^2 with pulse width 10 ps.

3.3.4 Spatial and temporal pressure variation

The pressure variation is one of the plasma parameters. It is depends on the thickness of plasma layers [84, 87]. Figure (3.43) shows the spatial variation of the plasma pressure at the laser power density of 10^{11}W/cm^2 and pulse width of 10 ns. The maximum plasma pressure was 1Mbar at a distance of 200 μm and it began to decrease along the plasma length. When the plasma pressure decreased to reach the lowest value of pressure, the velocity began to increases rapidly.

The temporal variation of plasma pressure can be shown in Fig.(3.44), the plasma pressure of the plasma decreased to reach value lower than 0.01 Mbar at 1 ns, and then increased to value greater than 0.01 Mbar at 4 ns.

Fig.(3.45) shows that the maximum plasma pressure was 1 Mbar when power density increased to 10^{12}W/cm^2 and it stayed in the same value until the distance $\sim 84\ \mu\text{m}$ and then it decreased to reach value greater than 0.001 Mbar. Figure (3.46) represents the temporal variation of the plasma pressure when the laser power density was 10^{12}W/cm^2 . The maximum pressure was 1 Mbar and it decreased to reach value less than 0.01 Mbar at 1 ns.

Figure (3.47) represents the spatial plasma pressure variation when the laser power density was 10^{11}W/cm^2 and with pulse width of 10 ps. The plasma pressure was $\sim 1\text{Mbar}$ and then it decreased to value 0.009 Mbar after 82 μm . The temporal variation of the plasma pressure can be shown in Fig.(3.48), The maximum pressure was 1 Mbar and it decreased to reach value less than 0.01 Mbar at 1 ns, and then it increased to reach value more than 0.01 Mbar after 4 ns.

Fig.(3.49) shows the spatial variation of the plasma pressure when the laser power density increased to 10^{12} W/cm². The maximum plasma pressure was 1 Mbar and it stayed until ~ 84 μ m and then it decreased to reach value larger than 0.001 Mbar. Figure (3.50) represents the temporal variation of the plasma pressure when the laser power density was 10^{12} W/cm². The maximum pressure was 1 Mbar and it decreased to reach value less than 0.01 Mbar at 1 ns.

The variation of the plasma pressure when the laser power density increased to 10^{13} W/cm² at the same pulse width can be shown in Fig. (3.51). The maximum pressure was ~ 1 Mbar and it increased to 10 Mbar at 100 μ m, and then it decreased to reach 0.002 Mbar at 1150 μ m. Figure (3.52) represents the temporal variation of the plasma pressure began from 1 Mbar and decreased rapidly to 0.007 Mbar after 10 ns.

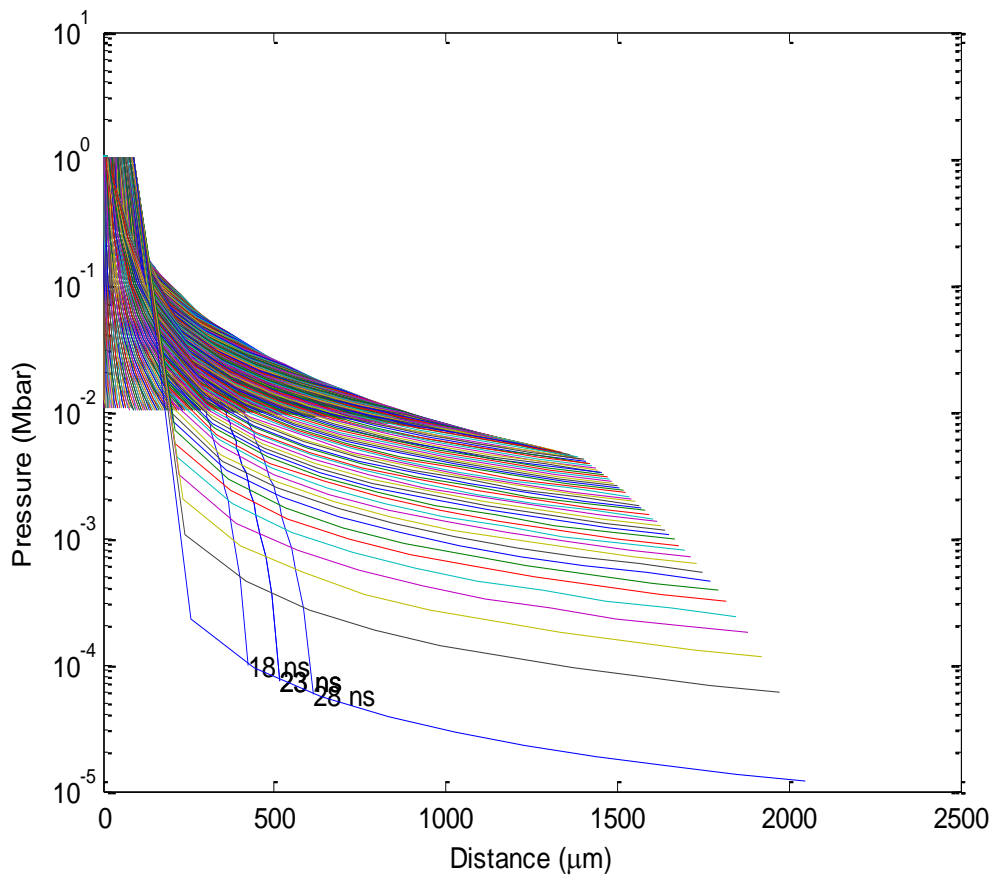


Fig.(3.43) Spatial variation of plasma pressure at intensity 10^{11} W/cm^2 with pulse width 10 ns.

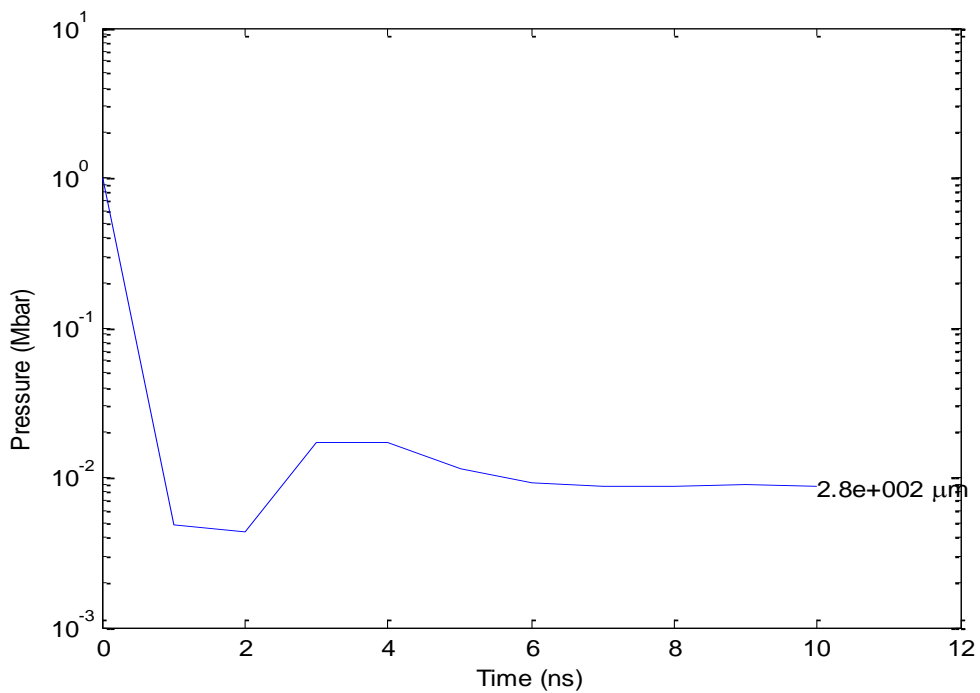


Fig.(3.44) Temporal variation of plasma pressure at intensity 10^{11} W/cm^2 with pulse width 10 ns.

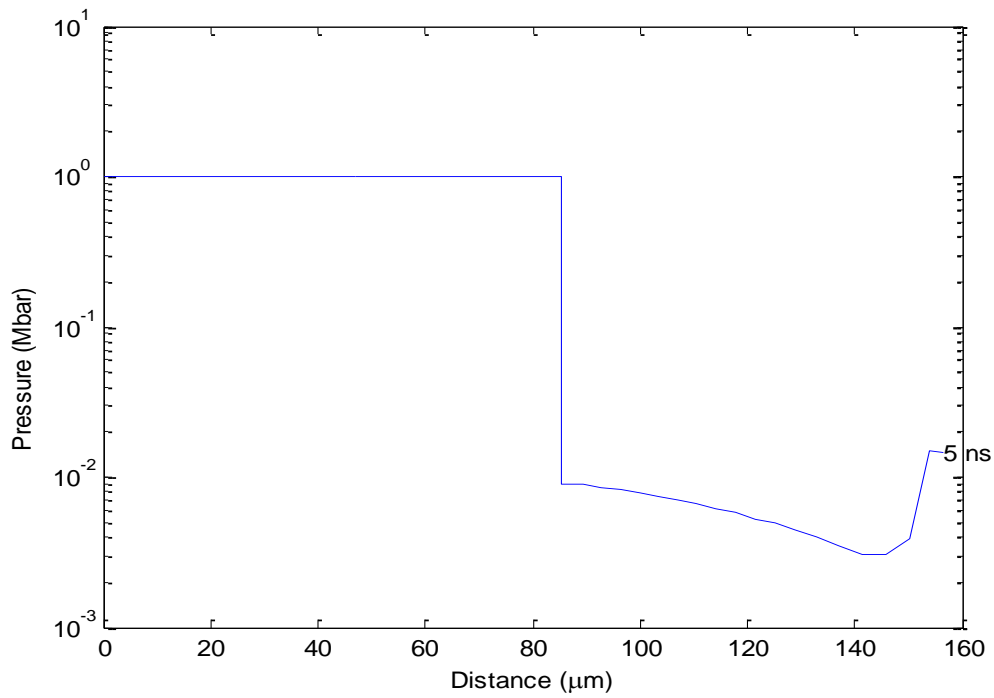


Fig.(3.45) Spatial variation of plasma pressure at intensity 10^{12} W/cm² with pulse width 10 ns.

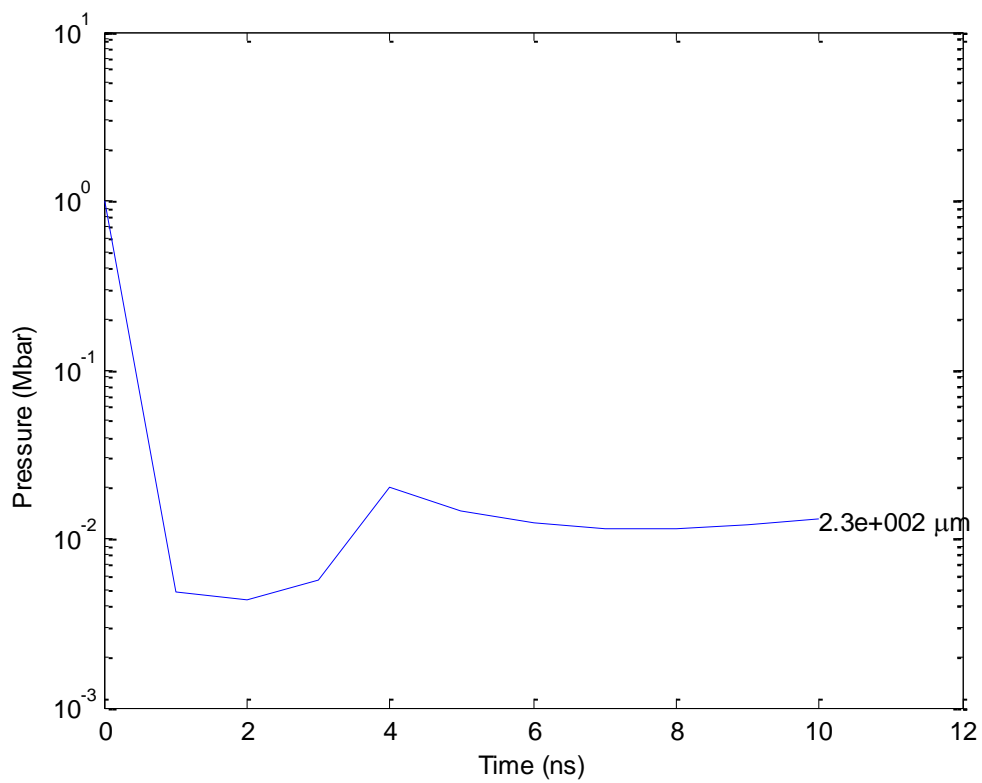


Fig.(3.46) Temporal variation of plasma pressure at intensity 10^{12} W/cm² with pulse width 10 ns.

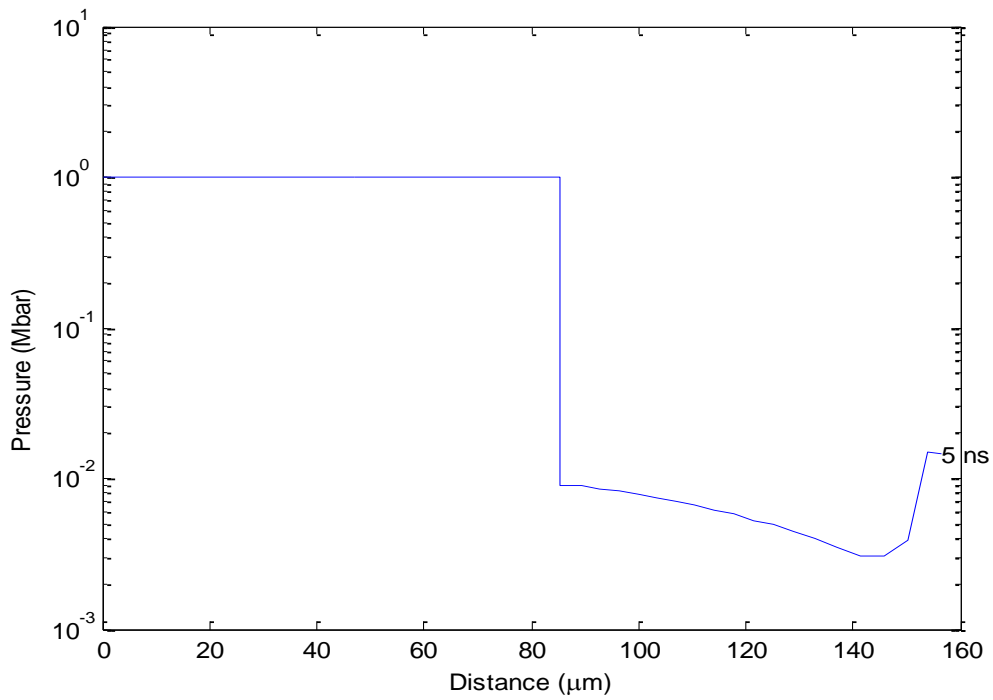


Fig.(3.47) Spatial variation of plasma pressure at intensity 10^{11} W/cm² with pulse width 10 ps.

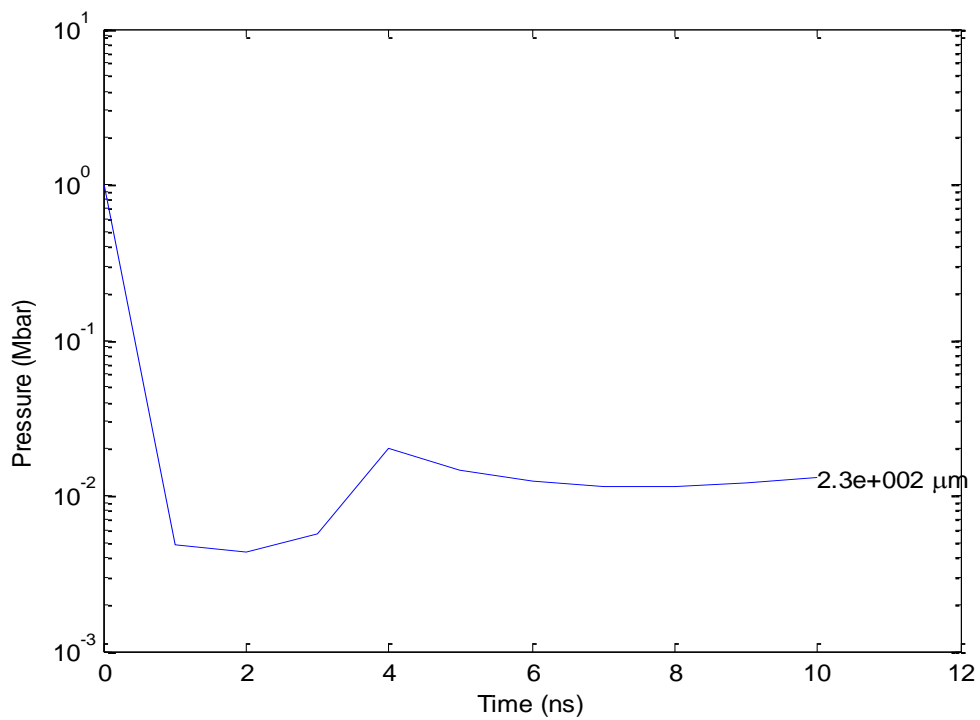


Fig.(3.48) Temporal variation of plasma pressure at intensity 10^{11} W/cm² with pulse width 10 ps.

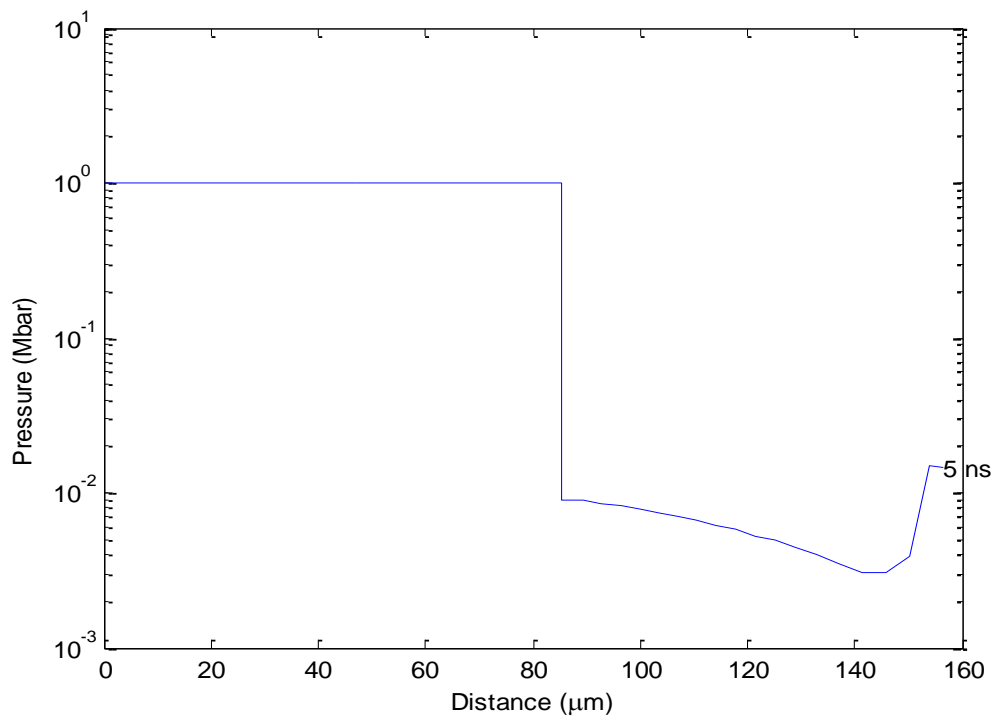


Fig.(3.49) Spatial variation of plasma pressure at intensity 10^{12} W/cm^2 with pulse width 10 ps.

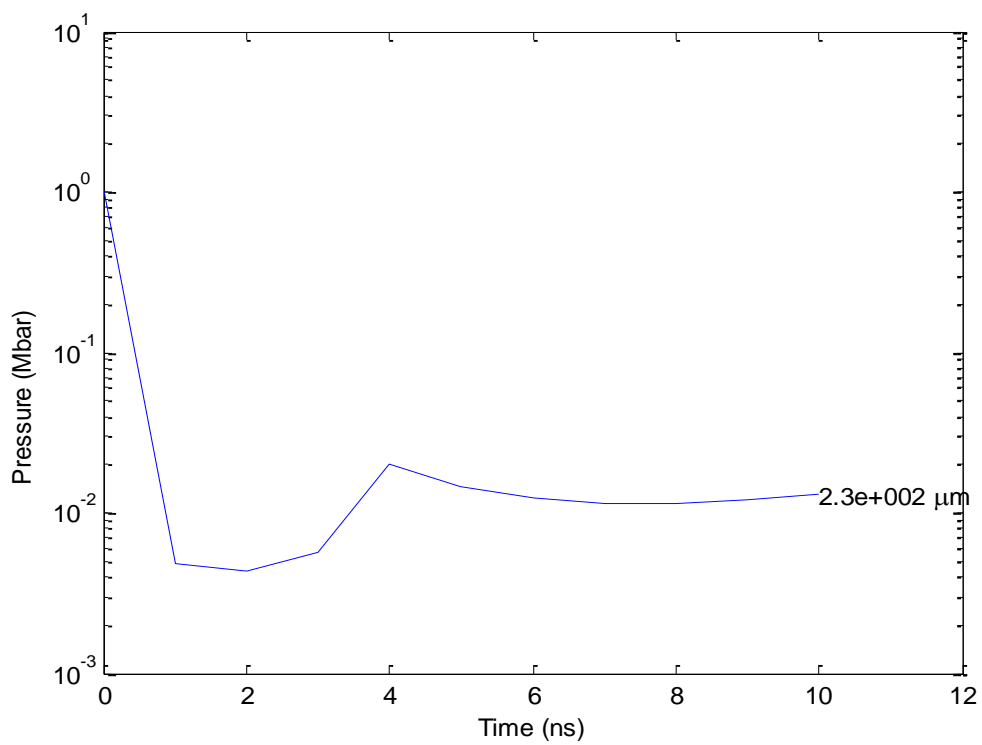


Fig.(3.50) Temporal variation of plasma pressure at intensity 10^{12} W/cm^2 with pulse width 10 ps.

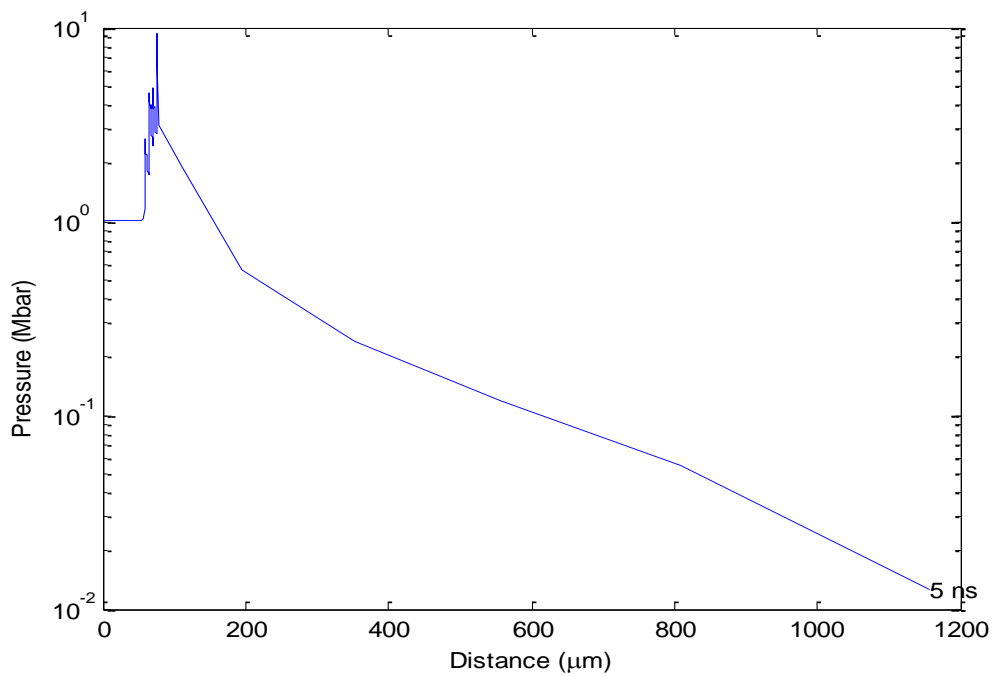


Fig.(3.51) Spatial variation of plasma pressure at intensity 10^{13} W/cm² with pulse width 10 ps.

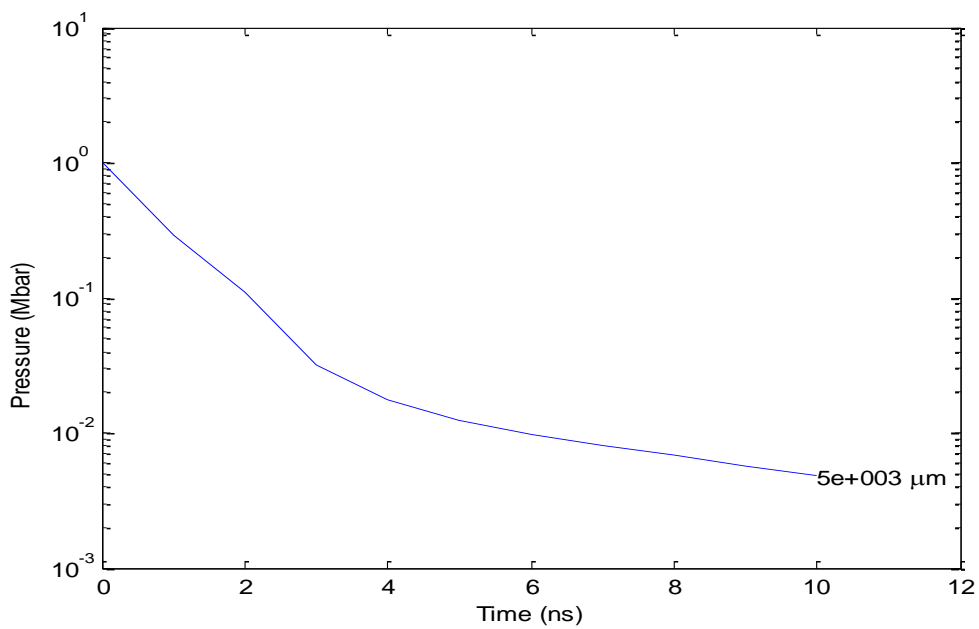


Fig.(3.52) Temporal variation of plasma pressure at intensity 10^{13} W/cm² with pulse width 10 ps.

3.3.5 Spatial and temporal average ionization variation (Z^*)

Figure (3.53) represents the spatial variation of the plasma average ionization when the laser power density was 10^{11}W/cm^2 with pulse width of 10 ns. The average ionization began from 2.1 and it increased to reach 3.42 at a distance $\sim 152\ \mu\text{m}$. The temporal variation of the plasma average ionization is shown in Fig.(3.54), the average ionization began from 2.45 and stayed with constant value .

The spatial variation of the plasma average ionization when the laser power density was 10^{12}W/cm^2 and with the pulse width is of 10 ns can be shown in Fig. (3.55). The maximum average ionization reached the value 2.5 at $\sim 150\ \mu\text{m}$. The temporal variation of the average plasma ionization is shown in Fig.(3.56), moreover, the average ionization stayed at the value 2.5 until $\sim 4\ \text{ns}$ and then it increased to reach 11 after 9 ns.

Figure (3.57) and Fig.(3.58) represent the spatial and temporal variation of the average plasma ionization when the laser power density was 10^{11}W/cm^2 and pulse width of 10 ps. The average ionization had value similar to that when the laser power density was 10^{12}W/cm^2 and pulse width is 10 ns.

The spatial variation of the plasma average ionization when the laser power density was 10^{12}W/cm^2 and with pulse width of 10 ps can be shown in Fig. (3.59). The average ionization stayed at 2.2 until $155\ \mu\text{m}$ and it increased rapidly to reach 3.35. The temporal variation of the average plasma ionization is shown in Fig.(3.60), the average ionization began from 2.3 and it increased to reach 13 after 0.9 ns. Figure (3.61) represents the spatial variation of the average plasma

ionization when the laser power density was $10^{13}\text{W}/\text{cm}^2$ and pulse width of 10 ps. The maximum average ionization was 13 at $20\ \mu\text{m}$ and it stayed with the same value at a long distance. The temporal variation of average plasma ionization Z began from 3.6 and increases rapidly to reach 13 after 0.8 ns.

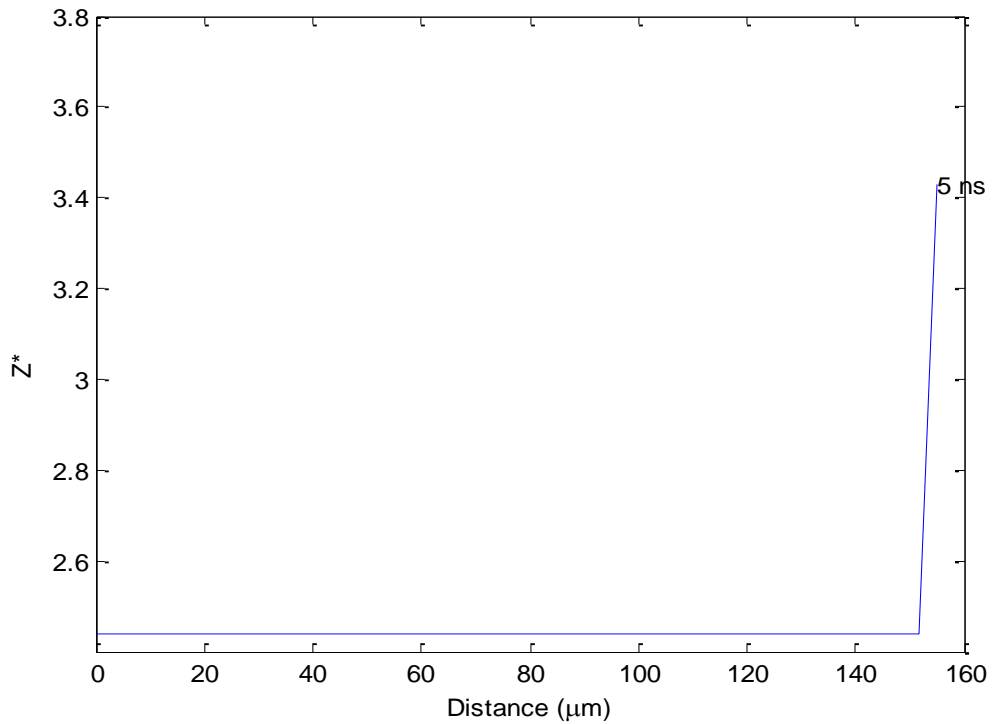


Fig.(3.53) Spatial variation of plasma average ionization at intensity $10^{11}\text{W}/\text{cm}^2$ with pulse width 10 ns.

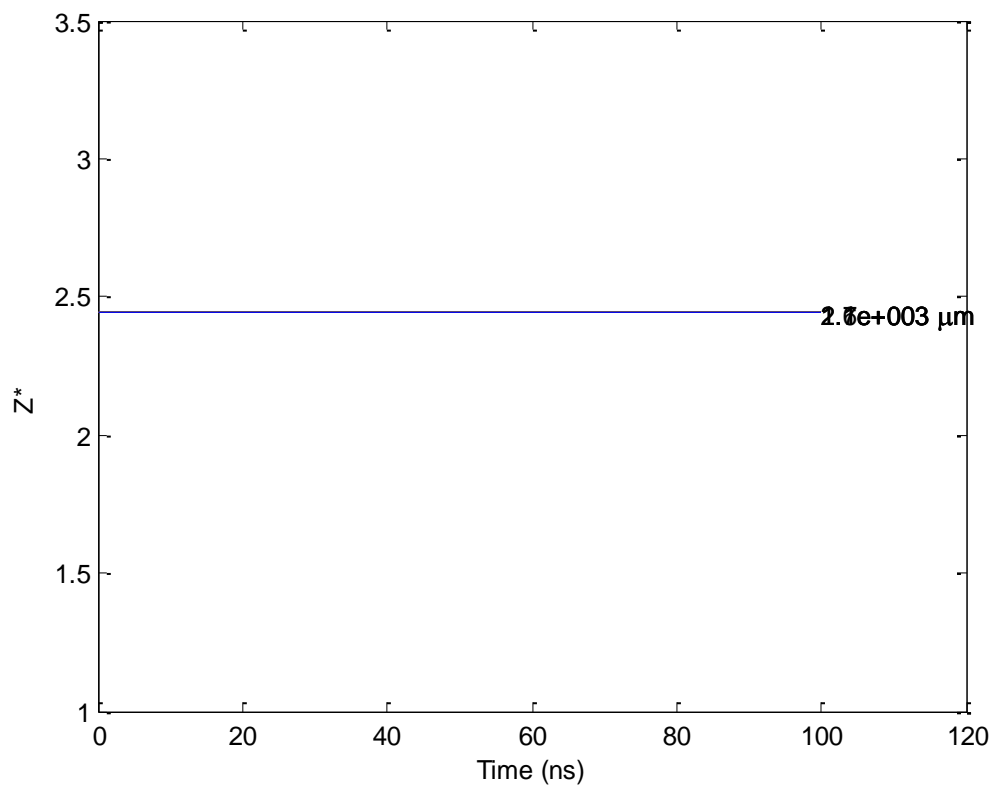


Fig.(3.54) Temporal variation of plasma average ionization at intensity 10^{11} W/cm^2 with pulse width 10 ns.

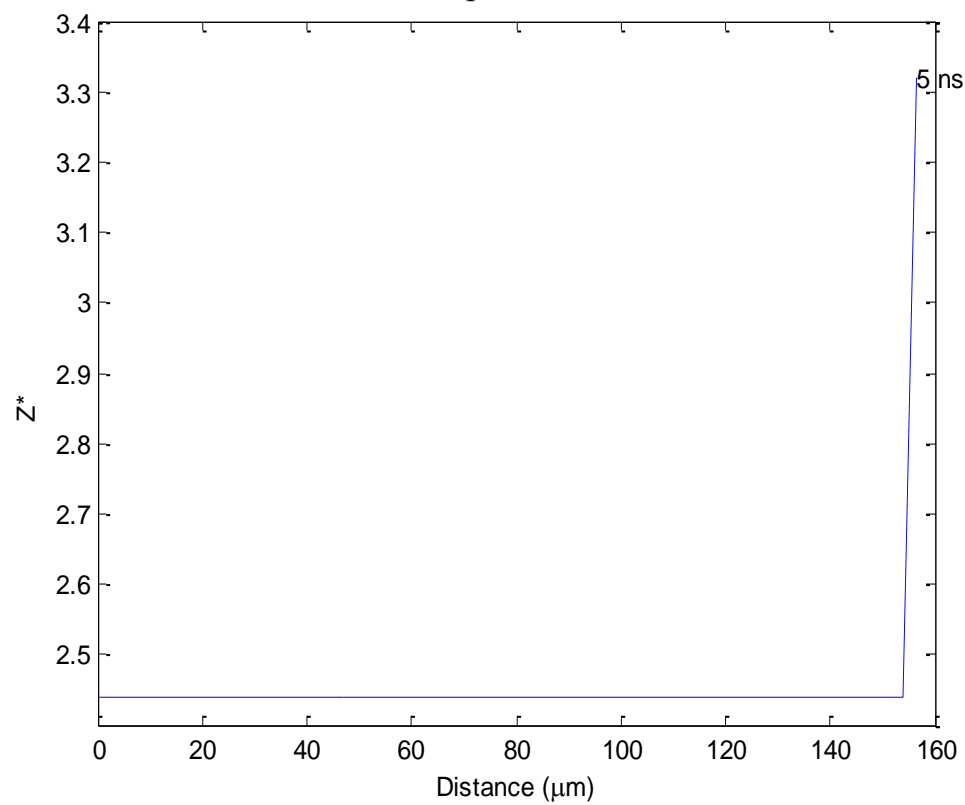


Fig.(3.55) Spatial variation of plasma average ionization at intensity 10^{12} W/cm^2 with pulse width 10 ns.

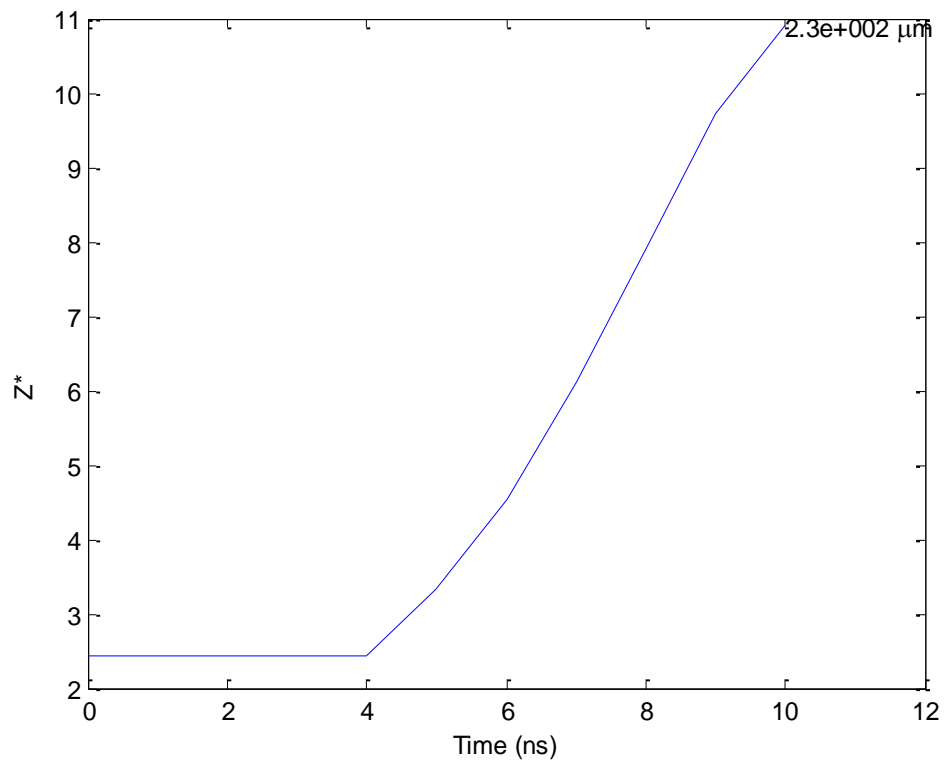


Fig.(3.56) Temporal variation of plasma average ionization at intensity 10^{12} W/cm^2 with pulse width 10 ns.

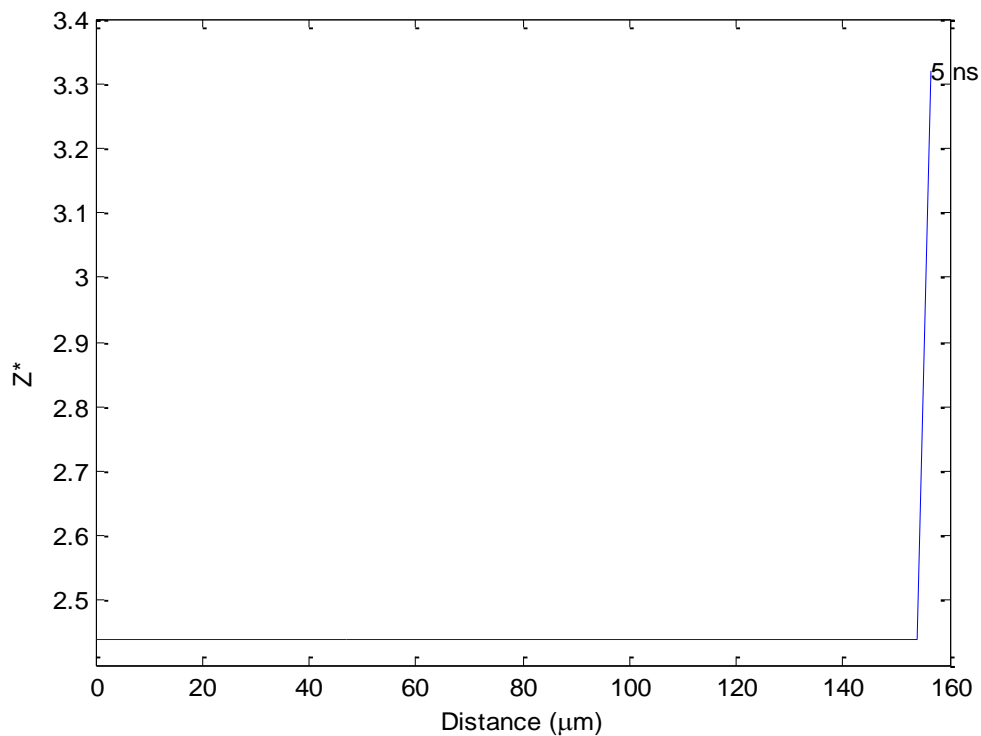


Fig.(3.57) Spatial variation of plasma average ionization at intensity 10^{11} W/cm^2 with pulse width 10 ps.

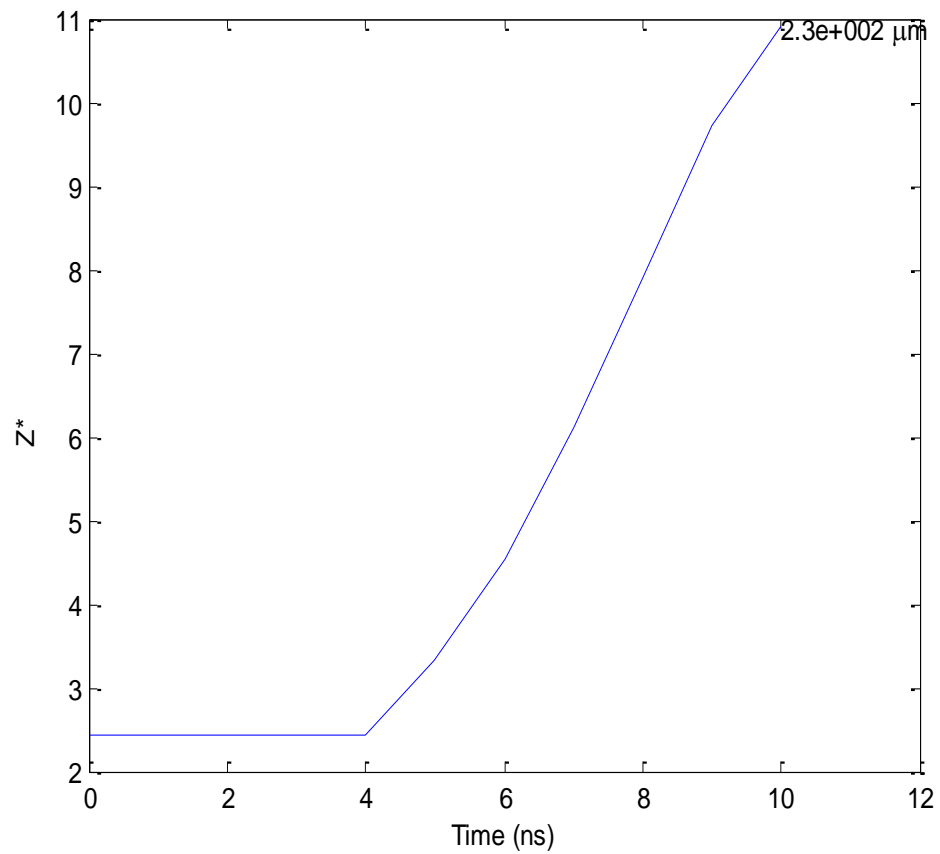


Fig.(3.58) Temporal variation of plasma average ionization at intensity 10^{11} W/cm² with pulse width 10 ps.

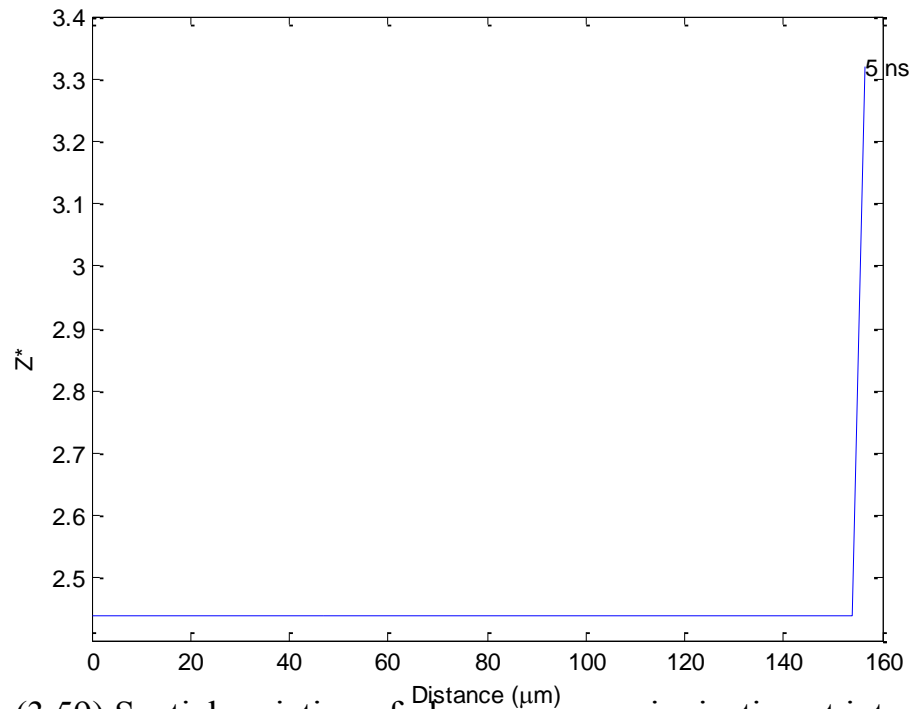


Fig.(3.59) Spatial variation of plasma average ionization at intensity 10^{12} W/cm^2 with pulse width 10 ps.

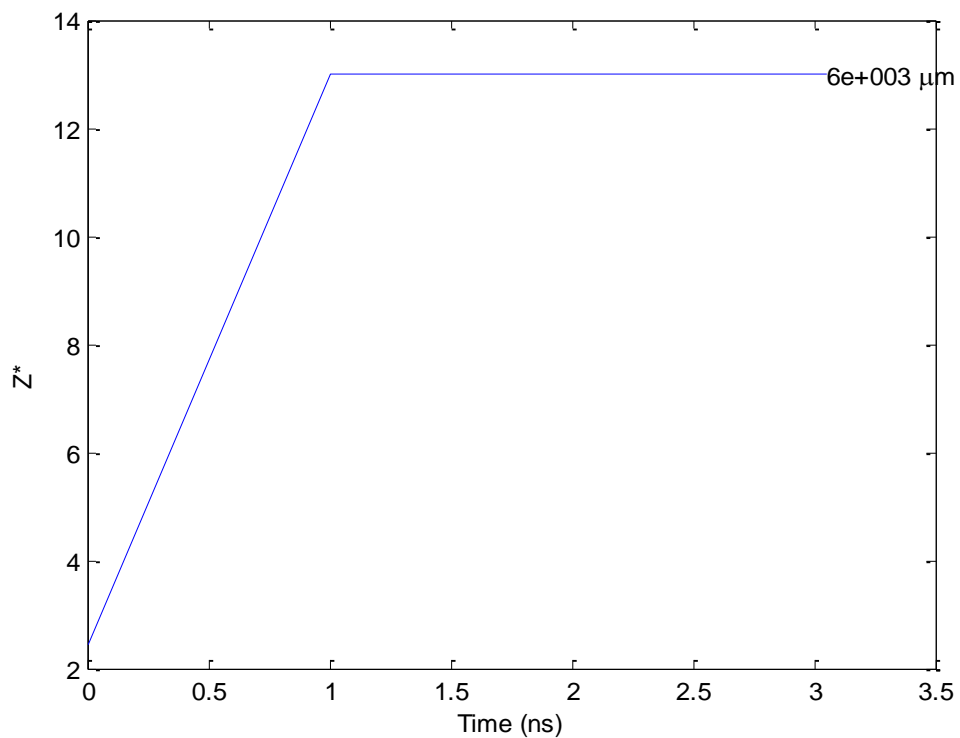


Fig.(3.60) Temporal variation of plasma average ionization at intensity 10^{12} W/cm^2 with pulse width 10 ps.

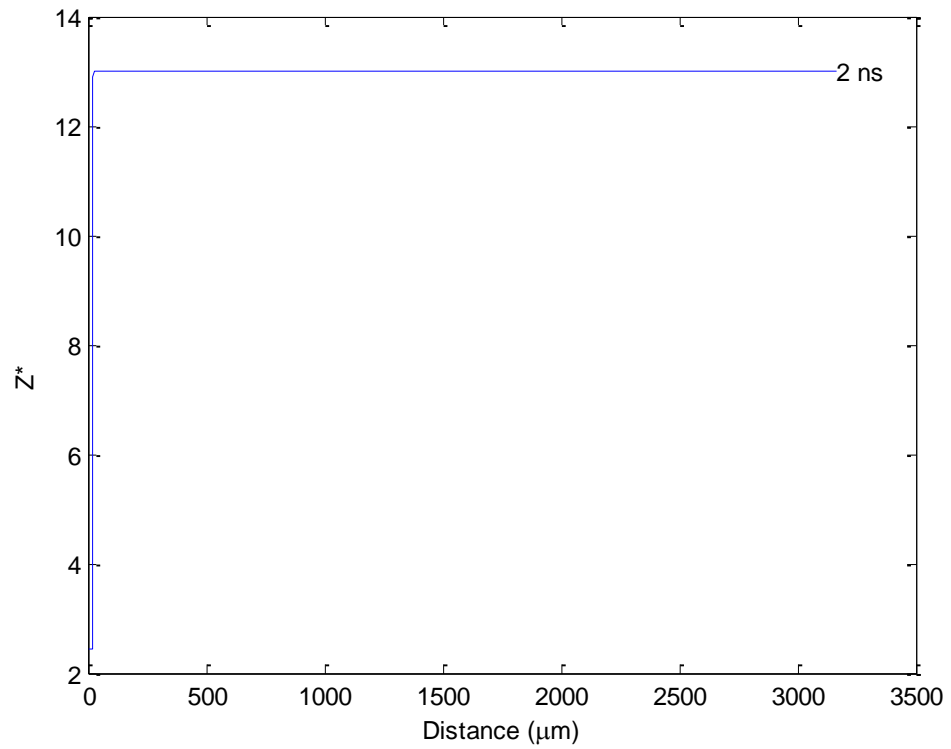


Fig.(3.61) Spatial variation of plasma average ionization at intensity 10^{13} W/cm^2 with pulse width 10 ps.

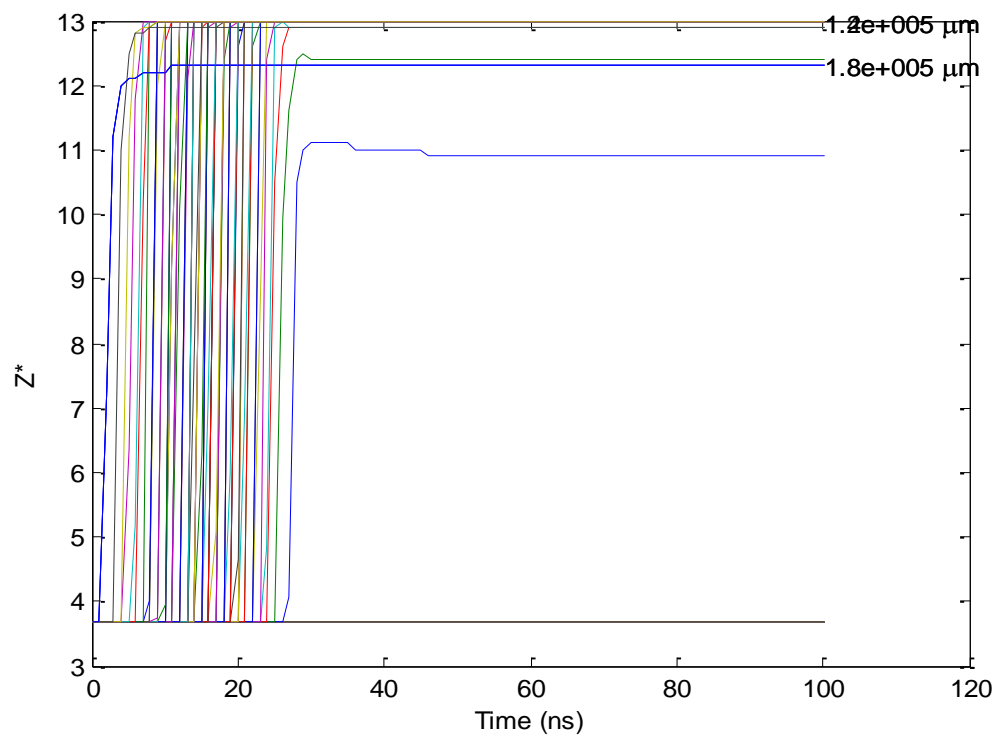


Fig.(3.62) Temporal variation of plasma average ionization at intensity 10^{13} W/cm^2 with pulse width 10 ps.

3.4 Conclusions

This work can give the information for all the processes in the atomic structure and the description of emission spectra steps for aluminum target (Cowan code) and also can give all hydrodynamic properties of the plasma (MEDUSA code).

- 1- The emission spectra of aluminum can give a strong oscillator strength of 1.82 with wavelength of 10 nm of the AlV, which can be considered a promising source for lithography.
- 2- The three laser intensities (10^{11} , 10^{12} and 10^{13} W/cm²) with pulse duration of 10 ns gave high ionization stages for aluminum.
- 3- The average ionization (Z) range has been obtained from the 1064 nm with 10 ns pulse width was obtained from 2.4-11 for electron temperature range from 16.5-3000 eV.
- 4- The average ionization (Z) range for laser pulse duration of 10 ps was 3.35-13 while the electron temperature range was from 16.5 to about 2000 eV.
- 5- The laser pulse width in nanosecond has been given more suitable results than the pulse width in picosecond because of the laser can be considered as a thermal source, so it needs more time to heat and creating plasma.

3.5 Future work

Many points can be taken in consideration to improve this work and get more suitable results. These points are:

- 1- Selecting different materials to study the emission spectra for each one in details and trying to find another emission sources in the XUV regions.
- 2- Using different laser wavelengths and study the effect of these wavelengths on the emission spectra.
- 3- Choosing different laser power densities for a certain laser wavelength at different laser pulse widths and trying to find the optimum parameters to produce the desired emission spectrum.
- 4- The most important point is building up an experimental setup for the next generation lithography manufacturing.

-
-
- 1- F. F. Chen, "Introduction to Plasma Physics and Controlled Fusion", Plenum Press, New York (1984).
 - 2- D. H. Lowndes, D. B. Geohegan, A. A. Puretzky, D. P. Norton, and C. M. Rouleau, Synthesis of novel thin-film materials by pulsed laserdeposition, *Science*, Vol. 273, No. 5277, August 1996, pp. 898-903.
 - 3- D. R. Nicholson, Introduction to Plasma Theory, © Wiley, New York, (1983).
 - 4- C. Uberoi, Introduction to unmagnetized plasmas, © PHI Pvt. Ltd. New Delhi (1988).
 - 5- M. Borghesi, A. Giulietti, D. Giulietti, L.A. Gizzi, A. Macchi, O. Willi, *Phys. Rev. E* 54,6769 (1996).
 - 6- L.A.Gizzi, D. Giulietti, A. Giulietti, T. Afshar-Rad, V. Biancalana, P. Chessa, E. Schifano, S. M. Viana, O. Willi, *Phys. Rev. E* 49, 5628 (1994).
 - 7- J. White, Opening the extreme ultraviolet lithography source bottleneck:Developing a 13.5-nm laser-produced plasma source for the semiconductor industry. PhD thesis, University College Dublin (2006).
 - 8- C. K. Birdsall and A. B. Longdon, "Plasma Physics Via Computer Simulation", Adam Hilger, Bristol (1991).
 - 9- V. L. Ginzburg, "The Properties of Electromagnetic Waves in Plasma", Pergammon, New York (1964).
 - 10- M. V. Allmen and A. Blatter, "Laser-Beam Interaction with Materials", Springer, New York (1995).
 - 11- G.P.Karman , McDonald GS, New GHC and Woerdman JP. *Natur.*, 402:138 (1999).

-
-
- 12- W. Duley, Laser Welding, John Wiley & Sons, New York,:67 (1999).
 - 13- W. L. Kruer, "The Physics of Laser Plasma Interaction", Addison-Wesley, Boston (1988).
 - 14- S. Suckewer, C.H. Skinner, H. Milchberg, C. Keane, and D. Voorhees. Amplification of stimulated soft-X-ray emission in a confined plasma column. *Phys. Rev. Lett.* 55(17), 1753-1756 (1985).
 - 15- W.L. Kruer, The physics of laser plasma interaction, Addison-Wesley (1988).
 - 16- D. Giulietti and L.A. Gizzi, "X-ray emission from laser-produced plasmas," *LaRivista del Nuovo Cimento*, vol. 21, number 10 (1998).
 - 17- W. L. Kruer, " Introduction to the physics of large amplitude plasma waves", *Physica Scripta*, T30 (1990).
 - 18- D. Giulietti and L.A. Gizzi, "X-ray emission from laser-produced plasmas," *LaRivista del Nuovo Cimento*, vol. 21, number 10 (1998).
 - 19- R. More, "Atomic physics of laser produced plasmas," *Handbook of Plasma Physics*, vol. 3, chap. 2, editors: Rosenbluth and Sagdeev, (1991) Elsevier.
 - 20- D. R. Corson and P. Lorrain, "Electromagnetic Fields and Waves", Freeman, New York (1988).
 - 21- R. K. Singh and J. Narayan, " Pulsed- laser evaporation technique for deposition of thin films: Physics and theoretical model", *Phy. Rev.*, B41 (1990).

-
-
- 22- R. W. Dreyfus, "Cu⁰, Cu⁺, and Cu₂ from excimer-ablated copper", *Journal of Appl. Phys.*, 69 (1991).
- 23- H. R. Griem, "Plasma Spectroscopy", Mc-Grew-Hill Book Company, New York (1964).
- 24- D. Salzmann, "Atomic Physics in Hot Plasma", Oxford University Press, Oxford (1998).
- 25- P. Hough, "Laser, Optical and Electrical Diagnostic of Colliding Laser-Produced Plasmas", Ph. D. Thesis, Dublin City University, (2010).
- 26- T. P. Hughes, "Plasma and Laser Light", Hilger, Bristol, U.K. (1975).
- 27- P. K. Carroll and E. T. Kennedy, " Laser-Produced Plasmas", *Contemp. Phys.* 22 (1981).
- 28- J. Richler, "Plasma Diagnostics", North –Holland Publishing Company, Amsterdam (1968).
- 29- C. Phipps, *Laser Ablation and its Applications*. Springer Science + Business Media,(2007).
- 30- V. Bakshi, editor. *Proceedings of the 3rd International EUVL Symposium*, Miyazaki, Japan,(2004).
- 31- B.E. Jurczyk, E. Vargas-Lopez, M.N. Neumann, and D.N. Ruzic. Illinois debris-mitigation EUV applications laboratory. *Microelectron. Eng.* 77(2), 103-109 (2005).
- 32- JA R Samson, "Techniques of vacuum ultraviolet spectroscopy", Wiley, NewYork (1967).
- 33- D.T. Attwood. *Soft X-rays and EUV radiation*. Cambridge University Press, Cambridge,UK (1999).

-
-
- 34- P. Marczuk and W. Egle, EUV Sources for Lithography, ed. V. Bakshi, ch. 33 Grazing-Incidence EUV Collectors, pp. 873–892. SPIE Press, Bellingham, WA, (2006).
- 35- K. Ota, Y. Watanabe, V. Banine, and H. Franken, EUV Sources for Lithography, ed. V. Bakshi, ch. 2 EUV Source Requirements for EUV Lithography, pp. WA, 27–43. SPIE Press, Bellingham, (2006).
- 36- D. Nagel, C.M. Brown, M.C. Peckerar, M.L. Ginter, J.A. Robinson, T.J. McIlrath and P.K. Carroll, “Repetitively pulsed-plasma soft x-ray source”, *Appl. Opt.*, 23, No.9 (1984).
- 37- R. E. Shanon, "System Simulation: The Art of Science", Prentice Hall, New Jersey (1975).
- 38- J. A. Payne, "Introduction to Simulation", Mc Graw Hill, New York (1985).
- 39- J. W. Schmidt, and R. E. Tay, "Simulation and Analysis of Industrial System", Irwin Home Wood, (1970).
- 40- R. D. Cowan, "Theoretical Calculations of Atomic Spectra Using Digital Computers", *Journal of Optical Society of America*, 58 (1968).
- 41- R. D. Cowan, "The Theory of Atomic Structure and Spectra", California University Press (1981).
- 42- O. Svelto, *Principles of Lasers*. Plenum Press, (1998).
- 43- J. P. Christiansen, D. E. Ashby and K. V. Roberts, "MEDUSA A One-Dimensional Laser Fusion Code", *Comp. Phys. Commun.*, 7 (1974).
- 44- S. J. Rose and R. J. Evans, "Radiation Transport in Medusa", Rutherford Appleton Laboratory Report: RL-83-040, RAL, Didcot, U. K., (1983).

-
-
- 45- Rodgers, P.A., Rogoyski, A.M., Rose, S.J., Rutherford Appleton Laboratory Internal Report, RAL-89-127,(1989).
- 46- A. R. Bell, "New Equations of State for Medusa", Rutherford Appleton (1980).
- 47- C. Moore, "Atomic Energy Levels", U.S. Government Printing Office, Washington (1949).
- 48- R. Bates, A. Kingston and R. Mowhrter," Recombination Between Electrons and Atomic Ions. I. Optically Thin Plasmas", Proc. Roy. Soc.A, 267 (1962).
- 49- J. A. Bearden and A. F. Burr," Reevaluation of X-Ray Atomic Energy Levels", Reviews of Modern Physics, 39(1) (1967).
- 50- U. Fano and J. Cooper," Spectral Distribution of Atomic Oscillator Strength", Rev. Mod. Phys. 40(1968).
- 51- M. Mansfield and J. P. Connerade," The Absorption Spectrum of Sr I between 40 and 95 angstrom", Proceedings of The Royal Society, A 342 (1975).
- 52- J. C. Ganthier and J. Geindre," A study of shock and ionisation waves in laser gas-breakdown using near-resonant absorption of nanosecond tunable-laser light", Rev. de Phys. 14 (1979).
- 53- I. Martinson," The spectroscopy of highly ionised atoms", Reports on Progress in Physics, 52(1983).
- 54- J. Costello, J. Mosnier, E. Kennedy, P. Carroll and G. O'Sullivan," X-UV Absorption Spectroscopy with Laser-Produced Plasmas: A Review", Physica Scripta, T34 (1991).

-
-
- 55- P. Sladeczek, H. Feist, M. Feldt, M. Martins and P. Zimmermann," Photoionization Experiments with an Atomic Beam of Tungsten in the region of the $5p$ and $4f$ excitation", *Phys. Rev. Lett.*, 75 (1995).
- 56- G. O'Sullivan, P. Carroll, P. Dunne, R. Faulkner, C. Mc Guinness and N. Murphy," Supercomplex spectra and continuum emission from rare-earth ions: Sm, a case study", *J. Phys. B: At Mol. Opt. Phys.*, 32(8) (1999).
- 57- A. Neogi, M. Martins, C. Mc Guinness, G. O'Sullivan, E. Kennedy, J. Mosnier, P. Van Kampen, J. Costello, " Vacuum-ultraviolet absorption spectrum of the Rb^{2+} ion in a laser generated plasma *Journal of Physics B: Atomic, Molecular and Optical Physics*, 35 (2002).
- 58- A Cummings, G O'Sullivan, P Dunne, E Sokell, N Murphy and JWhite" Conversion efficiency of a laser-produced Sn plasma at 13.5 nm, simulated with a one-dimensional hydrodynamic model and treated as a multi-component blackbody" *Physics Department, University College Dublin, Belfield, Dublin 4, Ireland* (2004).
- 59- N. Shaikh, S. Hafeez, B. Rashid and M. Baig," Spectroscopic Studies of Laser Induced Aluminium Plasma Using Fundamental, Second and Third Harmonics of a Nd:YAG Laser", *The European Physical Journal D*, 44 (2007).
- 60- P. Hough, C. Mcloughlin, T. Kelly, P. Hyden, S. Harilal, J. Mosnier and J. Costello," Electron and Ion Stagnation at the Collision Front Between Two Laser Produced Plasmas", *Journal of Physics D: Applied Physics*, 42 (2009).

-
-
- 61- C. Suzuki, C. Harte, D. Kilbane, T. Kato, H. Saku, I. Murakami, D. Kato, K. Sato, N. Tamura, S. Sudo, M. Goto, R. D'Arcy, E. Sokell, and G. O'Sullivan," Interpretation of spectral emission in the 20 nm region from tungsten ions observed in fusion device plasmas" *Journal of Physics B: Atomic, Molecular and Optical Physics*, 44 (2011).
- 62- M. Hanif, M. Salik, and M. A. Baig "Spectroscopic Studies of the Laser Produced Lead Plasma" *Atomic & Molecular Physics Laboratory, Department of Physics, Quaid-I-Azam University, Islamabad 45320, Pakistan, Plasma Science and Technology, Vol.13, No.2, (2011).*
- 63- C. Pagano, A. A. Goncharov, and J. G. Lunney" Compression and focusing a laser produced plasma using a plasma optical system" *American Institute of Physics Journal of Modern Physics* 3, 1663-1669 (2012).
- 64- M. Hanif, M. Salik, and M. A. Baig " Optical Spectroscopic Studies of Titanium Plasma Produced by an Nd : YAG Laser" *National Center for Physics (NCP), Quaid_E_Azam University Campus, Islamabad, pakistan, (2013).*
- 65- H. Hegazy, E. AlAshkar, H. H. Abou-Gabal, M. Naguib Aly, and N. Hamed "Spectroscopic Evolution of Plasma Produced by Nd-YAG Laser" *Ieee transactions on plasma science, V.42,no. 6,(2014).*
- 66- M. Favre¹, H. M. Ruiz², D. Cortes¹ F. Merello¹, H. Bhuyan¹, F. Veloso¹ and E. Wyndham¹ " Collision dynamics of laser produced carbon plasma Plumes" *Journal of Physics: Conference Series* **720** (2016).

-
-
- 67- C. Iorga, V. Stanculescu, V. Pașca "A study of the laser-produced aluminum plasma by means of computer simulation" National Institute for Laser Plasma and Radiation Physics, Atomistilor 409, P. O. Box MG-36, Magurele-Ilfov, 077125 Romania EU, Romanian Reports in Physics, Vol. 68, No. 1, P. 294–304, (2016).
- 68- E. U. Condon and G. H. Shortley, "The Theory of Atomic Spectra", Cambridge University Press (1935).
- 69- J. C. Slater, "The Quantum Theory of Atomic Structure", McGraw-Hill-Book Company, New York, (1960).
- 70- E. U. Condon and H. Odabasi, "Atomic Structure", Cambridge University Press, (1978).
- 71- M. Bonitz, N. Horing and P. Ludwig, "Introduction to Complex Plasmas", Springer, New York, (2010).
- 72- D. R. Hartree, "The Wave Mechanics of an Atom with a Non-coulomb Central Field: Part III, Term Values and Intensities in Series in Optical Spectra." Proceeding of The Cambridge Philosophical Society, 24 (1928).
- 73- V. Fock, "Approximation method for solving the quantum-mechanical many-body problem" *Zphysics*, 61 (1930).
- 74- J. C. Slater, "The Theory of Complex Spectra", *Phys. Rev.* 34 (1929).
- 75- T. Koopmans, "About the assignment of wave functions and eigenvalues of the individual electrons one atom", *Physica* (1934).
- 76- E. Clementi and C. Roetti, "Tables of Root-mean-Square Hartree-Fock Wavefunctions", *Atomic Data and Nuclear Data Table*, 14 (1974).

-
-
- 77- W. Eissner, M. Jones and H. Nussbauma," Techniques for the calculation of atomic structures and radiative data including relativistic corrections", *Comp. Phys. Commun.* 8 (1974).
- 74- A. Hibbert," CIV3 — A general program to calculate configuration interaction wave functions and electric-dipole oscillator strengths", *Comp. Phys. Commun.*, 9 (1975).
- 75- R. D. Cowan, L. J. Radziemski and V. Kanfman," Effect of continuum configuration interaction on the position of $s p^6$ in neutral chlorine, other halogens", *Journal of The Optical Society of America*, 64 (1974) .
- 76- C. Froese, Fisher, "The Hartree-Fock Method for Atomic: A numerical Approach", John Wiley and Sons, New York (1972).
- 77- D. A. Dirac," The Quantum Theory of the Electron Ibid", *Proceedings of The Royal Society*, 117 (1928).
- 78- R. D. Cowan," Atomic Self-Consistent-Field Calculations Using Statistical Approximations for Exchange and Correlation", *Phys.Rev.*, 163 (1967).
- 79- R. D. Cowan, Programs RCE (Mod11) Computational of Atomic Energy Levels and Spectra, Los Alamos National Laboratory, (1993).
- 80- R. D. Cowan, Programs RCN36/RCN2 (Mod36), Computational of Atomic Radial Wavefunctions, Los Alamos National Laboratory, Aug. (1993).
- 81- D. Atwood, *Soft X-Rays and Extreme Ultraviolet Radiation: Principles and Applications*, Cambridge University Press, (1999).

-
-
- 82- J. P. Christiansen and K. V. Roberts," OLYMPUS a standard control and utility package for initial-value FORTRAN programs", *Comp. Phys. Commun.*,(1974).
- 83- A. Djaoui, "A user Guide for The Laser Plasma Simulation Code MED103", Rutherford Appleton Laboratory Report: RAL-TR-96-099, RAL, Didcot, U. K., (1996).
- 84- P. Shaaf, "Laser Processing of Material, Springer, New York (2010).
- 85- G. O'Sullivan, A. *Cummings*, P. Dunne, K. Fahy, P. Hyden, L. McKinney, N. Murphy, E. Sokell and J. White, "Recent Progress in The Development of Sources for EUV Lithography", *AIP Conf. Proc.*,(2005).
- 86- R. W. Coons, S. Harilal, M. Polek and A. Hassanein," Spatial and temporal variations of electron temperatures and densities from EUV-emitting lithium plasmas", *Anal. Bioanal. Chem*, 400 (2011).
- 87- P. T. Mannion, S. Fvre, C. Mullan, D S Ivanov, G. O'Connor, T. J. Glynn, B. Doggett and J. G Lunney," Langmuir probe investigation of plasma expansion in femto-and picosecond laser ablation of selected metals", *J. of Physics: Conference Series*, 59 (2007).

الخلاصة

تم في هذه الرسالة دراسة الخصائص الهيدروداينميكية للبلازما المتولدة بالليزر. ان الغرض من هذا العمل هو توليد مصدر ضوئي ضمن منطقة الاشعة فوق البنفسجية البعيدة وهو مهم جدا في عملية الطباعة النقشية وتصنيع اشباه الموصلات.

تم استخدام برنامج (Cowan) لحساب الأنتقالات الألكترونية بين التوزيعات الذرية بأستعمال طريقة (HartreeFock) الرياضية.

باستخدام برنامج Medusa (Med103) المطور ذو البعد الهيدروداينميكي الواحد مثل (السرعة, كثافة الألكترون, الضغط, درجة حرارة الألكترون, كثافة الأيون, درجة حرارة الأيون ومعدل الأيونات) للبلازما المنتجة من الالمنيوم.

تم اتمام هذا العمل باستخدام مصدر ليزري ذو طول موجي 1064 نانومتر وبثلاث شدات مختلفه (10^{11} , 10^{12} , 10^{13} واط/سم³) وكان عرض النبضة الليزرية المستخدمة هو (10 نانوثانية و 10 بيكوثانية).

ان الليزر المستخدم بشدات مختلفه مع عرض النبضه 10 نانومتر اعطى معدل تأين عالي للألمنيوم من (2.4 – 11) مع معدل درجة حرارة الالكترن من (16.5-3000) الكترن-فولت. بالنسبه لعرض نبضه الليزر 10 بيكوثانية كان معدل التاين من (13-3.35) بينما كان معدل درجة حرارة الكترن من (16.5-2000)الكترن فولت.

ان الألمنيوم قد اعطي طيف انبعائي جيد في المنطقة فوق البنفسجية البعيدة عند 10 نانومتر مع قوة انتقال بمقدار 1.82.



وزارة التعليم العالي والبحث العلمي

جامعة بغداد

معهد الليزر للدراسات العليا

دراسة حسابيه للأنبعاثات الطيفية للألمنيوم في مدى
الأشعة فوق البنفسجية البعيدة باستخدام ليزر النديميوم-
ياك

رسالة مقدمة الى

معهد الليزر للدراسات العليا / جامعة بغداد / لاستكمال متطلبات نيل شهادة
ماجستير علوم في الليزر / الفيزياء

من قبل

شيماء نعمه عياش

بكالوريوس علوم الفيزياء - 2014

بإشراف

المدرس الدكتور محمود شاکر محمود